ISTANBUL TECHNICAL UNIVERSITY ★ GRADUATE SCHOOL

IDENTIFYING THE LOCATIONS OF OBSERVATION WELLS FOR VARIOUS BOUNDARY CONDITIONS FOR GEOTHERMAL RESERVOIRS

Ph.D. THESIS

Ufuk ÖZTÜRK

Department of Petroleum and Natural Gas Engineering

Petroleum and Natural Gas Engineering Programme

SEPTEMBER 2021

ISTANBUL TECHNICAL UNIVERSITY ★ GRADUATE SCHOOL

IDENTIFYING THE LOCATIONS OF OBSERVATION WELLS FOR VARIOUS BOUNDARY CONDITIONS FOR GEOTHERMAL RESERVOIRS

Ph.D. THESIS

Ufuk ÖZTÜRK
(505112501)

Department of Petroleum and Natural Gas Engineering

Petroleum and Natural Gas Engineering Programme

Thesis Advisor: Prof. Dr. Ömer İnanç TÜREYEN

SEPTEMBER 2021

İSTANBUL TEKNİK ÜNİVERSİTESİ ★ LİSANSÜSTÜ EĞİTİM ENSTİTÜSÜ

JEOTERMAL REZERVUARLAR İÇİN FARKLI DIŞ SINIR KOŞULLARINDA UYGUN GÖZLEM KUYUSU YERLERİNİN BELİRLENMESİ

DOKTORA TEZİ

Ufuk ÖZTÜRK
(505112501)

Petrol ve Doğal Gaz Mühendisliği Anabilim Dalı

Petrol ve Doğal Gaz Mühendisliği Programı

Tez Danışmanı: Prof. Dr. Ömer İnanç TÜREYEN

EYLÜL 2021

Ufuk ÖZTÜRK, a Ph.D. student of ITU Graduate School student ID 505112501 successfully defended the thesis/dissertation entitled "IDENTIFYING THE LOCATIONS OF OBSERVATION WELLS FOR VARIOUS BOUNDARY CONDITIONS FOR GEOTHERMAL RESERVOIRS", which he prepared after fulfilling the requirements specified in the associated legislations, before the jury whose signatures are below.

Thesis Advisor : **Prof. Dr. Ömer İnanç TÜREYEN** ....
Istanbul Technical University

Jury Members : **Prof. Dr. Abdurrahman SATMAN** ....
Istanbul Technical University

Prof. Dr. Niyazi AKSOY ....
Dokuz Eylül University

Prof. Dr. Serhat AKIN ....
Middle East Technical University

Asst. Prof. Dr. Didem KORKMAZ BAŞEL ....
Istanbul Technical University

Date of Submission : 09 August 2021
Date of Defense : 15 September 2021

To my family and beloved wife,

FOREWORD

Firstly, I would like to express my deepest gratitude to my thesis supervisor Prof. Dr. Ömer İnanç TÜREYEN for his invaluable guidance, support, continuous motivation, insight and guidance throughout my Ph.D. study. He was always supportive and positive within the passing years.

I would like to express my gratitude to my jury member Prof. Dr. Abdurrahman SATMAN for his constructive support and valuable advises during my thesis study. Secondly, I would like to express my special thanks to my other jury member Prof. Dr. Niyazi AKSOY for his valuable comments and suggestions that help me to improve the quality of my thesis study.

I also would like to express my sincere thanks to ITU Petroleum and Natural Gas Engineering family, namely Prof. Dr. Mustafa ONUR, Asst. Prof. Dr. İ. Metin MIHÇAKAN, Asst. Prof. Dr. Şenol YAMANLAR, Assoc. Prof. Dr. Murat ÇINAR for their insight in the lectures I took.

I really thank my dear colleagues Turgay İNCEIŞÇI and Harun KIRMACI for their friendship during long journeys to İstanbul.

I greatly appreciate my mentor Dr. Tayfun Yener UMUCU for his encouragement to start my Ph.D. study.

I want to thank my managers in TPAO and colleagues from my department for their understanding and support in finalizing this study.

I would like to thank my family, especially my mother Fatma, my father Ömer, my sister Burcu and my niece Mila for their continuous support, encouragement and trust since the beginning of my long journey.

At last but not the least, I would like to say my deepest thanks to my beloved wife Yağmur Venüs for her support, patience and motivation in finalizing this study.

September 2021 Ufuk ÖZTÜRK
(Petroleum and Natural Gas Engineer)

TABLE OF CONTENTS

Page

LIST OF FIGURES

Page

LIST OF TABLES

SYMBOLS

A	: Drainage area, m^2
B	: Water formation volume factor, m^3/sm^3
C_r	: Specific heat capacity of the rock, J/kg
c_t	: Total compressibility, 1/bar
h	: Height of the production zone, m
$h_{w,i}$	: Specific enthalpy of the injected water, J/kg
$h_{w,r}$	: Specific enthalpy of the recharge water, J/kg
$h_{w,p}$	: Specific enthalpy of the produced water, J/kg
k	: Permeability of the reservoir, m^2
k_x	: Permeability in the x direction, m^2
k_y	: Permeability in the y direction, m^2
N_{tim}	: Number of timesteps
p	: Pressure, bar
p_D	: Dimensionless pressure, dimensionless
p_i	: Pressure of grid i, bar
p_i^n	: Pressure of grid i at the n^{th} time step, bar
p_w	: Wellbore pressure, bar
p_r	: Average Reservoir pressure, bar
p_{wf}	: Wellbore flowing pressure, bar
$p_i(t)$	: Pressure of i^{th} grid as a function of time, bar
$p_r(t)$	: Average reservoir pressure as a function of time, bar
p_{wD}	: Dimensionless wellbore pressure, dimensionless
p_0	: Initial pressure, bar
$p(t)$	: Average pressure in the tank at a given time, bar
Δp	: Pressure difference between the tanks, bar
Δp_u	: Pressure drop caused by unit mass flow rate, bar
$\Delta p(t)$	: Pressure change of a tank as a function of time, bar
Δp_A	: Pressure drop at point A, bar
$\Delta p_{B,A}$	: Pressure drop at point A caused by well B, bar

$\Delta p_{C,A}$: Pressure drop at point A caused by well C,bar
q : Flow rate, sm^3/s
q_B : Flow rate of well B, sm^3/s
q_C : Flow rate of well C, sm^3/s
r : Radius, m
r_D : Dimensionless radius, dimensionless
r_e : Drainage radius, m
r_o : Effective well grid radius, m
r_w : Well radius, m
s : Skin factor of the well, dimensionless
T : Temperature of the reservoir, °C
T_0 : Initial temperature, °C
t : Time, s
t_D : Dimensionless time, dimensionless
t_{DA} : Dimensionless time based on the drainage area, dimensionless
t_0 : Initial time, s
t_n : n^{th} timestep, s
Δt_1 : Initial timestep difference, s
u_w : Specific internal energy of water, J/kg
V_b : Bulk volume, m^3
V_i : Bulk volume of grid i, m^3
w_{acc} : Mass accumulation rate of water, kg/s
w_i : Water injection rate, kg/s
w_{i,j_l} : Water flow rate from grid i and j_l, kg/s
w_p : Water production rate, kg/s
$w_{p,net}$: Net production rate of water, kg/s
w_r : Recharge rate of water, kg/s
w_{well} : Production rate from the well, kg/s
w_{well1} : Production rate from Well1 in shallow reservoir, kg/s
w_{well2} : Production rate from Well2 in deep reservoir, kg/s
WI : Peaceman's well index, kg/ bar-s
x_i : x coordinate of the i^{th} image well
Δx : Width of the grid, m
y_i : y coordinate of the i^{th} image well

Δy	: Length of the grid in y direction, m
Δz	: Length of the grid in z direction, m
α	: Recharge index, kg/ bar-s
α_r	: Recharge index to the reservoir, kg/ bar-s
α_{i,j_l}	: Recharge index between grid i and j_l, kg/ bar-s
α_{ir}	: Recharge index between the inner aquifer and the outer aquifer, kg/bar-s
α_{or}	: Recharge index between the outer aquifer and recharge source, kg/bar-s
α_{r1}	: Recharge index between the aquifer and the shallow reservoir, kg/bar-s
α_{r2}	: Recharge index between the aquifer and the deep reservoir, kg/bar-s
α_{r12}	: Recharge index between the deep and the shallow reservoir, kg/bar-s
α_a	: Recharge index between the aquifer and recharge source, kg/bar-s
β_r	: Thermal expansion coefficient, 1/°C
κ	: Storage capacity of a tank, kg/bar
κ_i	: Storage capacity of grid i, kg/bar
κ_r	: Storage capacity of the reservoir, kg/bar
κ_{ia}	: Storage capacity of the inner aquifer, kg/bar
κ_{oa}	: Storage capacity of the outer aquifer, kg/bar
κ_{r1}	: Storage capacity of the shallow reservoir, kg/bar
κ_{r2}	: Storage capacity of the deep reservoir, kg/bar
κ_{ar}	: Storage capacity of the aquifer, kg/bar
μ	: Viscosity of water, cp
ρ_r	: Density of rock, kg/m^3
ρ_w	: Density of water, kg/m^3
$\rho_{w,i}$	: Density of water in grid i, kg/m^3
ϕ	: Porosity of the reservoir rock, %
ϕ_0	: Initial porosity, %
ϕ_i	: Porosity of grid i, %
φ_i	: Absolute percentile difference, %

IDENTIFYING THE LOCATIONS OF OBSERVATION WELLS FOR VARIOUS BOUNDARY CONDITIONS FOR GEOTHERMAL RESERVOIRS

SUMMARY

In the last two decades, the importance of renewable energy sources has increased due to global warming and environmental concerns. Having suitable geological conditions, Turkey’s geothermal potential is high. In the last sixteen years, with new investments, the installed geothermal capacity of Turkey greatly increased. In the near future, geothermal energy can contribute more to the domestic energy needs and could be an important alternative energy resource for our country.

In geothermal projects, optimum reservoir management is one of the most important aspects of sustainable production. It affects the project's economy and the sustainability of the resources. In order to manage the reservoir optimally, future predictions have to be made by using reservoir simulation techniques. In reservoir simulation, the volumetric average reservoir pressure is one of the most important data that can be obtained from the reservoir. One can use well tests or observation wells to determine the volumetric average reservoir pressure. This study aims to contribute to answering the best possible location for the observation well that represents the average reservoir pressure. The pressures observed from the observation well can then be used for reservoir engineering practices. In case the observation well location does not represent the average reservoir pressure behavior, reservoir engineering practices may lead to unreliable future performance predictions. Thus, placing an observation well at a place where actual volumetric average reservoir pressure can be recorded is crucial for the economic development of the geothermal reservoir.

In this thesis, a numerical work is conducted to study the proper location of an observation well to be selected for different boundary conditions and various well configurations. In all examples a square-shaped reservoir is assumed and no-flow or constant pressure outer boundaries are used. The cases studied usually have either one production or reinjection well or a pair of them. Even though the results obtained in the studied cases show results from a single well or a pair of wells, they can be used to generalize to production and reinjection regions in a field. A production well can represent a production region (where all or most of the production wells in the system are located) or an injection well might represent an injection region. The results of this study provide decision maps for various boundary and well configurations from which the engineer may be able to determine qualitatively where to place the observation well. It is determined that in the case where there is a high reinjection ratio (most of the produced fluid is reinjected back into the reservoir) the effects of the outer boundary on the location of the observation well becomes negligible. The location of the observation well in such cases depends mostly on the configuration of how the production and reinjection wells are placed. Furthermore, it should also be noted that the location of an observation well may change depending

on how the locations of production and reinjection wells change over time, and also on the production and reinjection amounts. It is important to note that the results obtained from this study should be interpreted qualitatively. A study that provides the proper locations of an observation well does not exist in the geothermal engineering literature. The original contribution of this study is to fill this gap which could be very important.

JEOTERMAL REZERVUARLAR İÇİN FARKLI DIŞ SINIR KOŞULLARINDA UYGUN GÖZLEM KUYUSU YERLERİNİN BELİRLENMESİ

ÖZET

Artan nüfus ve sanayileşme ülkelerin enerji ihtiyacını arttırmaktadır. İç kaynakları ile bu enerji ihtiyacını karşılayamayan ülkeler, dışarıdan kaynaklarla bu açığı kapamaya çalışmaktadır. Ancak artan çevresel kaygılar ve küresel ısınma, ülkelerin farklı enerji kaynaklarına yönelmesine sebep olmuştur. Temiz, sürdürülebilir ve ucuz olması sebebiyle jeotermal gibi temiz enerji kaynakları geliştirilmeye çalışılmaktadır. Bu noktada belli başlı coğrafi, jeolojik özellikler jeotermal kaynaklarının geliştirilebilmesi için gerekmektedir. Türkiye de bu noktada jeotermal kaynaklar açışından avantajlı bir durumda yer almaktadır. Örneğin Afrika plakasının kuzeye hareketi nedeniyle Suudi Arabistan plakası kuzeye doğru itelenmekte, Suudi Arabistan plakası da Anadolu plakasını batıya doğru bir yılda 2-3 cm kadar ötelerken, Anadolu'nun özellikle batıdaki Ege Bölgesinde oluşan graben yapıları ve incelen kabuk jeotermal sistemler için uygun ortamlar oluşturmaktadır. Ülkemizde son yıllarda jeotermale yapılan yatırımların arttığı, yeni projelerin hayata geçirildiği ve jeotermal kaynağı üretiminin ve kullanımın arttığı gözlenmektedir. Türkiye'nin yıllık üretim değerlerine bakıldığında da dünya çapında önemli bir konumda yer aldığı ve bu pozisyonunu ileride üretime geçirebileceği yeni projelerle daha da ilerletebileceği beklenmektedir. Bu noktada jeotermal sahaların da verimli olarak üretilmesi ve kaynakların verimli bir şekilde harcanması jeotermal üretiminin sürdürülebilirliğinde önemli bir husus olarak dikkat çekmektedir. Bu sebeple son yıllarda ülkemizin dışa bağımlılığını azaltacak jeotermal enerjinin verimli ve doğru bir şekilde üretilmesi için yapılan çalışmaların sayısı arttığı gözlenmektedir.

Bir jeotermal sahasına yapılan yatırımın büyüklüğü düşünülünce saha üretiminin verimli yapılması gerektiği anlaşılmaktadır. Sahanın verimli olarak üretilebilmesinde rezervuar mühendislerinin önemli bir yeri vardır. Rezervuar mühendisleri, jeoloji ve jeofizik mühendislerinin destekleriyle hazırlanan kavramsal statik modelleri ve daha sonra da üretim performansı verilerini kullanarak, sahanın geleceğini tahmin edilmesini sağlayacak dinamik modelleri oluşturmaktadır. Bu dinamik modeller yapılırken belli başlı parametrelerin de elde edilmesi gerekmektedir. Sahanın ortalama basıncının gözlenmesi ve tahmin edilmesi bu noktada modelleme konusunda en önemli verilerden biridir.

Sahanın ortalama basıncının takip edilmesi için iki farklı yöntem mevcuttur. Birincisi sahada yapılacak kuyu testleri olmakla birlikte, kuyu testleri yapılırken kuyu üretimine ara verilmesi gerekmektedir. Kuyu sayısı fazla olan sahalarda, kuyular arasında girişim etkileri olabilmektedir. Bu etkileşim de yapılacak tahminlerde sahanın ortalama basınç hesabının yanlış yapılabilmesine sebebiyet verebilir.

Ortalama rezervuar basıncının takibinin yapıldığı bir başka yöntem ise sahada delinen gözlem kuyuları ve bu kuyulara yerleştirilen basınç ölçme aletleriyle

gözlenmesidir. Gözlem kuyuları üretim ve enjeksiyon operasyonlarının yapılmadığı ancak delinen diğer kuyularla aynı özellikleri taşıyan kuyulardır. Bu kuyuların amacı sahada yalnızca basıncın takibinin yapılmasıdır ve sektörde yaygın bir şekilde kullanılmaktadır. Bir jeotermal sahasında birden fazla gözlem kuyusu olabilmektedir ancak gözlem kuyularının maliyetleri de normal üretim yada enjeksiyon maliyetlerine yakın olduğu için ve üretime katkıda bulunmadıkları için sayıları az tutulmaktadır. Sahada üretim ve enjeksiyon operasyonları olması sebebiyle basınç doğrusal bir şekilde dağılmamaktadır. Üretim kuyularına yakın noktalarda basınçların düşme eğiliminde olduğu ve enjeksiyon kuyularına yakın noktalarda ise basınçların artma eğiliminde olduğu bilinmektedir. Bir sahanın ekonomik ömrü boyunca, ortalama basıncının gözlendiği noktalar, açılan üretim ve enjeksiyon kuyuları yerlerine, debilerine göre ve sahaya bağlı kısıt koşullarına göre değişim gösterebilmektedir. Dolayısıyla gözlem kuyusunun nereye yerleştirildiği ve bu noktadan sahanın ortalama basıncının gözlenebildiğinden emin olunması gerekmektedir.

Bu çalışma sahadaki ortalama basıncının gözlendiği noktaların belirlenmesinde kolaylık sağlaması ve belli başlı senaryolarda nerelerde gözlem kuyularının yerleştirilmesine ışık tutmasını amaçlamıştır. Çalışmanın ilk kısmında oluşturulan sayısal model anlatılmıştır. Kullanılan sayısal model 2 boyutlu bir sistemi varsaymış ve tek fazlı su barındıran bir rezervuar modellenmiştir. Ayrıca rezervuardaki sıcaklık değişimleri ihmal edilmiştir. Sayısal modelin teorik altyapıları anlatılmasını takiben, oluşturulan sayısal modelin doğrulanması yapılmıştır. Modelin doğrulanması üç farklı yöntemle yapılmıştır. İlk aşamada doğruluğu bilinen analitik modellerle kıyaslama yapılarak doğrulanmıştır. İkinci aşamada bir paket programdaki sonuçlarla kıyaslama yapılmış ve sonuçların örtüştüğü gözlenmiştir. Son aşamada ise literatürde kullanılan yarı-kararlı akış denklemindeki sonuçlarla kıyaslama yapılmıştır. Üç aşamada da doğrulama sağlanmıştır.

Çalışmanın ikinci aşamasında tank modelleri ile ilgili teorik bilgiler verilmiştir. Bu bölümde bir optimizasyon algoritması tanımlanarak ters modelleme yöntemi ile verilen basınç datalarıyla uyumlu tank modeli parametrelerinin tahmin edilmesini sağlayan program oluşturulmuştur. Bu program yardımıyla gözlem kuyularının seçilme yerleri etkilerini belirten bir takım örnekler yapılmıştır. Bu örnekler sonucunda gözlem kuyusunun yerleştirilmesi gereken bölge hakkında ilk izlenimler edinilmiştir. Ayrıca yanlış gözlem noktası seçilmesinin rezervuarı temsil eden tank parametrelerinin tahmininde ne kadar sapmaya yol açtığı ve saha basınç tahminlerinin ne kadar etkilendiği ile ilgili de bilgiler paylaşılmıştır.

Çalışmanın üçüncü aşamasında ise süperpozisyon yöntemi tabanlı Larsen yöntemi ve bu yöntemin çok kuyulu sahalarda iki kez süperpozisyon yöntemi kullanılarak uygulanabileceği metodun teorik altyapısı anlatılmıştır. Çok kuyulu saha yönteminin doğrulaması da yapılmıştır. Bu yöntemi kararlı akışın olduğu senaryolarda kullanarak farklı kısıt koşulları ve kuyu yerleşimi durumlarda gözlem kuyu yerinin seçiminde kullanılmıştır. Bu örneklerin sonucunda önemli sonuçlar çıkarılmıştır.

- Tek üretim kuyusunun olduğu sistemlerde, ortalama basıncın gözlendiği bölge üretim kuyusu ile sabit basınç sınırı arasında olduğu gözlenmiştir.

- Gözlem kuyusu kesinlikle üretim kuyusu yada enjeksiyon kuyusuna yakın yerleştirilmemelidir. Üretim kuyusu basınç okumalarının düşük olmasını, enjeksiyon kuyuları da basınç okumasının yüksek olmasına sebebiyet verebilir.

- Enjeksiyon kuyusunun olmadığı ve yalnızca üretim kuyusunun olduğu sistemlerde, eğer üretim kuyuları sabit basınç sınırına yakın bir lokasyona yerleştirilirse ortalama basınç bölgesi iki yerde gözlenebilir. Birincisi üretim kuyusu ile sabit basınç sınırı arasında. İkinci bölge ise kuyunun yakınında bulunduğu sabit basınç sınırının aksi yönünde yer alır.
- Enjeksiyon kuyusunun bulunduğu sistemlerde, ortalama basınç bölgesi üretim kuyusu ile enjeksiyon kuyusu arasında yer almaktadır.
- Enjeksiyon yüzdesinin yüksek olduğu durumlarda sınır etkileri gözlem kuyusu yeri seçiminde etki etmemektedir.
- Birden fazla üretim bölgesi yada birden fazla enjeksiyon bölgesi bulunan sistemlerde ortalama basınç bölgesi en etkin üretim bölgesi ile en etkin enjeksiyon bölgesi arasında yer almaktadır.
- Fay olan sistemlerde, sabit basınç sınırı ile fay iletişim halindeyse, fay da bir sabit basınç sınırıı etkisi göstermektedir. Aynı şekilde üretim yada enjeksiyon kuyuları fayın içinde yer alıyorsa fay da bir kuyu gibi davranarak doğrusal bir kuyu etkisi yapmaktadır. Dolayısıyla sistemdeki fayın etkisine dikkat edilmelidir.

Tezin son kısmında ise çalışmadan çıkarılan sonuçlar ve çalışmanın sonuçları kullanılarak ileride yapılabilecek çalışmalar hakkında bilgiler verilmiştir.

1. INTRODUCTION

The word “geothermal” comes from the Greek word “Geo”, which means Earth and “therme” which means heat respectively. With the same logic, geothermal energy describes the energy generated and stored in the Earth. Below the Earth's crust, in the layer called magma, heat is continuously produced by the decay of radioactive particles. As we move to the center of the Earth the temperature increases which is also termed as the geothermal gradient. Areas having more tectonic activities, mainly around the boundaries of the plates, the underground temperatures are higher where the major geothermal resources are located (URL-1) .In Figure 1.1, the red areas are showing the major geothermal provinces over the world where major tectonic activities are taking place.

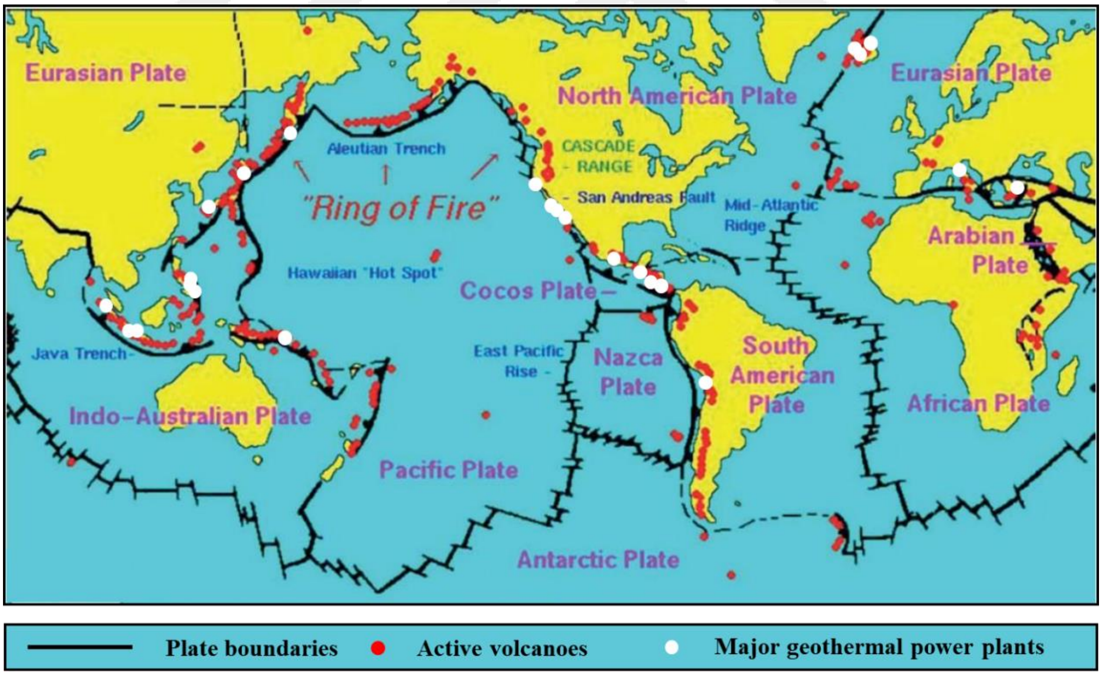

Figure 1.1 : Major geothermal provinces over the world (URL-2).

It can be seen that most of the geothermal rich areas are located between the boundaries of the tectonic plates or places having high earthquake activity.

Geothermal energy has been used as a heating source since 10000 BC in North America (URL-3). The first use of geothermal energy for electricity generation took place in 1904 in Italy (URL-3). In early applications, geothermal energy was not as economic as the most widespread energy resources i.e. fossil fuels. However, as the price of fossil fuels, mainly oil, increases countries tend to diversify their main source of energy besides fossil fuels. Being a safe, reliable, and clean source of energy, geothermal energy usage started to increase over the last decades. Figure 1.2 shows the world geothermal capacity change between the years 2000 and 2020 together with forecasts until 2025.

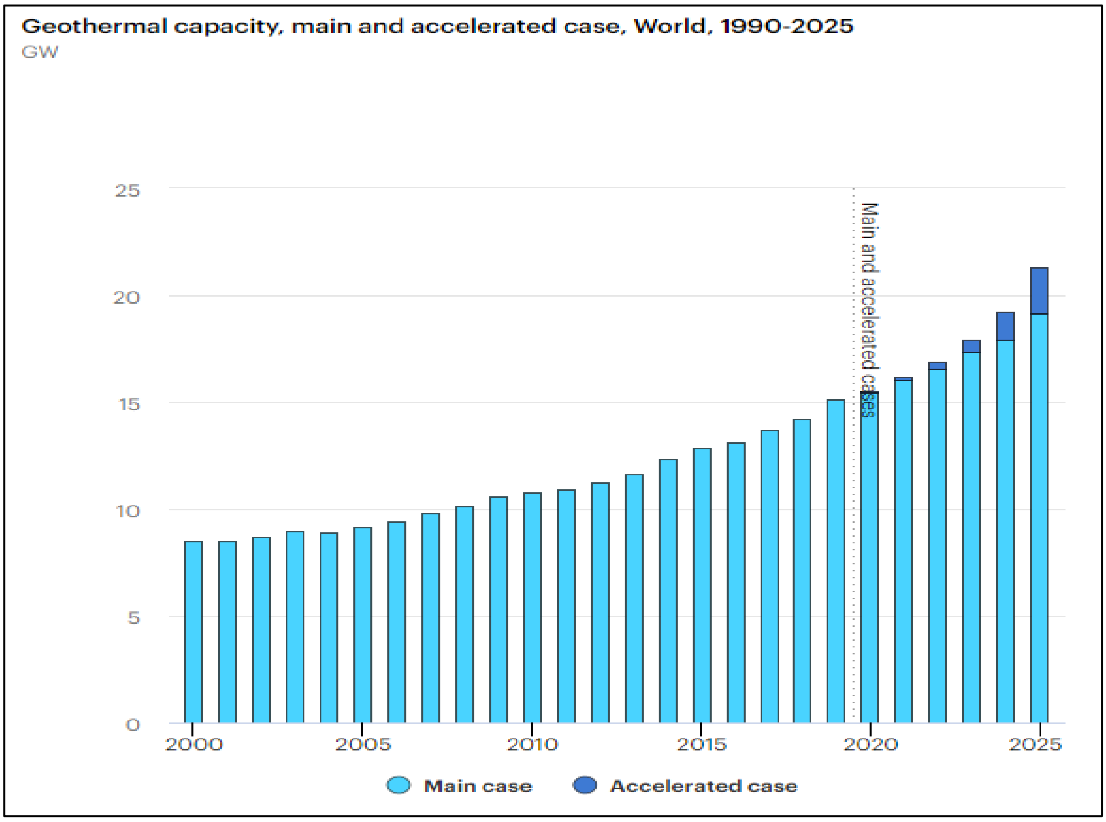

Figure 1.2 : World installed geothermal capacity (URL-4).

It is seen that the installed geothermal capacity of the world has increased from 8.5 GWe to 15 GWe in the last two decades and expected to reach around 20 GWe by 2025, which is a clear indication that the usage of geothermal energy will continue to increase in the near future globally. When the domestic capacity of geothermal energy is considered, Turkey has a respectable position in the world. Figure 1.3 shows the country-based installed capacity of geothermal energy.

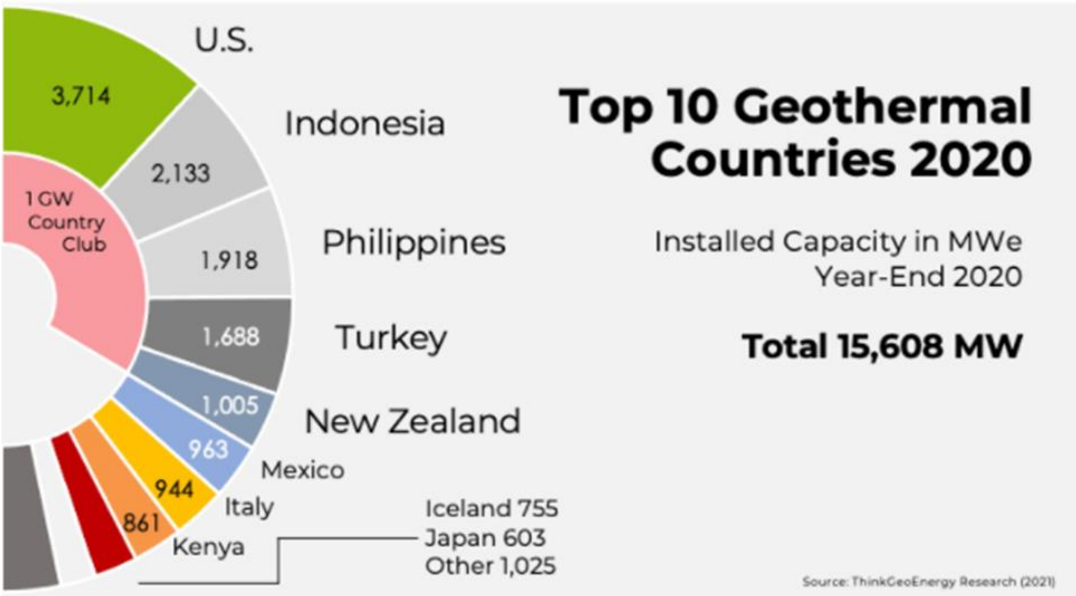

Figure 1.3 : Countrywise installed capacity of geothermal energy (URL-5).

It can be seen that in terms of the installed geothermal capacity, Turkey is the fourth biggest country in the world. Turkey's installed geothermal capacity has increased from 0.1 GWe to 1.35 GWe between the years 2010 and 2019 (URL-4) which is a huge increase when the global change all over the world is considered between the same period. Figure 1.4 shows the important geothermal fields of Turkey.

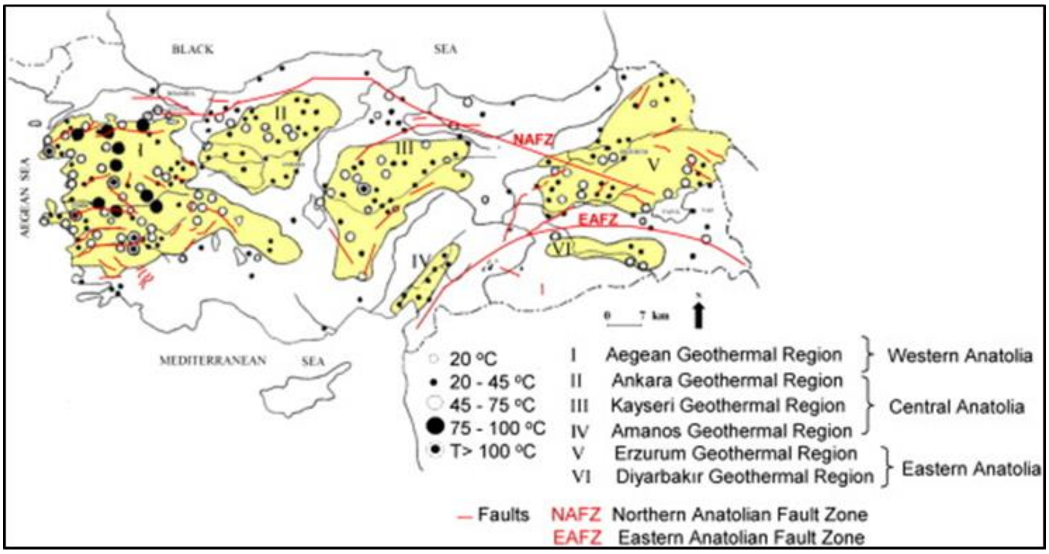

Figure 1.4 : Important geothermal sites and regions in Turkey (Korkmaz et al. 2014).

The circles in the figures indicate the fields in Turkey. By 2025, International Energy Agency's expectation for Turkey's installed geothermal capacity is around 2 GWe which is nearly 10% of the geothermal energy capacity of the world (IEA, 2020). It can easily be said that geothermal energy will become more crucial in the upcoming years. For this reason, the sources of geothermal energy, geothermal reservoirs have to be understood well to produce the energy more optimally. At first, simple reservoir models were built to determine the behavior of the reservoirs, however as time passed new and more complicated models in reservoir modeling and computer-aided systems have been developed. These models helped to forecast the production regime of the fields.

1.1 Literature Review

It is always important to predict the performance of a geothermal field. The need for optimal and effective production performance prediction leads to the development of the reservoir modeling concept. Companies try to decrease their drilling and operational costs together with an increase in the production of the fields they own. It is understood that drilling more wells does not mean that the field will produce effectively. Moreover, there is a certain number of wells that should be drilled into a field to maintain optimal production performance.

The behavior of the field has to be known when we drill wells. The best way to do this is to model the behavior of the reservoirs while they are producing. The reservoir modeling starts with the integration of data from the field. Even with the first well lots of information can be obtained. However to honor this information a model should be built. The reservoir engineer together with the subsurface team tries to predict the geological features of the reservoir (faults, boundaries, etc.) and model it. By this way, the team will have an idea about setting the optimal production strategy for the field. As new wells are drilled or operations are made, new data is acquired and clues for a less flawed model are obtained. The improvement of the model lasts until the field is abandoned. In Figure 1.5 a basic workflow of the reservoir modeling is shown. It can be seen from Figure 1.5 that every piece of data obtained from the reservoir improves the quality of the model and gives better predictions. For that reason, reservoir models take a crucial role in a field's production campaign. There are two conventional methods for modeling geothermal reservoirs. The first one is numerical modeling and the second one is lumped parameter modeling.

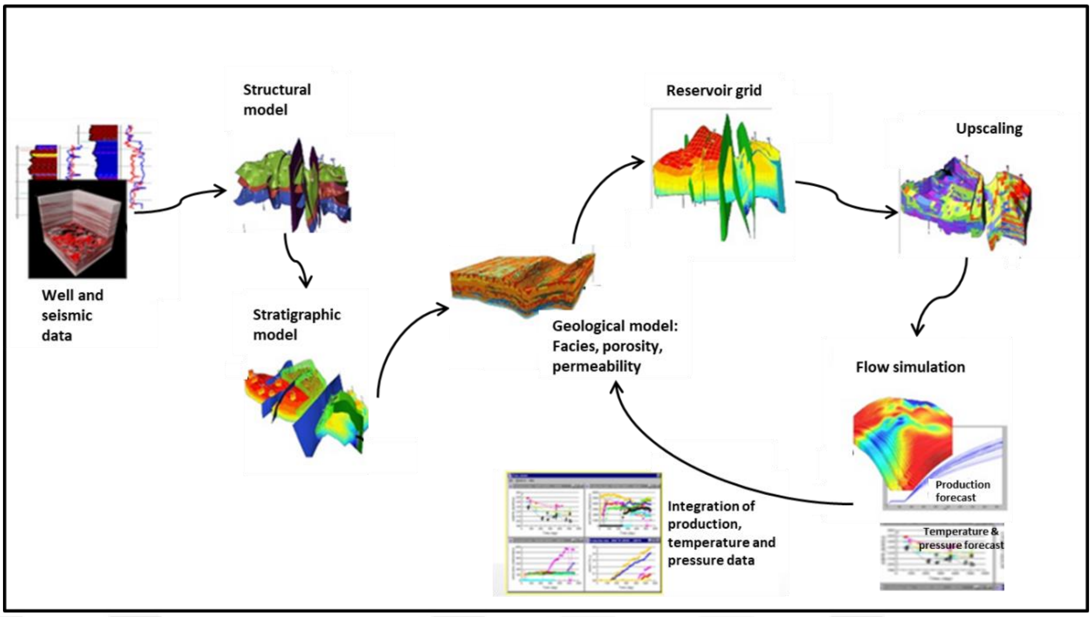

Figure 1.5 : Basic workflow of reservoir modeling (URL-6).

1.1.1 Numerical modeling of geothermal reservoirs

In the numerical models, the reservoir is divided into smaller blocks that represent certain parts of a reservoir. The number, size, and shape of the grids are generally defined by the user to honor the complexity of the reservoir. The heat and mass flow between these grids takes place based on the principle of conservation of mass and conservation of energy. With the help of computer systems, these conservation equations are solved simultaneously and the behavior of the reservoir can be modeled. The most important strength of the numerical models is the ability to solve many equations together in a very short time. Thus, many companies use numerical models in order to obtain an understanding of the reservoir. Using more number of grids will result in increased accuracy with the price of increased run time and CPU power. This can be noted as a disadvantage for the numerical models. Another disadvantage of this kind of model is that it needs more data to represent the reservoir. Even in the early times of a production campaign when the availability of much data is not possible, one should input a significant amount of data to build the model.

In the 1970s, with the developing computer technology first attempts of numerical models were generated. Horne and O'Sullivan (1977) used a numerical model for predicting the performance of the Wairakei geothermal reservoir which has been producing since the mid-1950s. In their study, a hypothetical reservoir was investigated and the wells produced fluids from the top layers of this reservoir. This production led the reservoir pressure to decrease and the liquid level to change. With the help of the model generated, pressure response of the reservoir was predicted.

Coats (1977) described a three-dimensional geothermal model which dealed with single-phase or two-phase, heterogeneous, or fractured reservoirs. In this model for each grid in the system mass balance and energy balance were solved implicitly. Also in this study, model stability for certain time step limits for various cases was studied.

Pruess and Schroeder (1979) developed a simulator called SHAFT79 which was using an integrated finite difference method. In this study, it was emphasized that having phase changes in the reservoir and coupling between mass and energy flows generates nonlinear equations which decrease the applicability of analytical approximations, the need for the numerical models has arisen. This simulator proposed a solution for one, two, and three-dimensional reservoirs having up to 350 elements. It was also compatible with reservoirs having irregular geometries.

In Zyvoloski and O'Sullivan's (1980) study, a finite difference approximation was solved by the Newton-Rapshon method presented to deal with the two-phase cases having carbon dioxide and water. It was assumed that the noncondensable gas present in the reservoir is composed of CO_2 which dominates the flow's thermodynamic characteristics. The result of this study was limited with few cases but it showed the significant effect of CO_2 on pressure transients.

In 1981, Goyal and Kassoy presented a two-dimensional model for the East Mesa Geothermal Field. The model assumes that the fault located in the system charges the reservoir and an impermeable clay cap present in the top layers of the system. The prediction results of the model was reasonable and the assumption of the fault-controlled-charging system was acceptable for the system.

Bodvarsson et. al. (1982) presented a two-dimensional fault-charged model that takes into account the heat losses caused by the surrounding layers in the system. This model was applied to the system in Susanville, California and reasonable matches were obtained for temperature profiles of the wells. The results obtained from this model gave some idea about the future development of the system.

In Marcou and Gudmundsson's (1986) study, a model was presented based on coupling both power plant performance and reservoir deliverability to obtain some economical results to optimize the development cost of the geothermal projects. Liquid-dominated reservoirs were considered in three different aspects which are reservoir performance, inflow performance, and wellbore performance. This model was used to match the production data of Ahuachapan and Wairakei fields.

Pruess (1987) presented the TOUGH model to the literature which can be used for one, two, and three dimensional, anisotropic, isotropic, and fractured systems. Later in 1991, Pruess presented an improved version of this program, TOUGH2 which includes the capability to handle different fluid mixtures and to input the geometry data that describes the volume elements and their connections. Both TOUGH and TOUGH2 are part of the MULKOM family of codes which belongs to Lawrence Berkeley Laboratory. O'Sullivan et. al. (1998) used TOUGH2 for the Wairakei field and check the effectiveness of the model for the field. Moreover, in this study, they presented new options to the model including a function that enables the user to graphically edit the geometry and permeability structure of the model.

Arihara et al. (1995) presented a simulation study by using the STARS software which is developed by Computer Modeling Group. In this study, a two layered reservoir, Kakkonda geothermal field is modeled by using dual porosity property of STARS software. Having highly heterogeneous fracture network, they succeeded in developing a history matched numerical model for the 13 years production period. Also history matched model indicated the partial pressure support from the lower reservoir section.

In Butler et al.'s (2000) study, a 3D numerical model of Cerro Prierto field is shown. A two staged modeling strategy is presented and TETRAD simulator is used to model the field. In the first stage the initial state model is generated mainly to match temperature distribution, heat transfer and mass discharge of the field are inserted to the TETRAD simulator. In the second stage the production history match and parameter adjustment is done. Based on the matched model, the possible future scenarios for the field is compared and future development strategies are suggested. Further studies are presented by Bromley et al. (2013), Llanos et al. (2015), Feng et al. (2016) and Quinao and Zarrouk (2018) by using TOUGH2 software for various geothermal fields.

1.1.2 Lumped parameter modeling of geothermal reservoirs

Lumped parameter modeling is a technique in which, a reservoir is represented by a series of tanks that can have different properties. Mainly, lumped parameter models need fewer amounts of data compared to numerical models. In lumped parameter modeling, mass and / or energy balance equations are solved on various control volumes for modeling the pressure and / or temperature. These control volumes may represent the reservoir, the outer part, the recharge source, a part of the reservoir and etc. The reservoir is referred to as the region of the geothermal system where the wells are located (usually located towards the center parts of the reservoir). The outer part refers to the region that surrounds the reservoir and provides a water influx into the reservoir as water is produced through the wells. The recharge source on the other hand is any source that replenishes the water in the outer part as it is produced from the reservoir. In Figure 1.6 a simple geothermal system is shown.

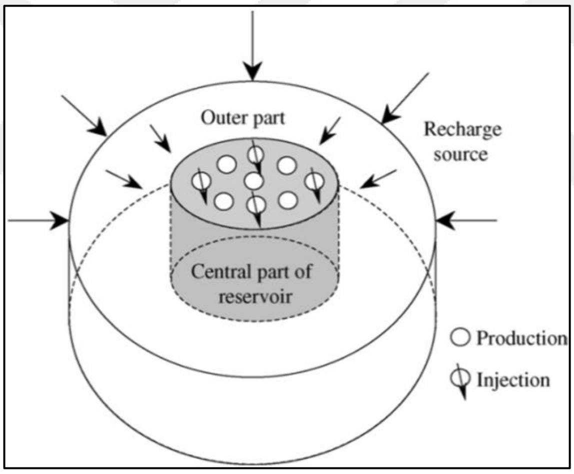

Figure 1.6 : A simple geothermal system (Sarak et al. 2005a).

Lumped parameter models can be divided into two types: isothermal and non-isothermal. In isothermal lumped parameter models, the change in the temperature is not taken into account. On the other hand, in non-isothermal lumped parameter models, the temperature change in the system is taken into account. These models have to be used when temperature changes occur, such as in cases where cooling due to reinjection needs to be modeled.

Whiting and Ramey (1969) developed the first lumped parameter model in the literature. In their model both mass and energy balance are honored and the flow is assumed to be isothermal liquid water having constant enthalpy, viscosity, and compressibility. Three flow geometries are valid for this model which is: hemispherical, linear, and radial. In this study, an illustrative example is presented for the Wairakei field.

Castanier et al. (1980) presented an analytical model which can be used for all liquid, all steam, and two-phase cases with radial geometry. In this model the reservoir is divided into 3 distinct regions which are: the innermost zone where production takes place, the intermediate zone where fluid flow and heat transfer takes place, and lastly, the outermost zone where injection operations around the field take place. In this model, the innermost zone is treated as a tank and the pressure of this tank is calculated by using the wells located in the boundary of the innermost and intermediate zone. In this study, the model is applied to the East Mesa field and acceptable results are obtained. On top of it, several production forecast scenarios are presented for the field.

In 1984, Olsen presented a study which targets mainly liquid dominated reservoirs. In this study, different influx models are used to match the field data of the Svartsengi geothermal field which is located in Iceland. It is observed that the match is increased as the influx models are implemented to the model. The best-performing influx model is obtained with Hurst's simplified solution.

Axelsson (1989) used the lumped parameter approach for modeling several geothermal reservoirs present in Iceland. These reservoirs are mainly low-temperature reservoirs and temperature change within the system is neglected. In this method, a network of capacitors is defined and these capacitors are connected via series of resistors. An iterative non-linear least-squares technique is used for estimating the model parameters used to represent the reservoir.

Sarak et al. (2005a) presented a study that can be used for low-temperature geothermal reservoirs. In this study analytical expressions have been obtained for various configurations of tanks connected together for modeling the geothermal reservoir. These models have then been incorporated in a history matching algorithm. The developed models have been used on Laugarnes field in Iceland and Balcova-Narlidere field in Turkey.

Li et al. (2017) presented a study that uses machine learning techniques to choose the best possible tank scheme among the various options. This method is used on the

Reykir field which is located in Iceland. Axelsson’s study and Sarak et al.'s (2005) study and Li et al.'s (2017) study were assuming isothermal systems.

Alkan and Satman's (1990) study is an example of non-isothermal lumped parameter models. In their study, the effect of carbon dioxide on reservoirs is taken into account and analytical formulations and mathematical expressions are presented. The model generated is applied to real-life geothermal reservoirs such as Cerro Prieto field in Mexico, Ohaaki field in New Zealand, Bagnore field in Italy, and Kizildere field in Turkey.

Onur et al. (2008) developed a model that can be used to predict both pressure and temperature of a low-temperature reservoir having single-phase liquid water. This model takes into account only the convectional heat exchange and neglects the heat transfer due to conduction. This model used on the Izmir Balcova-Narlidere field and two different scenarios are given for the pressure and temperature behavior of the field. Later, Tureyen et al. (2009) generalized this study to multiple tank cases.

The first study including the conduction effects was developed by Tureyen & Akyapı (2011) study. This model is a generalized model, which enhances one to represent a geothermal system with the desired number of tanks with different configurations. In this study, some applications are presented for injection well location selection, the effect of heat conduction on pressure and temperature, and lastly, the use of temperature data for reservoir characterization.

Nurlaela & Sutopo (2015) presented a model that is an extension of Onur et al.'s (2008) study to two-phase high-temperature geothermal reservoirs. The verification of the studied model is given together with two synthetic examples and for future studies, real-life cases will be used.

Hosgor et al. (2016) studied a new analytical expression for the liquid-dominated geothermal reservoirs having carbon dioxide. Since the presence of carbon dioxide is important for future predictions of the reservoir performance, having an expression for the change of carbon dioxide content depending on time, production, re-injection, and recharge enhance the understanding of the reservoirs having dissolved carbon dioxide.

Lastly, Qin et al. (2017) described a lumped parameter model which is used for two-phase superheated geothermal reservoirs. In this study, the "BFGS Quasi-Newton" optimization method to find the solutions is presented.

1.2 Structure of Thesis

In the following chapter, the statement of the problem is given. An example application is provided to emphasize the importance of the problem that is dealt with. In the third chapter, the mathematical models used in the study are summarized. Mainly, the numerical model, superposition model and lumped parameter models are discussed. In the fourth chapter, different examples are used to illustrate the understanding about the solution of the problem followed by a summary figure which can be used as a first guide for the cases having similar structure. In the final chapter, the conclusions obtained from the study are given together with the future work suggestions.

2. STATEMENT OF PROBLEM

The volumetric average reservoir pressure is the most critical parameter in lumped parameter models since the model basically describes the pressure behavior of a geothermal reservoir as a function of rate and time. In the practice of reservoir engineering, a relationship between the average reservoir pressure and the amount of production is usually sought for. Once such a relationship is obtained, then future predictions of average reservoir pressure could be made for a given production forecast.

A reservoir engineer could monitor the average reservoir pressure in two different ways. The first one is via well testing. By testing, certain wells occasionally will give an idea about how the reservoir pressure is changing. But, when the number of the wells in the field and the ongoing production/reinjection operations are considered, it is generally difficult to calculate the average reservoir pressure in the presence of interference effects. Also, it is generally not preferred economically to shut-in wells in the region that are heavily affecting the well that is going to be tested. Hence the average pressure measurements by the well tests may not represent the true volumetric average reservoir pressure for these kinds of instances.

The other method for obtaining the average pressure is by using observation wells. Observation wells are wells where no production or reinjection takes place, but the pressure is recorded at all times. This provides a continuous record of the observation well's pressure with time during production. An observation well is probably the most common way of keeping track of the average reservoir pressure. Furthermore, multiple observation wells may also be used for providing a more accurate record. However, there are two main problems with the use of the observation wells. One is that using an observation well is a costly procedure since a well or wells have to be designated for this purpose without performing any production or reinjection. The other problem with using observation wells has to do with the location of the observation well. It is a well-known fact that the pressure distribution in a geothermal reservoir will not be uniform spatially because of the production and reinjection operations. Closer to the production wells, the pressure will decline and away from the production wells the pressure will increase or closer to the reinjection wells, the pressure will increase and away from the reinjection wells it will decrease. During the lifetime of a geothermal reservoir, the locations which represent the average reservoir pressure could vary based on a number of factors such as the locations of the production and reinjection wells, the rates at which the wells are producing and re-injecting and the boundary conditions of the reservoir. In this case it becomes crucial that the observation well be placed at the location where the average pressure is observed.

In this chapter an example indicating the importance of the observation well location is shown.

2.1 Importance of Observation Well Location

In this subsection an example is used to illustrate the importance of the selection of observation well locations. As it has previously been stated the observation wells are considered to record volumetric average reservoir pressure. The effect if the location is not chosen correctly is explained with the example presented here.

Throughout the thesis study, reservoirs are assumed to have homogenous porosity and permeability distributions. The reservoir is filled with single-phase slightly compressible water.

For cylindrical reservoirs having r_e radius and one production well with a constant production rate located at the center of the reservoir, the location that the average reservoir pressure is observed for the constant pressure boundary and no-flow boundary conditions are shown in Figure 2.1 (Golan & Whitson, 1991).

It can be seen from Figure 2.1, the average reservoir pressure can be seen at $0.61r_e$ distance from the production well for the case having a constant pressure boundary. For the case having a no-flow boundary, this distance is shown as $0.47r_e$.

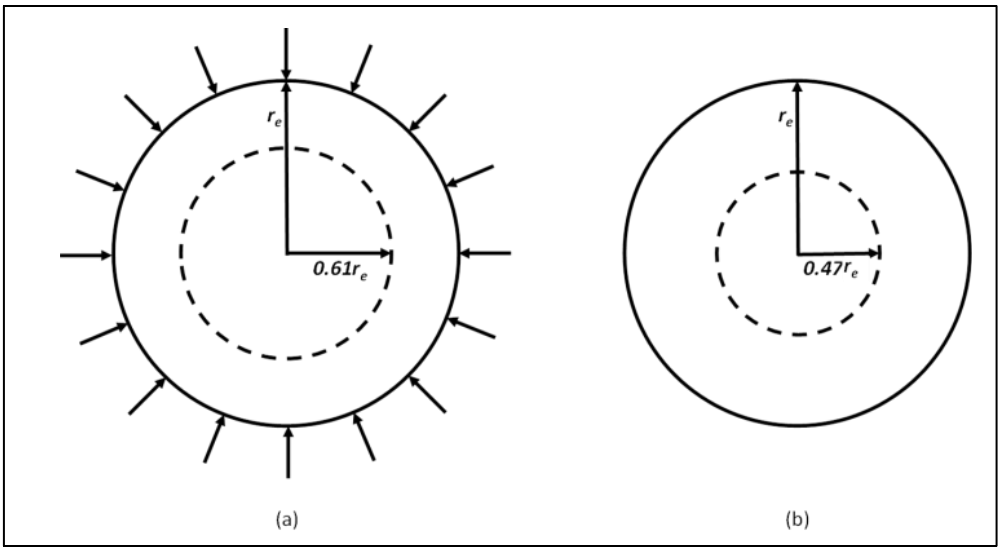

Figure 2.1 : The radius where the volumetric average reservoir pressure (indicated by the dashed line) is observed in a cylindrical reservoir with a well at the center. (a) Constant pressure outer boundary, (b) No-flow outer boundary

Consider a reservoir having a square shape with one side constant pressure boundary and remaining sides with no-flow boundary. The production well is located in the center of the reservoir and an arbitrary observation well location is chosen as shown in Figure 2.2.

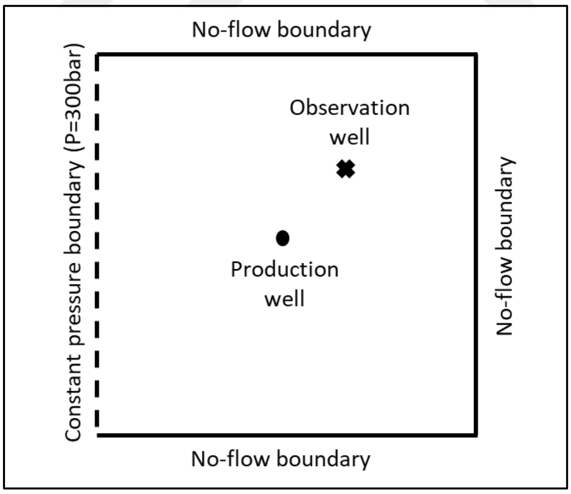

Figure 2.2 : Schematic of the reservoir with production and observation wells.

For the studied case the reservoir is assumed to be in equilibrium initially at a pressure of 300 bars. The system is composed of 40401 grids and both the production well and the observation well is located in the center of the grids where they are placed. The recharge index between the grids is 1 kg/bar-s and the storage capacity of each grid is 5385 kg/bar. Reservoir is assumed to have a storage capacity of $2.18{\times}10^8$ kg/bar. In Table 2.1 the parameters of the case are shown.

Table 2.1 : Parameters of the example.

Parameter	Value
Number of grids in x and y direction (numerical model)	201 × 201
Grid dimensions in x and y direction, m	49.75
Height of reservoir, m	500
Total length of the reservoir in x and y directions, m	10000
Storage capacity of a single grid, kg/bar	5385
Recharge index between grids, kg/bar-s	1
Initial pressure, bar	300
Porosity, fraction	0.1
Total compressibility, 1/bar	4.35×10^{-5}
Density of water, kg/m^3	1000
Viscosity of water, cp	1
Well radius, m	0.091
Production rate of the production wells, kg/s	110

The wells are assumed to have no wellbore storage and skin factor. The reservoir is assumed to be filled with single-phase slightly compressible water and all the thermal effects are neglected.

After 10 years of production, the observation well reading and the average reservoir pressure are shown in Figure 2.3.

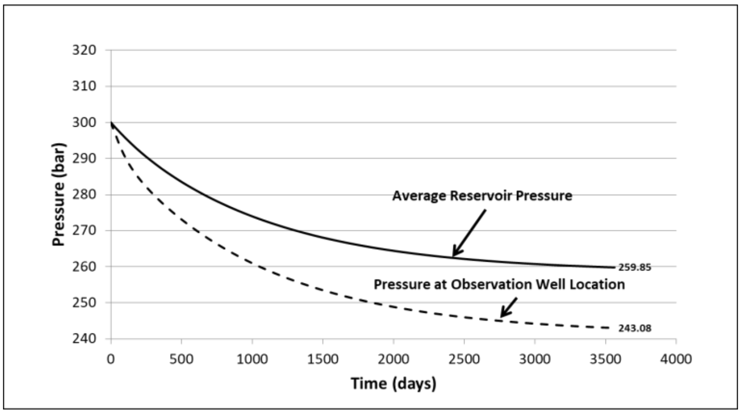

Figure 2.3 : The observation well pressure reading and average reservoir pressure.

It can clearly be seen that at the end of 10 years the observation well reading and average reservoir pressure has 16 bar difference.

As a next step, a single tank lumped parameter model (Sarak et al., 2005a) is used to match the average reservoir pressure history. Hence two parameters are determined as a result of the history matching process: the recharge index and the storage capacity. The recharge index is found to be 2.67 kg/bar-s using the single tank lumped parameter model over the average reservoir pressure history. The actual storage capacity is determined from the numerical model simply by taking the overall sum of all the recharge capacities of the grid blocks. The actual recharge index is determined by simply matching the actual average reservoir pressure.

When a history match is performed using the single tank lumped parameter model to the observation well pressure, the storage capacity is determined as 1.39×10^8 kg/bar and the recharge index is calculated as 1.94 kg/bar-s. Note that there exists considerable difference between the actual recharge index and the actual storage capacity (2.67 kg/bar-s and 2.18×10^8 kg/bar) and the ones obtained from the observation well pressure history match using the lumped parameter model (1.94 kg/bar-s and 1.39×10^8 kg/bar). As a next step, by using the parameters based on the observation well pressure and the actual reservoir pressure, future predictions are made for the next 10 years, this time doubling the flow rate. The results are given in Figure 2.4.

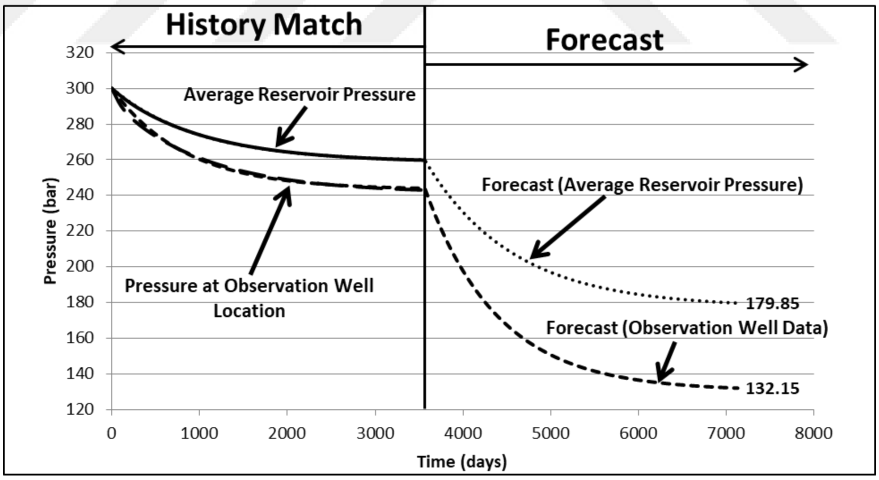

Figure 2.4 : Pressure predictions for the next 10 years.

Figure 2.4 clearly indicates that the prediction run gives a major deviation for the observation well pressure and average reservoir pressure. The effect of the inappropriate observation well placement leads to this misleading result. Even though a good match is obtained in the inverse model to the observation well, that does not mean that the parameters are representing the reservoir.

For each grid in the system, the percentile difference of grid pressure with the average reservoir pressure is calculated. Figure 2.5 gives the region where the actual volumetric average reservoir pressure is observed (at steady state conditions) along with the location of the observation well. The shaded area is showing the region where average reservoir pressure can be obtained.

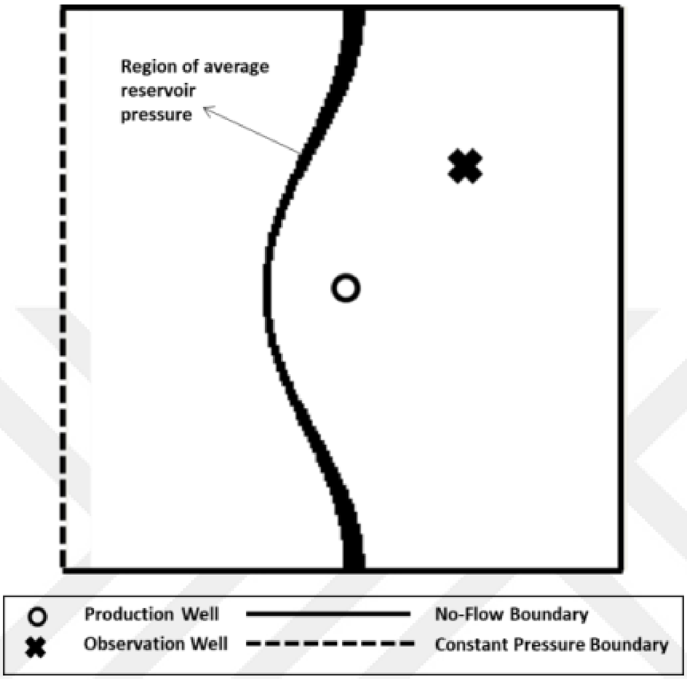

Figure 2.5 : Illustration of the region where actual volumetric average reservoir pressure is observed along with the location of the observation well.

It is clear from Figure 2.5 that the observation well is not placed correctly in this case leading to the errors shown in Figure 2.4.

In this study, the problem of the best possible locations for the volumetric average reservoir pressure observation is investigated. In Chapter 3 the detail of the mathematical models that are used in the study is provided. Following the theory and background of the numerical and superposition models, the validation of these models are also given in same chapter. In Chapter 4, various examples are given in order to understand the behavior of average pressure in the reservoir. In Chapter 5 major conclusions obtained from the study are presented together with proposed future studies.

3. MATHEMATICAL MODELS USED IN THE STUDY

In this chapter the theoretical background of the mathematical models that were used in the study is given. Firstly, the numerical model that was used is explained. In the second part of the chapter, the superposition model that was based on Larsen's study is explained. And in the last part of the chapter the validation of both models are given.

3.1 Numerical Model

In this section, the numerical model that is used in the study is described. The numerical model is mainly used for generating synthetic data and simulating the detailed grid-wise results to make necessary comparisons. Firstly, the theoretical background for the numerical model will be explained. Later, the validation of the numerical model will be shown.

3.2 Derivation of Numerical Model

The more general form of the model has been given previously by Tureyen and Akyapi (2011). In a numerical model, the system is formed of many grids, each of which representing some portion of the field. The flows between grids are generally described by mass and energy balances. In this study an isothermal system is considered, thus only mass balance is taken into account.

Some of the assumptions of the model are as follows:

- Every grid in the system is a porous material.
- The porous media of the grid is occupied fully with liquid water.
- The volume of the grid block is fixed.
- For any given time step, the production from the grid is by way of a fixed mass flow rate. However, this mass flow rate can change from time step to

time step. Thus, varying flow rates can easily be implemented to the model developed.

Firstly, the mass balance for a single tank should be understood. Consider a set of grids are present in the system as shown in Figure 3.1.

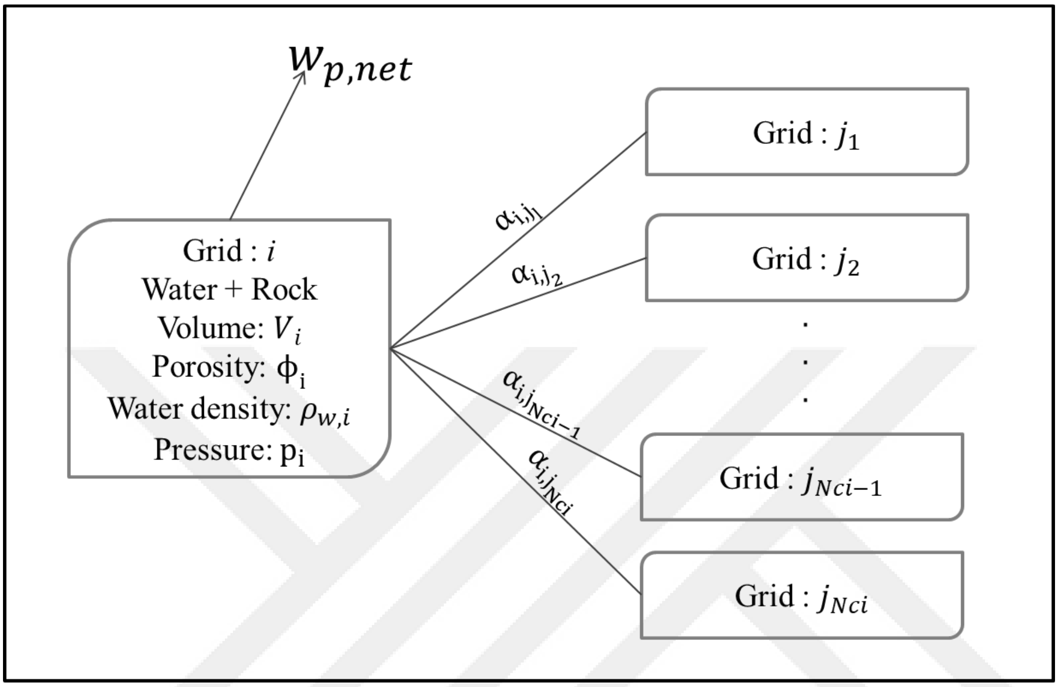

Figure 3.1 : Schematic of the system for multiple grids (Tureyen & Akyapı 2011).

Schilthuis's study (1936) presented a water influx model that describes the recharge rate between two tanks with the proportion of pressure difference between these two tanks. Equation (3.1) gives this relation:

$$w_r = \alpha[p_0 - p(t)] \tag{3.1}$$

where;

α is the recharge index, kg/bar-s,

p_0 is the initial pressure, bar,

$p(t)$ is the average pressure in the tank at a given time, bar,

w_r is the mass recharge rate of water to the tank, kg/s.

By using Equation (3.1), for the given system in Figure 3.1, the mass flow rate between grids i and j_l can be written as in Equation (3.2):

$$w_{i,j_l} = \alpha_{i,j_l}(p_{j_l} - p_i) \tag{3.2}$$

where;

α_{i,j_l} represents the recharge index between grid block i and j_l, kg/bar-s,

p_i is the pressure at grid i, bar,

p_{j_l} is the pressure at grid j_l, bar,

The mass balance for any grid i can be written as given in Equation (3.3):

$$\underbrace{V_i \frac{d(\rho_{w,i}.\emptyset_i)}{dt}}_{\substack{\text{Accumulation} \\ \text{rate of mass in} \\ \text{grid } i}} - \underbrace{\sum_{l=1}^{N_{c,i}} \alpha_{i,j_l}(p_{j_l} - p_i)}_{\substack{\text{Contribution of} \\ \text{mass from} \\ \text{neighboring tanks}}} + w_{p,net} = 0 \tag{3.3}$$

where;

$N_{c,i}$ denotes the total number of neighboring connections grid i makes with the neighboring grids,

$w_{p,net}$ represents the net mass flowrate from/to grid i (kg/s),

$\rho_{w,i}$ is the density of water in grid i (kg/m^3),

$\emptyset_i$ is the porosity of grid i (fraction),

V_i is the bulk volume of grid i (m^3).

By expanding the derivative term in Equation (3.3), we can obtain Equation (3.4):

$$V_i \rho_{w,i} \emptyset_i c_t \frac{dp_i}{dt} - \sum_{l=1}^{N_{c,i}} \alpha_{i,j_l}(p_{j_l} - p_i) + w_{p,net} = 0 \tag{3.4}$$

In this equation, c_t represents the total compressibility where the total compressibility is defined as the sum of water and rock compressibility. Writing equation (3.4) in terms of the storage capacity of grid i results in Equation (3.5).

$$\kappa_i \frac{dp_i}{dt} - \sum_{l=1}^{N_{c,i}} \alpha_{i,j_l}\left(p_{j_l} - p_i\right) + w_{p,net} = 0 \qquad (3.5)$$

where κ_i is the storage capacity of the grid i.

The time derivative in Equation (3.5) is handled numerically using a forward finite differencing scheme. Expanding the derivative numerically and further treating Equation (3.5) implicitly gives Equation (3.6).

$$\kappa_i \frac{({p_i}^{n+1} - {p_i}^{n})}{\Delta t} - \sum_{l=1}^{N_{c,i}} \alpha_{i,j_l}\left({p_{j_l}}^{n+1} - {p_i}^{n+1}\right) + {w_{p,net}}^{n+1} = 0 \qquad (3.6)$$

The superscript n denotes the current time and n+1 denotes the future time at which pressures will be computed.

Equation (3.6) represents the mass conservation equation to be solved numerically for grid i. All mass conservation equations are solved simultaneously to solve for all pressure in the system. It is important to note that the storage capacity κ and the recharge indices α between the grids are treated to be constant. This is a valid assumption to make when the fluid is a slightly compressible fluid such as water. A recharge source can be added to the system by defining a tank's volume as a very big number ($\approx 10^{99} m^3$).

The above equations connect the grids of the model to each other. The wells present in the field also have to be connected to the grids. Peaceman (1977) presented a study that can be used in numerical models while connecting wells to the grids of the model. In the simulations that have producing wells, a well index (WI) value has to be entered instead of α value. The WI is used as shown in Equation (3.7) for describing the communication between well (w) and the grid that well is located (i):

$$w_{i,w} = WI(p_i - p_{wf}) \qquad (3.7)$$

3.3 Superposition Models

This section starts with a brief explanation of the superposition principle. Later on, some approaches based on the superposition relation are presented. The first one is by assuming line source solution; the pressure distribution in space with time is shown. A general expression for the pressure drop in the system is presented. Secondly, a method based on Larsen's (1985) approach is presented. This method can be used to evaluate the results in the x and y direction together. Lastly, an approach for the cases having multiple production wells is shown by using the superposition principle again. In this way, a pressure map for the steady-state flow period is obtained.

3.3.1 Superposition method with line source solution

Superposition method is one of the widely used approaches used to model various production strategies in the reservoir. Superposition principle is used to determine the pressure drop at a certain location when there are multiple wells present in space. The principle states that for linear systems, the pressure drop at a certain location can simply be determined by adding the individual pressure drops of the wells as if they were producing alone.

The superposition is a straightforward approach. At any point of the reservoir, the total pressure drop is equal to the sum of each pressure drops caused by each well on that point of the reservoir. These added pressure drops are the drops when the wells are producing or injecting on their own. Consider a system composed of 2 wells located on points B and C as shown in Figure 3.2.

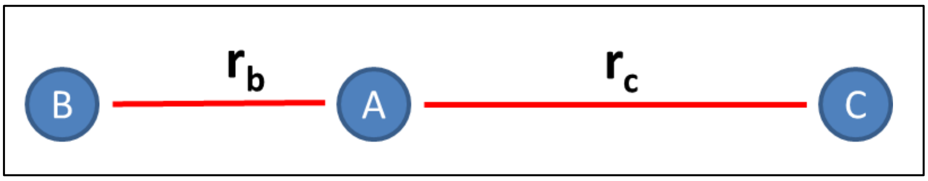

Figure 3.2 : Schematic of two well system.

The pressure drop at point A, Δp_A can be written as in Equation (3.8):

$$\Delta p_A = \Delta p_{B,A} + \Delta p_{C,A} \tag{3.8}$$

where;

Δp_A is pressure drop at point A,

$\Delta p_{B,A}$ is pressure drop at point A caused by well B when well B is the only producer,

$\Delta p_{C,A}$ is pressure drop at point A caused by well C when well C is the only producer.

Assuming that wells B and C are both line source wells without wellbore storage, the pressure drop can be formulated as in Equation (A.1). Formula is given in Appendix A.

Superposition method presents an easy approach to represent boundaries (no-flow boundary, constant pressure boundary) in the system. Consider well A is located with a distance L from the no-flow boundary as shown in Figure 3.3.

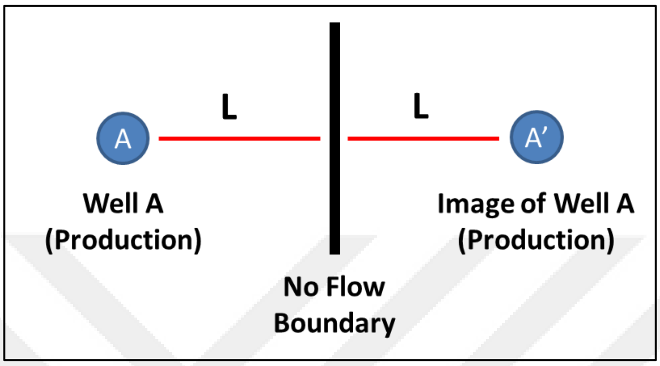

Figure 3.3 : Well near no-flow boundary.

The mathematical representation of this problem is placing an "image" well at 2L distance from the well A (Lee, 1982). This image well has the same production history as the original well A. By using this 2-well representation, the pressure distribution similar to a no-flow boundary is obtained.

Constant pressure boundaries can be represented in a similar way. Again, consider well A is located with a distance L from the constant pressure boundary as shown in Figure 3.4.

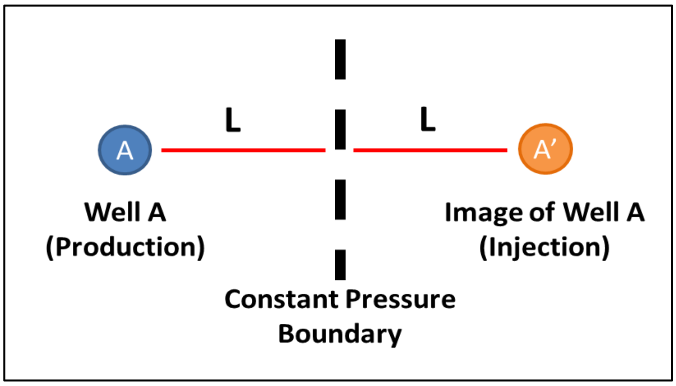

Figure 3.4 : Well near constant pressure boundary.

The mathematical representation of constant pressure boundary is obtained by adding an “image” well having 2L distance from the original well. However this time the image well will be an injection well (i.e. having the same rate).

The superposition principle eases the representation of complex reservoir cases by introducing image wells and forms a series of production and injection wells instead of the boundaries of the reservoir.

Instead of a four-sided reservoir, the line source solution is used for a reservoir bounded by a no-flow boundary from the right and a constant pressure boundary from the left. The producing well is located in the center as shown in Figure 3.5.

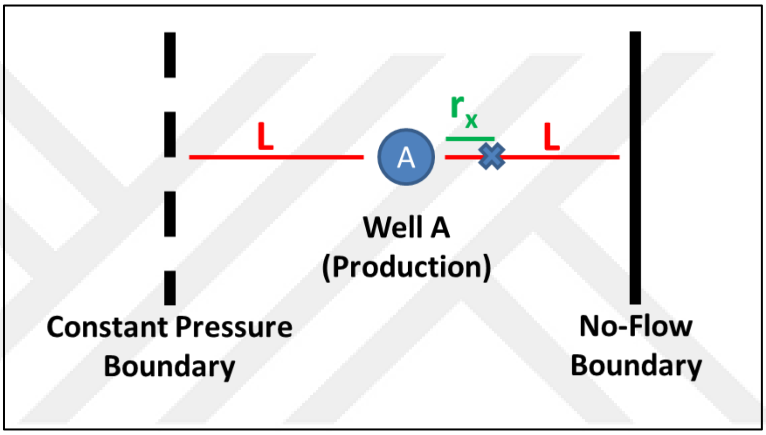

Figure 3.5 : Well and boundaries location in example.

The aim is to determine the pressure drop at point x. As it was explained in the superposition principle, the boundaries shown in the above figure could be represented by inserting image wells into the system. However, these image wells will also have image wells with respect to the boundaries in the system. The second set of image wells will be named as level two image wells. This insertion of the image of the image wells will keep on going infinitely and each set of image wells will be named according to the level of insertion. **Error! Reference source not found.** shows the level two image wells.

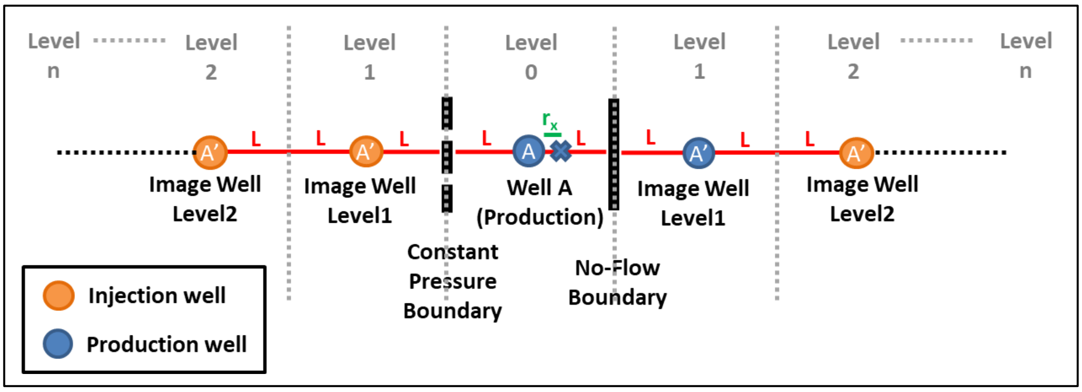

Figure 3.6 : The image well insertion to the system.

Figure 3.6 shows the sequence of the image well insertion. For simplicity the image well insertion sequence is shown in Figure 3.7 with more levels of added wells for distinguishing which wells become producers and which become injectors.

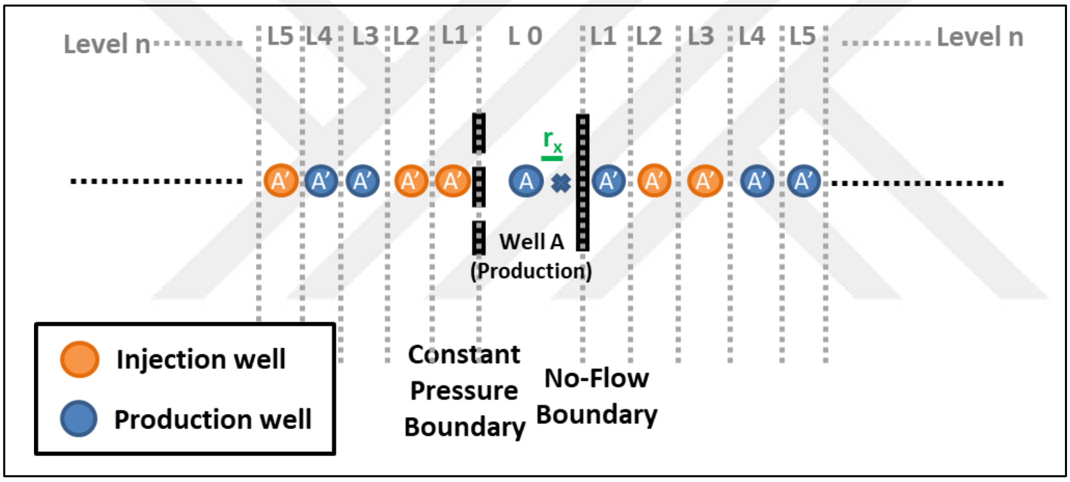

Figure 3.7 : The image well sequence of the system.

Details of the pressure calculation equations for each level of image well insertion and a sample example for this case is shown in Appendix A.

3.3.2 The Larsen method for 2D systems

In Larsen’s (1985) study, the superposition principle is given for 2-Dimensional systems. It introduces a practical way to calculate the pressure difference at a certain point of the reservoir, which has boundaries on four sides.

The basic idea is to add a regular infinite pattern of image wells to the actual well according to the type of boundaries. For example, if each image well is a producer, it means that the reservoir is a closed one. The infinite pattern of image wells is shown in Figure 3.8.

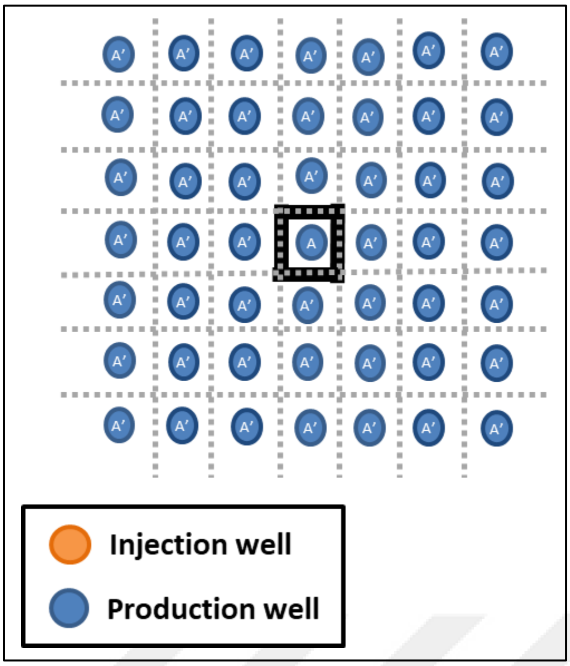

Figure 3.8 : Infinite pattern of image wells.

As in the superposition principle, each image well in the system will have an effect on the pressure drop at a chosen point in the reservoir. Let q_i be the rate of the i^{th} image well in the system above (negative for the injection wells) and $q = q_1 > 0$ is the rate of the actual well, then the dimensionless wellbore pressure drop for the actual well can be calculated by Equation (3.9):

$$\mathrm{p}_{wD}(\mathrm{t}_{DA}) = -\frac{1}{2}\sum_{i=1}^{\infty}\frac{q_i}{q}E_i\left(-\frac{{x_i}^2 + {y_i}^2}{4A\mathrm{t}_{DA}}\right) \tag{3.9}$$

where;

p_{wD} is dimensionless wellbore pressure drop,

t_{DA} is the dimensionless time based on the drainage area,

A is the drainage area,

x_i is x coordinate of the i^{th} image well,

y_i is y coordinate of the i^{th} image well.

In the above equation, it is again assumed that the wells are line source wells and (x_i, y_i) are the location of the i^{th} image well for $i \geq 2$. Also note that ${x_1}^2 + {y_1}^2 = {r_w}^2$.

At an arbitrary point (x_0, y_0) within the drainage area, the dimensionless pressure drop, P_D can be calculated by the Equation (3.10):

$$\mathrm{p}_D(x_0, y_0, \mathrm{t}_{DA}) = -\frac{1}{2}\sum_{i=1}^{\infty}\frac{q_i}{q}E_i\left(-\frac{(x_i - x_0)^2 + (y_i - y_0)^2}{4A\mathrm{t}_{DA}}\right) \tag{3.10}$$

In the above equation $x_1 = y_1 = 0$ and $x_0{}^2 + y_0{}^2 \geq r_w{}^2$. Note that p_{wD} will be obtained if $x_0{}^2 + y_0{}^2 = r_w{}^2$.

In Larsen's paper, two different methods are suggested: hexagonal summation patterns and rectangular summation patterns. For simplicity, only the rectangular summation pattern is taken into consideration. In the rectangular summation, the image wells are placed into rectangular grids as shown in Figure 3.9.

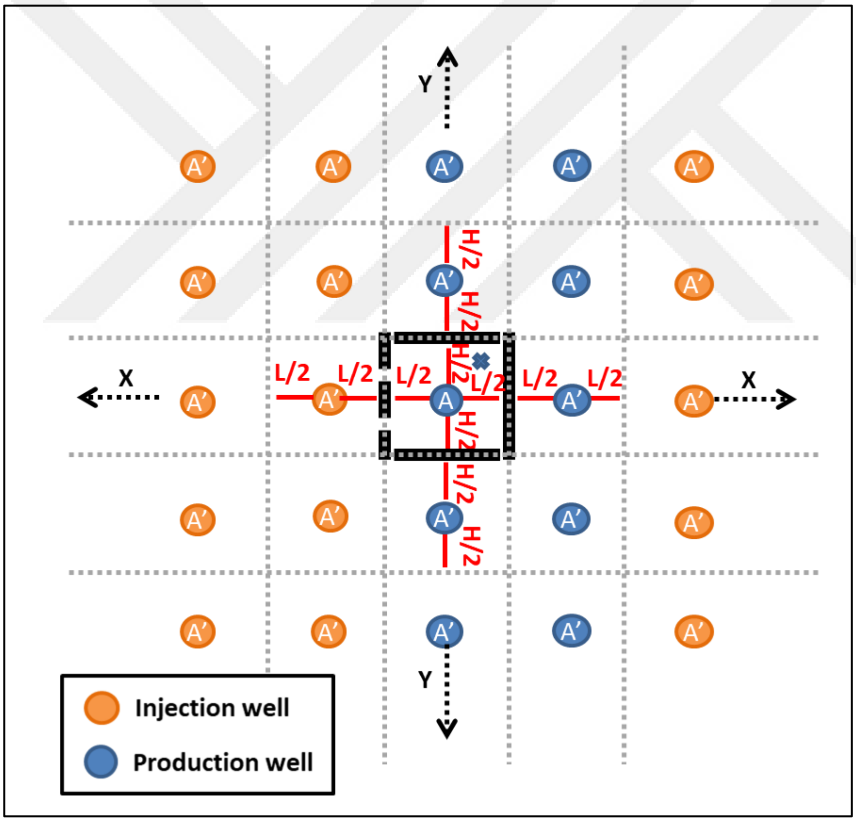

Figure 3.9 : The image well insertion for the rectangular summation pattern.

Consider a system having length L and height H as shown in Figure 3.9. The given shape will have the following ratio:

$$\mathrm{F} = \frac{H}{L} \tag{3.11}$$

The insertion of image wells is carried out by adding n_c number of columns on each side in the direction of X and n_r number of rows on each side in the direction Y. These numbers can be calculated by the following equations.

$$n_c = \text{the integer nearest } \left(1 + 4\sqrt{F t_{DA}}\right) \tag{3.12}$$

$$n_r = \text{the integer nearest } \left(1 + 4\sqrt{t_{DA}/F}\right) \tag{3.13}$$

The above numbers are calculated based on approximations and numerical verifications (Larsen, 1985). Like in the superposition principle, the image well will be injection if there is a constant pressure boundary on the corresponding side of the reservoir, and if there is no-flow boundary the image well will be a production well. Figure 3.10 shows a case where on the west boundary of the reservoir there is a constant pressure boundary and the rest of the boundaries are no-flow.

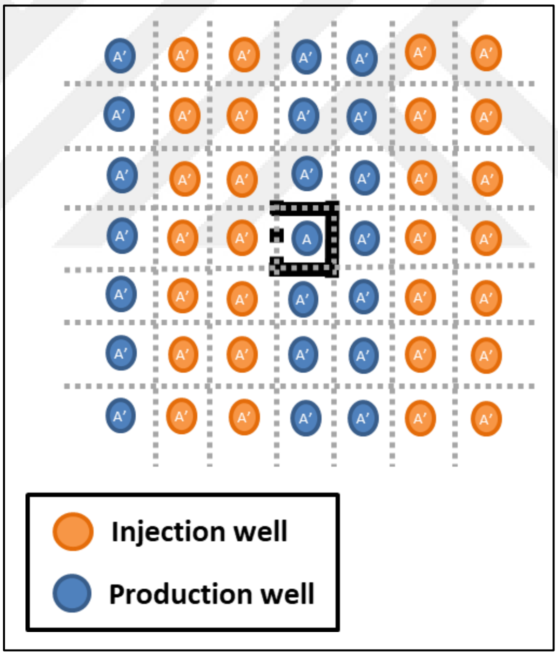

Figure 3.10 : Constant pressure on east and no-flow boundary on rest of the sides.

It is obvious that there is a pattern in the image well insertion and this pattern is modeled in order to validate the results with the numerical model.

3.3.3 Multi well approximation from single well models

In section 3.3.1 and 3.3.2, two different analytical approximations are described for the pressure drop match at a certain point in the reservoir. However, both of the cases give results when there is only one well in the system. In this section, a result for the multi well cases is obtained from single well cases. The logic behind this study is the superposition principle. When a single point is considered, all of the wells have an effect in decreasing the pressure at that point. One may ask if each well is treated separately to determine the single pressure drop for each well and later adding these values to calculate the multi-well pressure drop. This can be explained by the superposition principle applied twice in order to obtain the multi well case results. For this example a three well case is considered as shown in Figure 3.11.

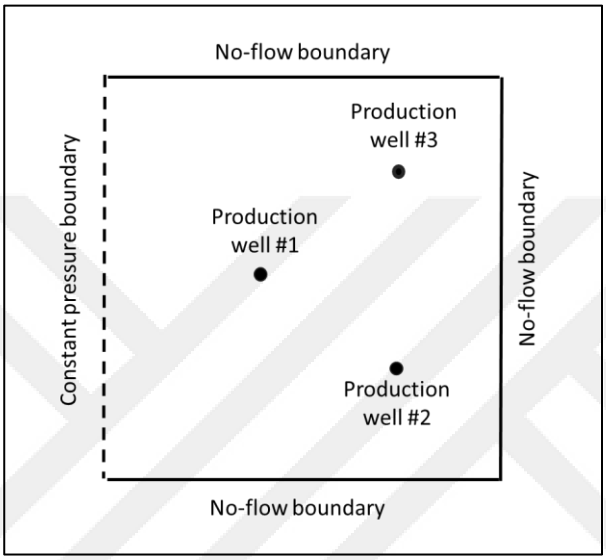

Figure 3.11 : The multi well example with three production wells.

The reservoir is assumed to be single-phase water and temperature changes are neglected. The production scheme for this reservoir lasts for 30 years. The input parameters for this case are shown in Table 3.1.

Table 3.1 : Parameters used in validation example.

Parameter	Value
Number of grids in x and y direction (numerical model)	201 × 201
Grid dimensions in x and y direction, m	49.75
Height of reservoir, m	500
Total length of reservoir in x and y directions, m	10000
Storage capacity of a single grid, kg/bar	5385
Recharge index between grids, kg/bar-s	1
Initial pressure, bar	300
Porosity, fraction	0.1
Total compressibility, 1/bar	4.35×10^{-5}
Density of water, kg/m^3	1000
Viscosity of water, cp	1
Well radius, m	0.091
Production rate of the production wells, kg/s	40

The wells created in the system, are assumed to have no wellbore storage and zero skin factor in order to keep the simplicity of the case. Figure 3.12 shows the final time step pressure drop results for each grid by using the numerical model.

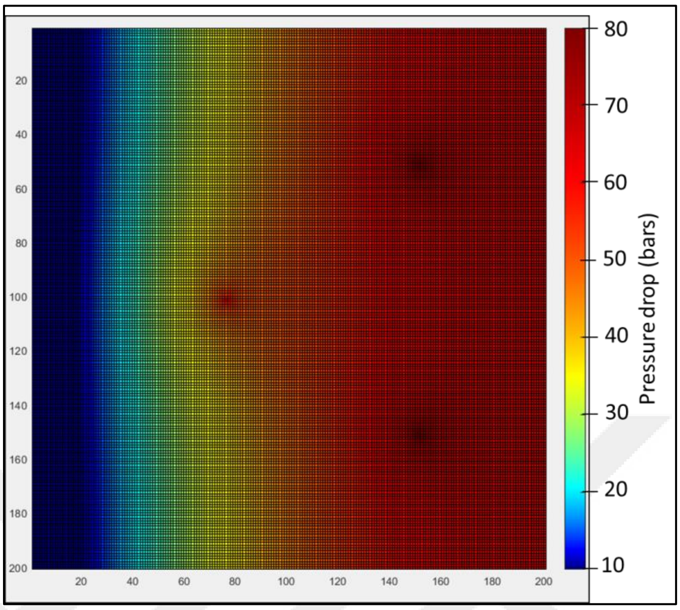

Figure 3.12 : The grid pressure drops at last time step with numerical model (multi-well case).

In the next step, the single well cases are run separately with the Larsen Method and the final time step results are shown in Figure 3.13.

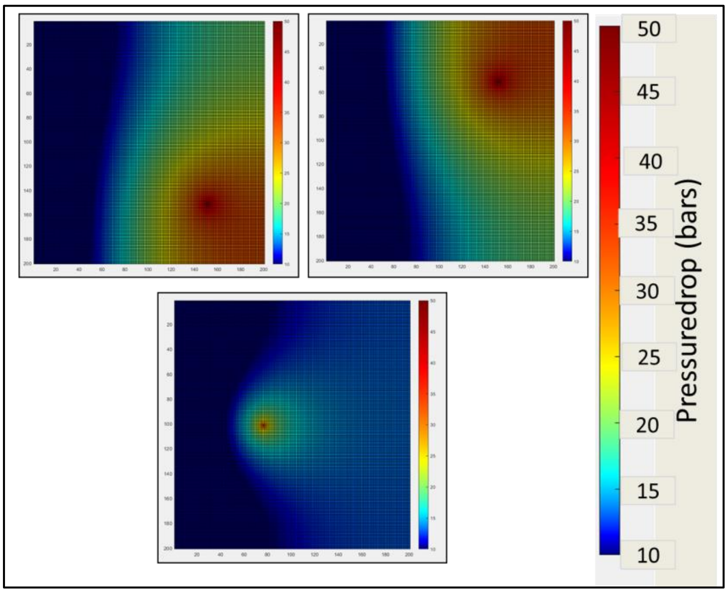

Figure 3.13 : The grid pressure drops at last time step with superposition model (single well cases).

From the last time step graphs, it is not easy to compare the results with the numerical model results. Thus, the summation of pressure drops for each single well case is calculated and the result is shown in Figure 3.14.

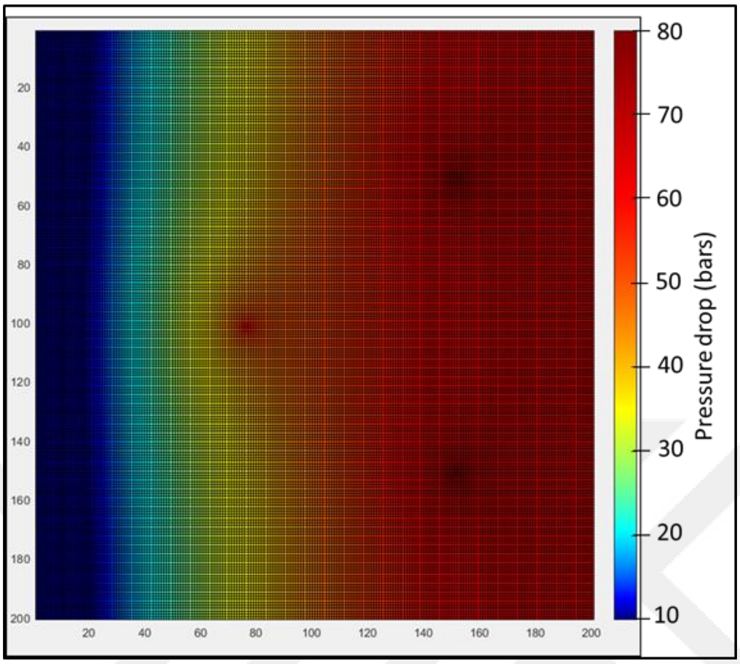

Figure 3.14 : Comparison of the pressures for two methods.

It can easily be seen that both methods give the same answers. In this case, only production wells were present. Further validation of the Larsen method is done with a multi well case where both production and injection well are present in the system. The case which was studied is shown in Figure 3.15.

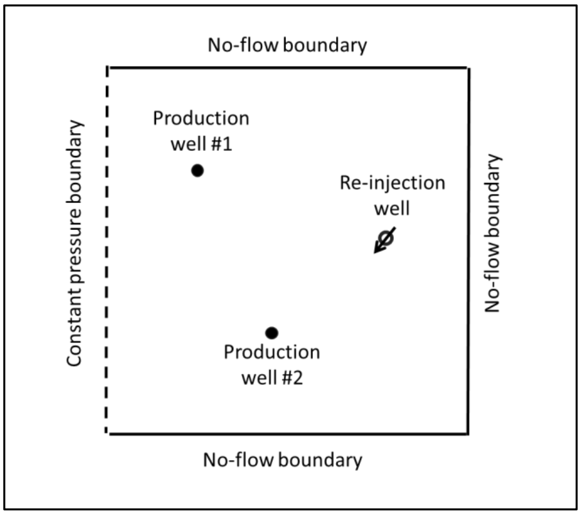

Figure 3.15 : The multi well example with two production and one injection wells.

The production wells are producing with 55 kg/s and also the injection well is injecting with the same amount. For this case, the pressure output of the numerical model and superposition model is compared. By this way validation of superposition model can be done. Figure 3.16 shows the outputs for the two models.

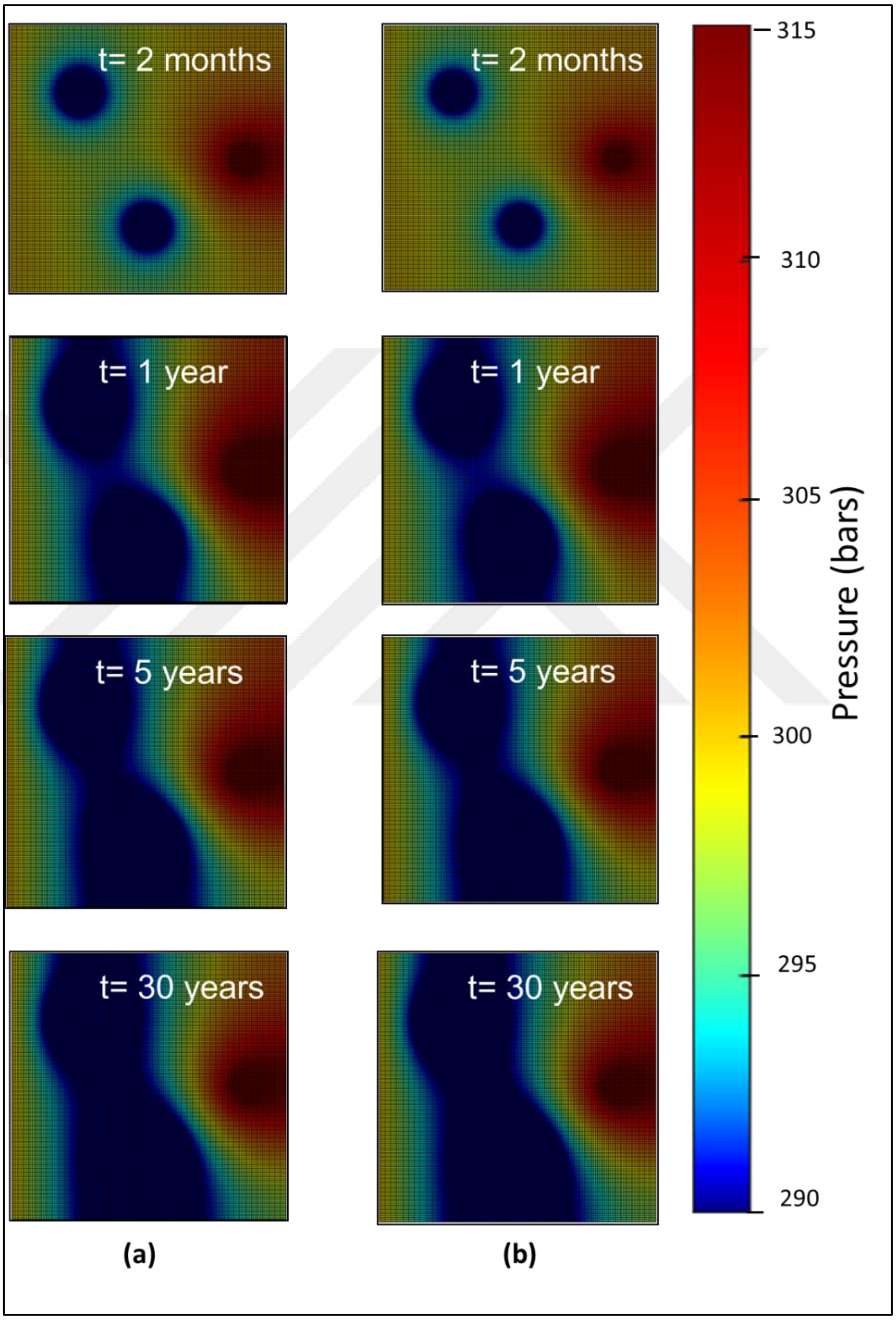

Figure 3.16 : Pressure distribution for various times (a) superposition (b) numerical model.

Figure 3.16 shows a clear result that two model outputs are giving a good match. This result is an important one for the study since for high gridded cases numerical model takes more time to solve than the time needed in the superposition model. In Section 4, various cases are run to identify the best location for the observation well.

3.4 Validation of Numerical and Superposition Models

In this section the validation of the models which are going to be used in the study is presented. In the first part the validation of numerical model is shown, later it is followed by the validation of the superposition method.

3.4.1 Validation of numerical model

A major pitfall that some engineers face is to be sure that generated model is giving correct answers. The accuracy of a numerical model is the most important property and needs to be checked with previously known models, analytical formulas, or softwares that can simulate similar problems. The generated numerical model is checked in two different ways. The first validation is with Sarak et al. (2005) lumped parameter model. The second validation is carried out with well-testing software Ecrin.

3.4.1.1 Validation with analytical formulas

Sarak’s (2004) study gave analytical formulas for certain lumped parameter models. In order to validate the developed numerical model, seven of these lumped parameter models are chosen and the same composition of tanks are generated in the numerical model. The outputs of the lumped parameter model cases and numerical model cases are compared. The chosen models are: one tank open, two tank closed, three tank open, and two reservoir tanks with aquifer models.

For all of the cases, all initial pressure is taken as 30 bar. The flow rates of all the production wells are constant. For the open cases, a recharge source is connected having a storage capacity equal to 1×10^{25} kg/bar. The details of the analytical formulas that was used in this section is given in Appendix B.

Single tank open model

The schematic of the single tank open model can be seen in Figure 3.17.

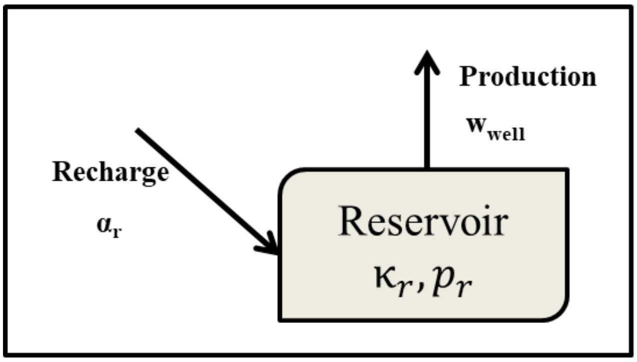

Figure 3.17 : Single tank open model schematic.

In order to calculate the pressure change in lumped parameter model Equation (B.1) is used. The input parameters for the case are tabulated in Table 3.2.

Table 3.2 : Inputs for single tank model**.**

Parameter	Value
κ_r,kg/bar	1.82×10^8
α_r, kg/bar-s	5
w_{well},kg/s C	15

By using the above input parameters both numeric and lumped parameter model case is run. The comparison of the outputs can be seen in Figure 3.18.

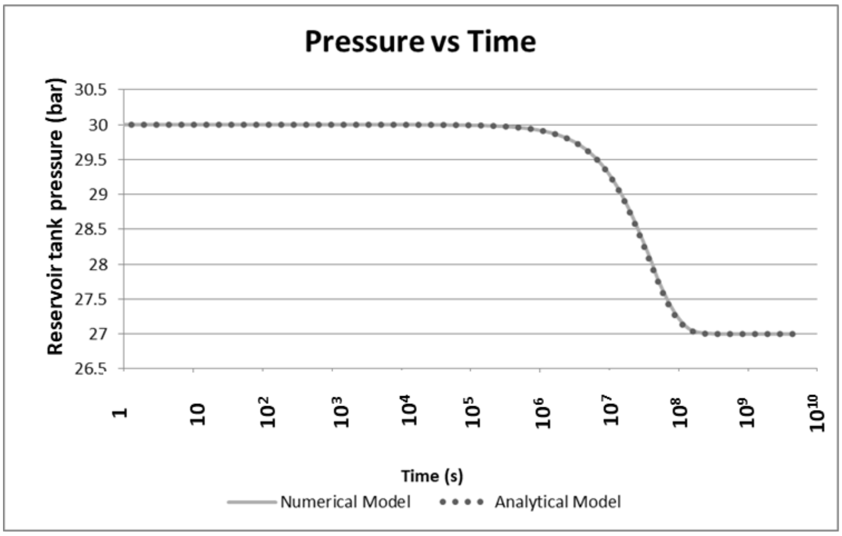

Figure 3.18 : Comparison for single tank open case.

It can easily be seen that both lumped parameter model and numerical model cases are giving similar results.

Two tank closed model

The schematic of two tank closed model can be seen in Figure 3.19.

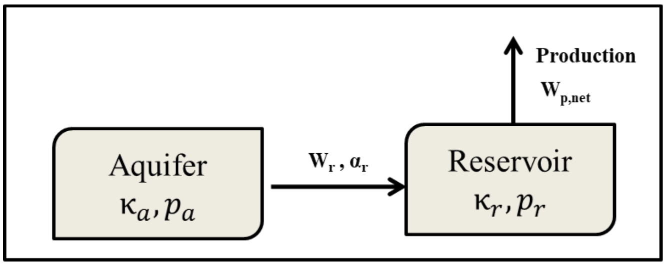

Figure 3.19 : Two tank closed model schematic.

In order to calculate the pressure change in lumped parameter model Equation (B.2) is used. The input parameters for the case are tabulated in Table 3.3.

Table 3.3 : Inputs for Two Tank Closed Model.

Parameter	Value
κ_r,kg/bar	1.82×10^8
α_r, kg/bar-s	5
κ_a,kg/bar	1×10^9
α_a, kg/bar-s	5
$w_{p,net}$,kg/s C	15

By using the above input parameters both numerical and lumped parameter model case is run. The comparison of the outputs can be seen in the Figure 3.20.

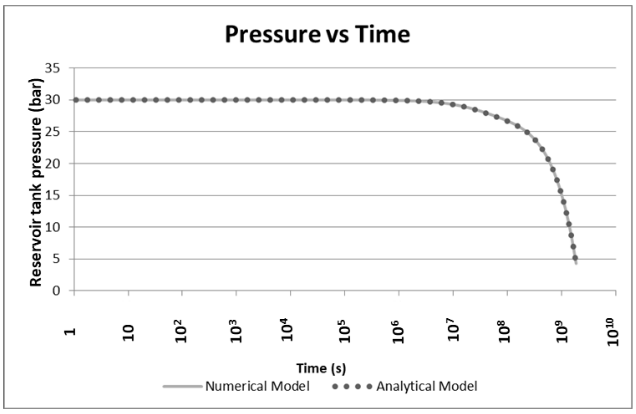

Figure 3.20 : Comparison for two tank closed case.

It can easily be seen that both lumped parameter model and numerical model cases are giving similar results.

Three tank open model

Three tank open system can be shown like in Figure 3.21.

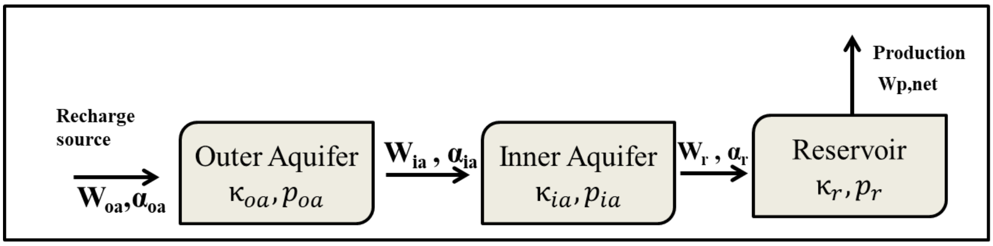

Figure 3.21 : Three tank open model schematic.

In this system, two levels of the aquifer are present in the system. The detail of the analytical formula that is used in this validation is shown in Appendix B. In order to calculate the lumped parameter model pressure change Equation (B.3) is used. The input parameters for the case are shown in Table 3.4.

Table 3.4 : Inputs for Three Tank Open Model.

Parameter	Value
κ_r,kg/bar	1.82×10^8
α_r, kg/bar-s	5
κ_{ia},kg/bar	4×10^8
α_{ia}, kg/bar-s	5
κ_{oa},kg/bar	8×10^8
α_{oa}, kg/bar-s	5
$w_{\mathrm{p,net}}$,kg/s C	15

By using the above input parameters both numerical and lumped parameter model case is run. The comparison of the outputs can be seen in the Figure 3.22.

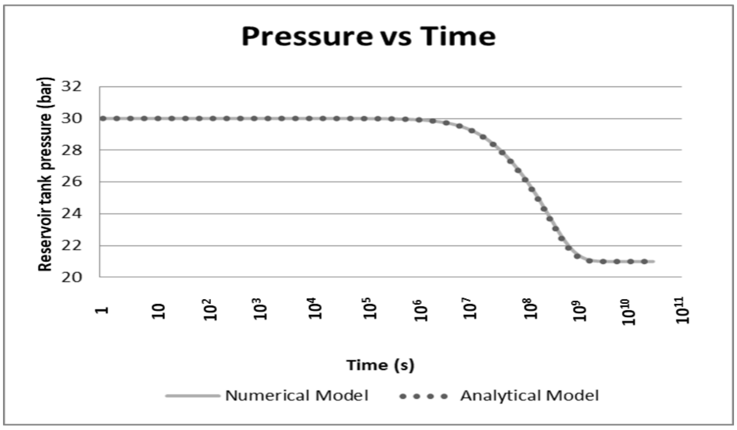

Figure 3.22 : Comparison for three tank open case.

Both numerical model and lumped parameter model give similar results.

Two reservoir tanks with aquifer model

This model is the last of the lumped parameter models that are used to validate the numerical model developed. In Figure 3.23 two reservoir tanks with aquifer model case is shown.

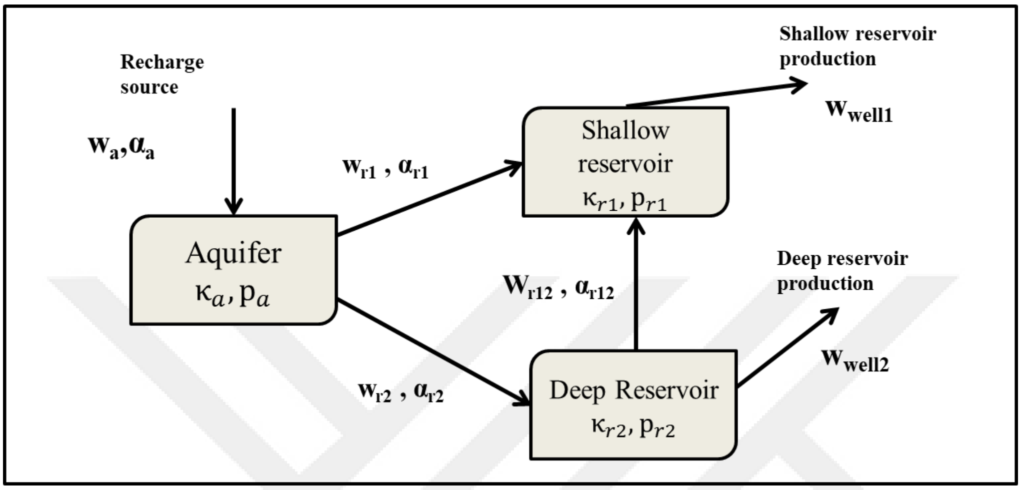

Figure 3.23 : Two reservoir tanks with aquifer model schematic.

The reservoir is composed of two different tanks from which production operation is ongoing. These two reservoir tanks are connected to an aquifer which is also supplied by a big recharge source.

In order to calculate the pressure change in the lumped parameter, model Equations (B.19) and (B.20) are used. The input parameters for the case are tabulated in Table 3.5.

Table 3.5 : Inputs for two reservoir tanks with aquifer model.

Parameter	Value
κ_{r1},kg/bar	1.82×10^8
α_{r1}, kg/bar-s	5
κ_{r2},kg/bar	1.82×10^8
α_{r2}, kg/bar-s	5
κ_a,kg/bar	1×10^9
α_a, kg/bar-s	5
α_{12}, kg/bar-s	5
w_{well1},kg/s C	20
w_{well2},kg/s C	10

The lumped parameter model and numerical model are solved by using the above input parameters. The comparison of the pressure outputs for shallow reservoir can be seen in Figure 3.24.

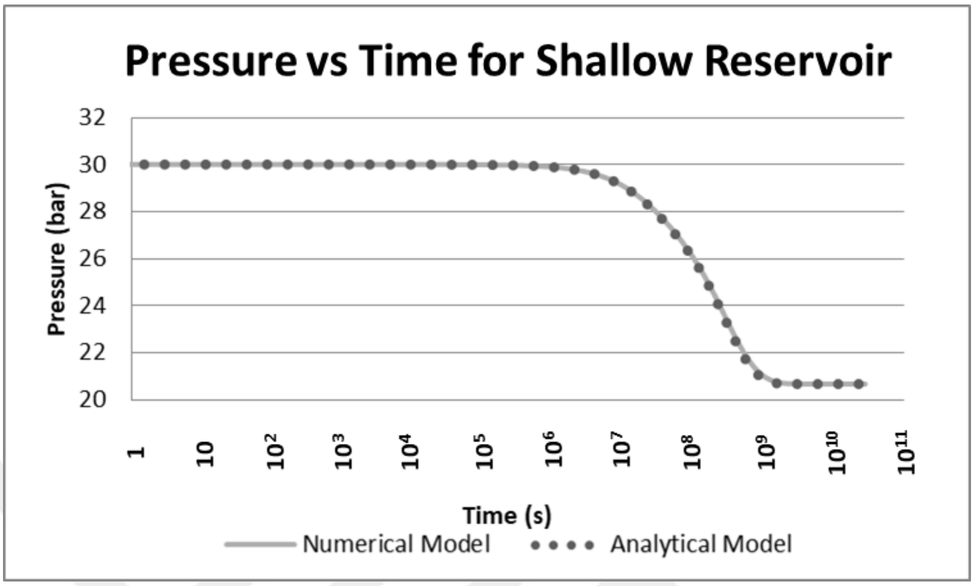

Figure 3.24 : Comparison for two reservoir tank with aquifer: shallow reservoir.

As it can be seen the pressure values for both of the models for the shallow reservoir is similar. The second reservoir tank which is deep reservoir pressure output results are shown in Figure 3.25.

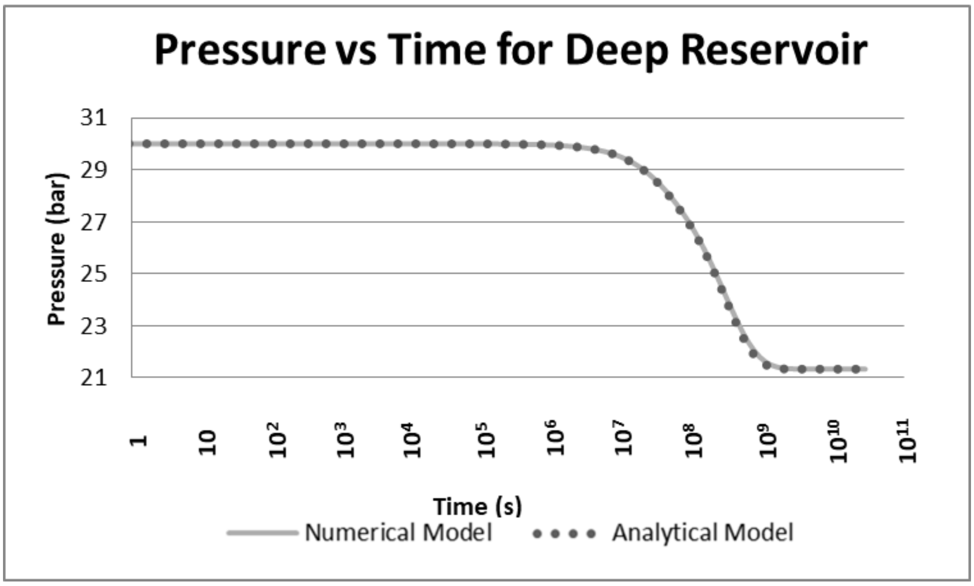

Figure 3.25 : Comparison for two reservoir tank with aquifer: deep reservoir.

It can easily be seen that for the deep reservoir tank, lumped parameter model and numerical model cases are giving similar results again.

Since the developed numerical model is giving similar results for four different lumped parameter model configurations, it can be said that the model is validated with a known analytical expression.

3.4.1.2 Validation with a software

In the previous part of the study validation of the numerical model is made with lumped parameter model that was presented by Sarak (2004). However, the production well’s downhole pressure response was not validated in that section. Thus, in order to honor this validation, the numerical model pressure is compared with Ecrin software’s well test design pressure response.

First of all, the description of the reservoir has to be done clearly. In the numerical model, a 101×101 grid system is generated. The length and the width of the reservoir are taken as 1010m, with a height of 10m. Thus, a grid block will have 10m×10m×10m dimensions. The reservoir is bounded with 4 sealing faults in North, South, East, and West directions. The structure of the reservoir is shown in Figure 3.26.

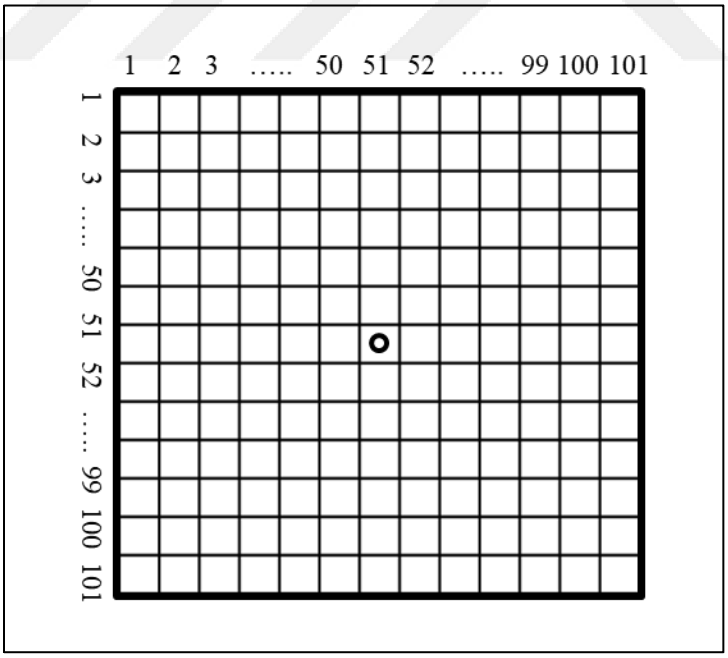

Figure 3.26 : Structure of the reservoir.

In the middle of the reservoir, a production well is placed with a constant production rate which is 0.01 kg/s. All of the grids in the reservoir are identical. The initial pressure of the reservoir grids is 300 bars. The recharge index between the entire grids is taken as 5 kg/bar-s and storage capacities of each grid are taken as 4.3511 kg/bar. The well index between the production well and the grid in the middle of the reservoir is taken as 10 kg/bar-s. Other inputs for the simulation run are tabulated in Table 3.6.

Table 3.6 : Inputs for downhole validation.

Parameter	Value
p_0,bar	300
ϕ, %	10
B,m^3/rm^3	1
μ, cp	1
c_t,1/bar	4.35×10^{-5}
ρ_w, kg/m^3	1000

Well pressure outputs of the numerical model are integrated into the Ecrin software. In the next step the test design tool of the software is used to generate synthetic data for the given reservoir structure. The pressure difference and derivative difference values for numerical model and test design output are shown in Figure 3.27.

Figure 3.27 : Comparison of numerical model output with synthetic software output.

As it can be seen from the figure two graphs are showing a perfect match in responses which means that the numerical model is validated with Ecrin software.

3.4.2 Validation of superposition model

In this subsection the validation of Larsen method with the numerical model is done. The considered reservoir is in 2D, having 201 grids on x direction and 201 grids on y direction with a total of 40401 grids. Each grid is identical, that has a width and a length of 49.75 m. The height of the reservoir is 500 m. The dimensions of the reservoir can be seen in Figure 3.28.

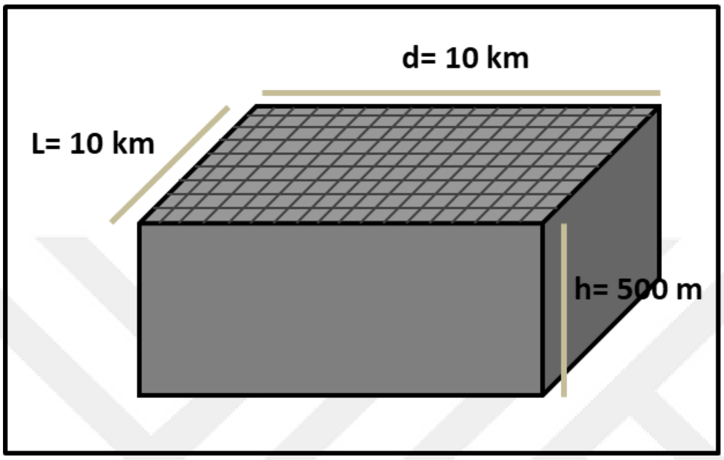

Figure 3.28 : The dimensions of the reservoir.

The storage capacity of a grid is 5384.93 kg/bar and the recharge indexes between the grids are the same which is 1 kg/bar-s. The initial pressure for each grid is 300 bars and for the wells created in the system, they are assumed to have no wellbore storage and skin factor for the simplicity of the case. The parameters that are used in the example are shown in Table 3.7.

Table 3.7 : Parameters used in the example**.**

Parameter	Value
Number of grids in x and y direction (numerical model)	201 × 201
Grid dimensions in x and y direction, m	49.75
Height of reservoir, m	500
Total length of the reservoir in x and y directions, m	10000
Storage capacity of a single grid, kg/bar	5385
Recharge index between grids, kg/bar-s	1
Initial pressure, bar	300
Porosity, fraction	0.1
Total compressibility, 1/bar	4.35×10^{-5}
Density of water, kg/m^3	1000
Viscosity of water, cp	1
Well radius, m	0.091
Production rate of the production wells, kg/s	110

In this case a production well is placed into the center of the reservoir. From the west side of the reservoir a constant pressure boundary is connected as shown in Figure 3.29.

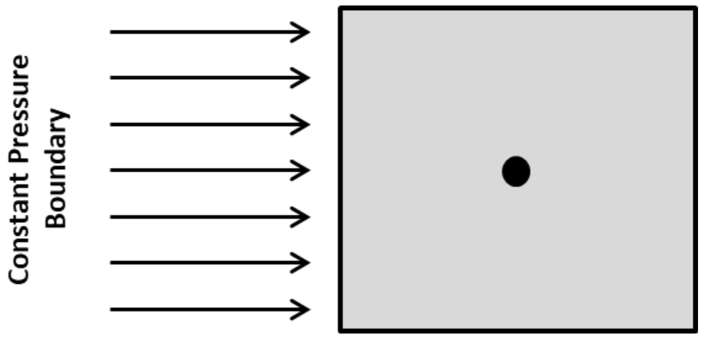

Figure 3.29 : Reservoir scheme for validation case.

After 10 years of production the pressure output for the given case for the numerical model and superposition model can be obtained as in Figure 3.30.

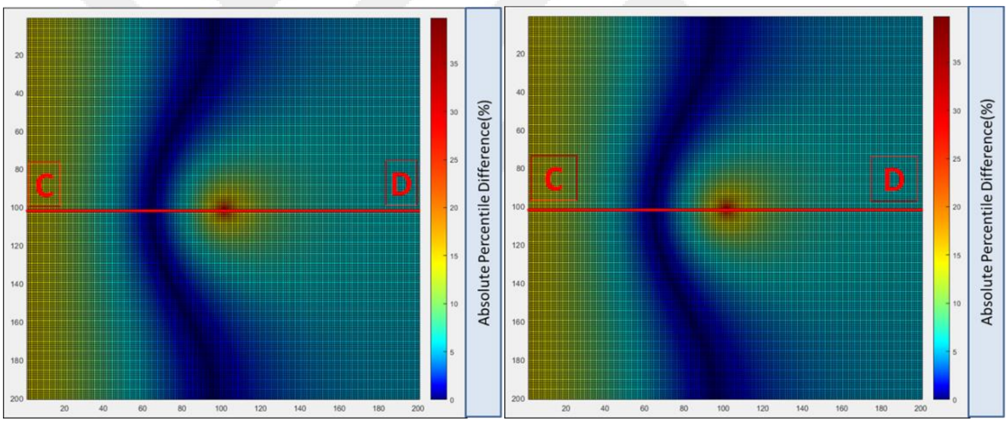

Figure 3.30 : Pressure outputs of (a) superposition model (b) numerical model.

In Figure 3.30, on the left hand side the pressure output for superposition model and on right hand side the numerical model pressure outputs can be seen. It can easily be understood that both schemes give similar output. The pressure outputs among C-D line are investigated separately as shown in Figure 3.31.

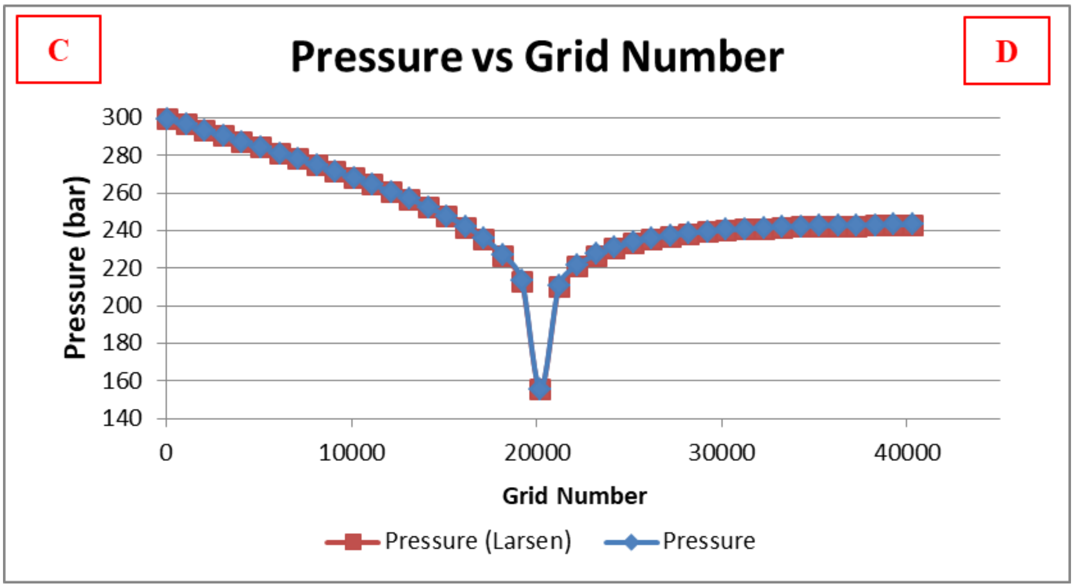

Figure 3.31 : Comparisons of the superposition and numerical model pressures among C-D line.

It can be seen that Larsen's method gives similar results with the numerical model results, which validates the superposition method.

4. BEHAVIOR OF AVERAGE PRESSURE IN RESERVOIR

In this chapter various cases are studied in order to understand the behavior of the regions of average reservoir pressure. By this way determining the best possible location for the observation well in the field is targeted. In the following examples, the hints for the correct observation well location are sought.

4.1 Behavior of the Volumetric Average Reservoir Pressure

In this section, the change in lumped parameter model parameters which are recharge index and storage capacity is investigated. Consider a system composed of a recharge source and a reservoir as shown in Figure 4.1.

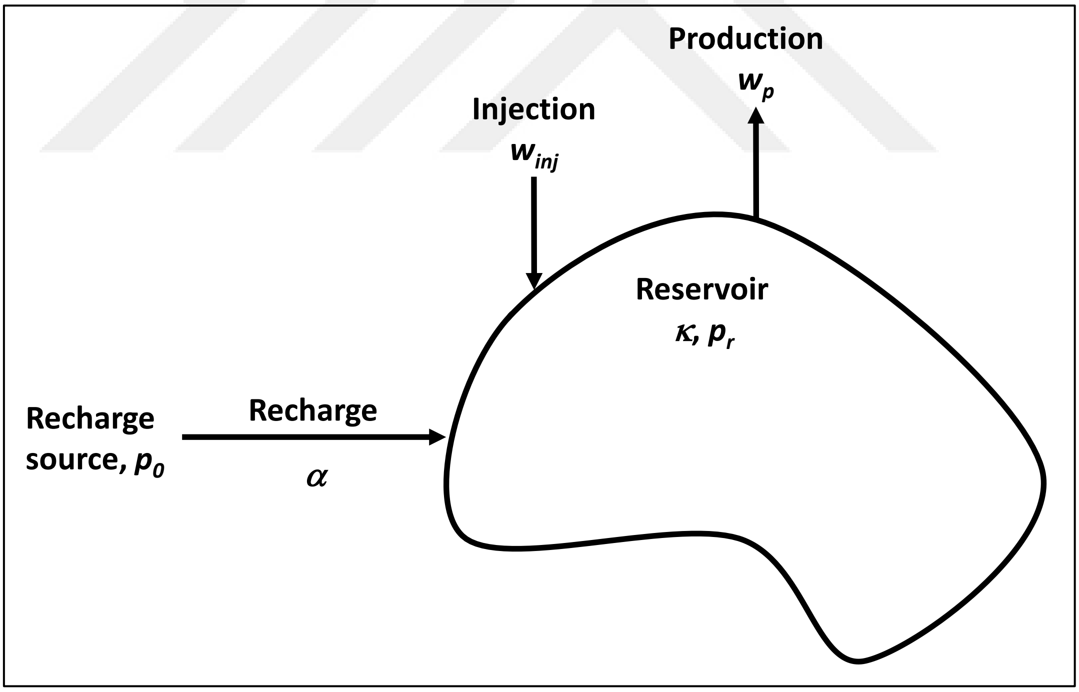

Figure 4.1 : Schematic of a lumped parameter model connected to a recharge source.

In the first step of the example, the change in average reservoir pressure match affected by the change in storage capacity and recharge index is examined. For the reservoir composition given in Figure 4.1 a synthetic example is generated with the input parameters given in Table 4.1.

Table 4.1 : Base case input parameters.

Parameter	Value
Storage capacity of the reservoir, kg/bar	1.0×10^8
Recharge index, kg/bar-s	2
Initial pressure, bar	300
Net production rate from the reservoir, kg/s	110

It is assumed that the system is isothermal and the reservoir is filled with single-phase slightly compressible water. The net production from the reservoir is 100 kg/s and the initial pressure of the system is assumed to be 300 bars.

The storage capacity will be the first parameter to be investigated. Figure 4.2 is showing the average reservoir pressure response with varying storage capacity.

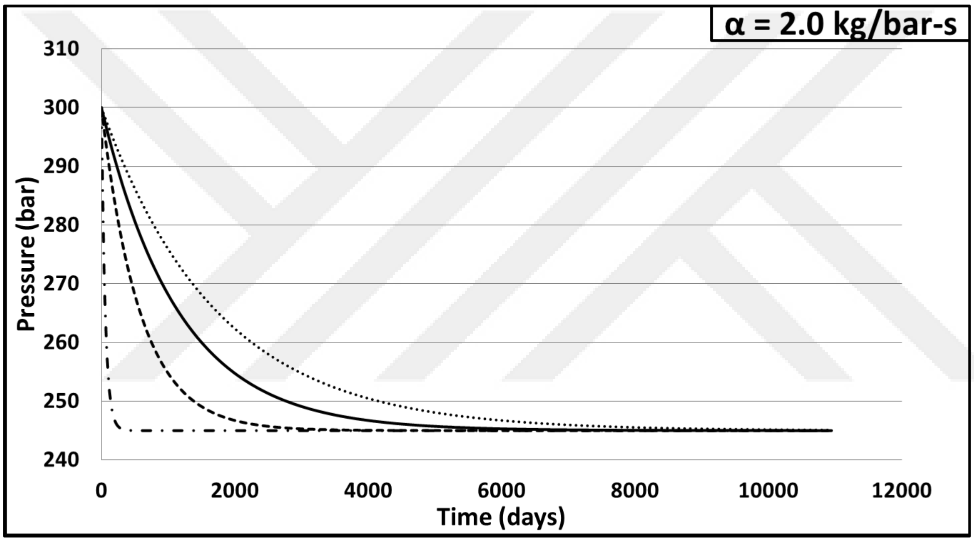

Figure 4.2 : Pressure responses for different storage capacities.

As it can be seen from Figure 4.2 the change in storage capacity has a great effect on the pressure responses. For the case that has the storage capacity value of 1×10^7 kg/bar, there is a sharp decline when production first starts. This sharp decline represents the period where transient flow is dominant. It can also be seen that the pressure line becomes flat when the steady-state period has been reached. Steady-state is reached since there is a recharge source connected to the reservoir that supplies water during the steady-state period. It was previously shown that for a system as shown in Figure 4.1, the pressure relation is given by Equation (B.1). The relationship of the average reservoir pressure (during the steady state flow) to the model parameters may be obtained by taking the limit of Equation (B.1) as time goes to infinity. The resulting formula is shown in Equation (4.1):

$$\Delta p_{ss} = \frac{w_{p,net}}{\alpha} \tag{4.1}$$

where the steady-state is shown with ss subscript. This equation clearly indicates that the steady-state pressure of the case is independent of time and depending only on two parameters which are the recharge index and the net flow rate from the reservoir. This is the main reason for each (case shown in Figure 4.2) reaching the same pressure value during steady-state period. The only change in these responses is the time when each case reaches steady state. Thus, it can be clearly said that storage capacity controls the steady-state time. Higher storage capacity leads to delayed time to reach the steady-state.

The second parameter that is going to be investigated is the recharge index. Figure 4.3 shows the pressure response of different cases for varying recharge indices.

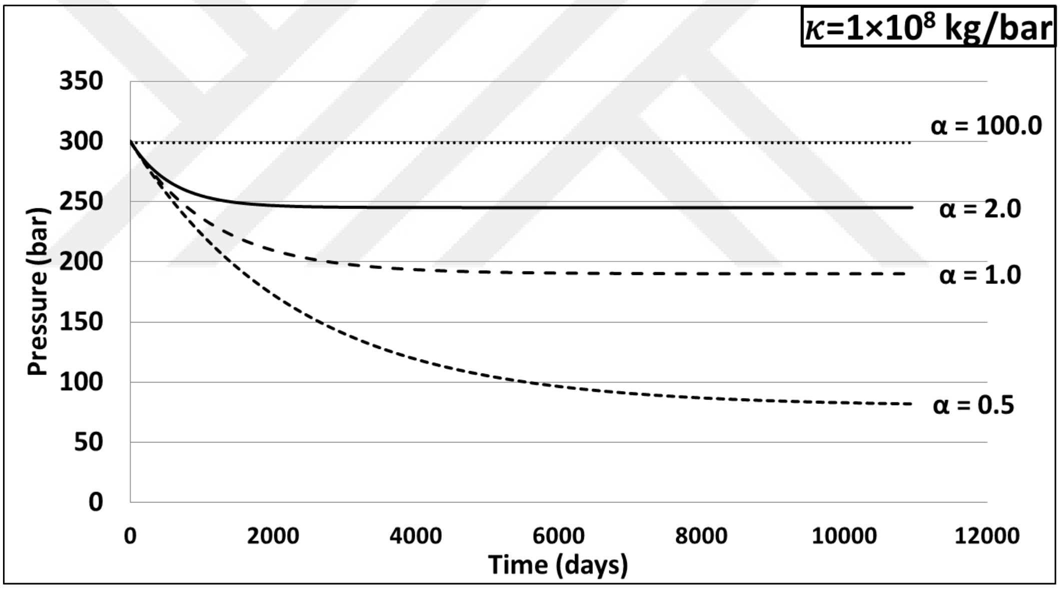

Figure 4.3 : Pressure responses for different recharge indices.

Storage capacity used for the above case is 1×10^8 kg/bar. It is known from the previous case that in the initial stages, transient period is dominant in pressure responses. It is clearly understood from Figure 4.3 that the steady-state pressures are different for each case. This is also explained in Equation (B.1) in which recharge index values control the value that the average reservoir pressure reaches during steady-state period. The greater the recharge index is, the higher the steady-state pressure values. In other words, high recharge index means higher pressure support from the recharge source and lower pressure drop during steady-state.

In the last part of the case, the change in the average reservoir pressure region with varying times is investigated. The numerical model that was explained in the previous chapter is used in order to identify the region where average reservoir pressure can be observed. The input parameters for the case are shown in Table 4.1. The schematic of the reservoir is also shown in Figure 2.2 (without the observation well). The map of the difference between the average reservoir pressure and each grid pressure is illustrated at various times as shown in Figure 4.4.

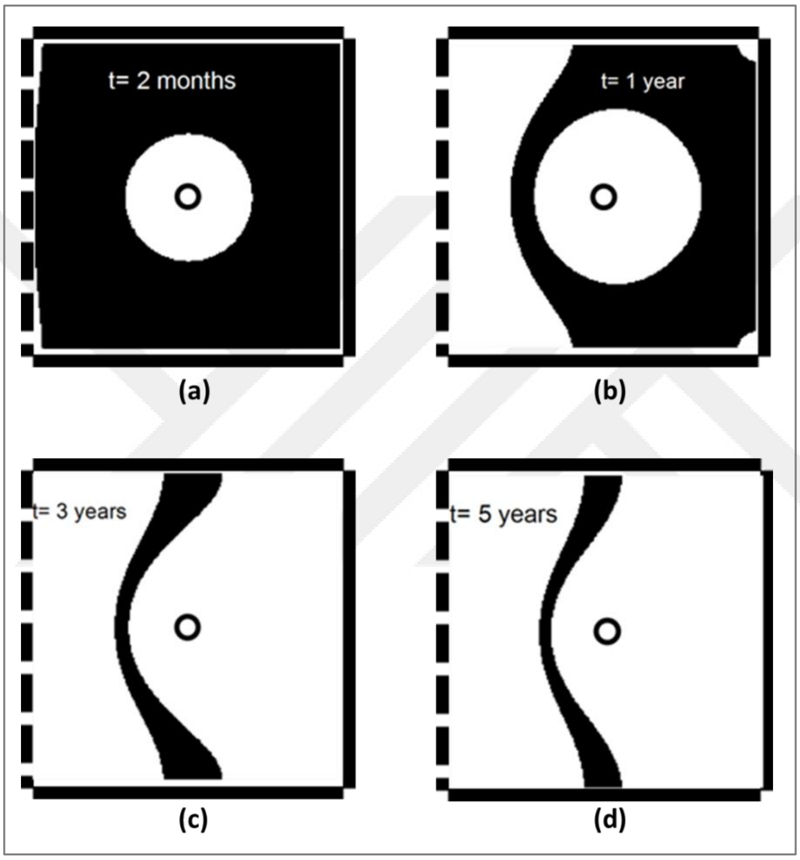

Figure 4.4 : The progression of the region that represents the volumetric average reservoir pressure for various times; (a) at the end of two months, (b) at the end of one year, (c) at the end of three years, (d) at the end of five years.

The dashed line represents the constant pressure boundary whereas solid lines represent the no-flow boundaries. The percentile difference of average reservoir pressure and grid pressure is calculated by using Equation 4.2.

$$\varphi_i = \left|\frac{p_i(t) - p_r(t)}{p_r(t)}\right| \times 100 \tag{4.2}$$

where φ_i represents the absolute percentile difference of the i^{th} grid pressure $p_i(t)$ with the average reservoir pressure $p_r(t)$ at time t.

In Figure 4.4, the dark region shows the places where average reservoir pressure can be seen. In other words, the grids in this region have the closest value to the average reservoir pressure with the smallest percentile difference values (where the dark region is the region where the absolute percentile difference is less than 1%). In early times, it can be seen that the dark region is formed away from the production well and the radial geometry of the region is changed slowly. This geometry change is mainly caused by the asymmetric placement of the boundaries of the system. Only one side of the reservoir is connected to the constant pressure boundary as shown in Figure 2.2. As the reservoir reaches the steady-state, the dark region tends to stabilize at some certain region. No matter how much time passes by, the region of volumetric average reservoir pressure becomes concave somewhere between the constant pressure boundary and the production point.

The reason for selecting 1% absolute difference will be explained at this point. In Figure 4.5 the output schemes for less than 0.5%, 1%, and 2% absolute percentile differences are shown. From Figure 4.5a and Figure 4.5d, the dark region formed between the well and the constant pressure boundary is rather thin whereas in Figure 4.5c and Figure 4.5f thicker dark region is observed when compared with the 1% difference outputs. Since 1% percentile difference gives acceptable results, throughout the study 1% percentile absolute percentile difference is used.

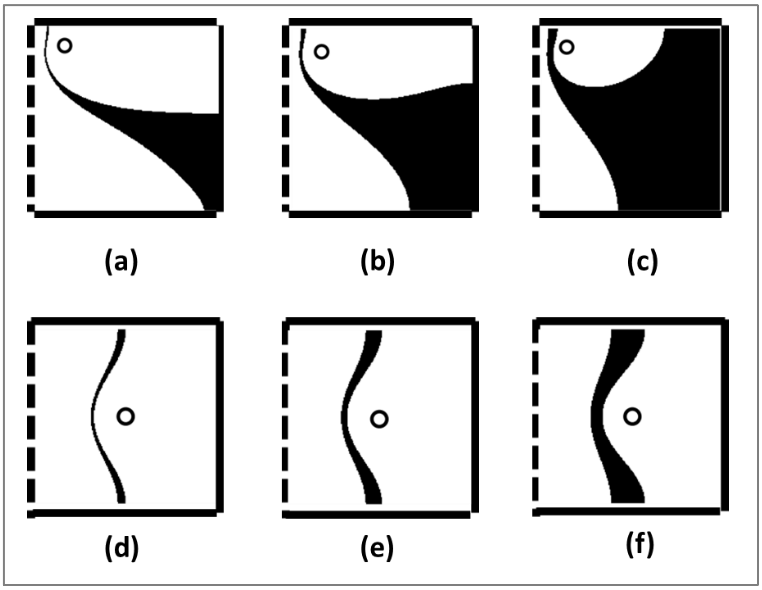

Figure 4.5 : Various outputs for different absolute percentile difference upper bound; (a) & (d) 0.5%, (b) & (e) 1%, (c) & (f) 2%.

4.2 Analysis of Observation Well Location in Future Predictions

In this example, several cases are presented for the observation well location selections for different reservoir compositions. In the first example, a detailed illustration for the calculation of average reservoir pressure will be shown. For each of these cases, the models that are generated by the formulas shown in this chapter are used. The calculations that are shown in this example will be considered when the steady-state flow condition is achieved in the reservoir.

At the end of each case, a region for possible locations of observation well is determined. In order to do this, the absolute percentile difference of each grid with the average reservoir pressure of that time step is calculated. Grids that have smaller percentile differences give the best place for the observation well location. Similarly, an increase in the value indicates a worse location for an observation well.

The considered reservoir is 2D, with 201 grids on x-direction and 201 grids on y-direction with a total of 40401 grids. Each grid is identical, which has a width and a length of 49.75 m. The height of the reservoir is 500 m. The dimensions of the reservoir can be seen in Figure 4.6.

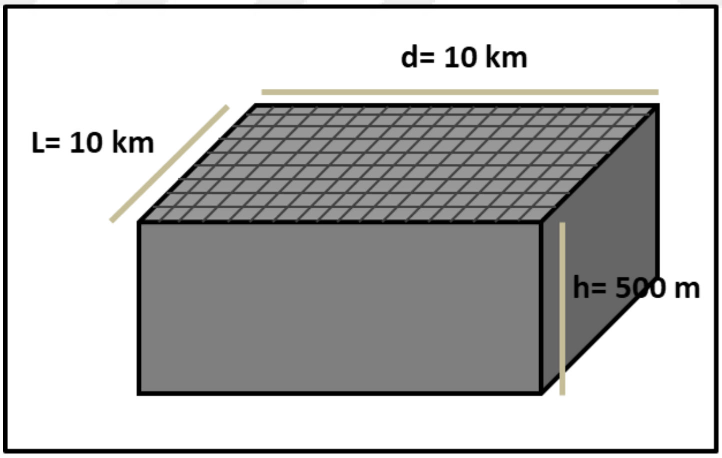

Figure 4.6 : The dimensions of the reservoir.

The storage capacity of a grid is 5384.93 kg/bar and the recharge indexes between the grids are constant, 1 kg/bar-s. The initial pressure for each grid is 300 bars. The wells created in the system, they are assumed to have no wellbore storage and skin factor for the sake of simplicity. The parameters that are used in the example are shown in Table 4.2.

Table 4.2 : Parameters used in the example**.**

Parameter	Value
Number of grids in x and y direction (numerical model)	201 × 201
Grid dimensions in x and y direction, m	49.75
Height of reservoir, m	500
Total length of the reservoir in x and y directions, m	10000
Storage capacity of a single grid, kg/bar	5385
Recharge index between grids, kg/bar-s	1
Initial pressure, bar	300
Porosity, fraction	0.1
Total compressibility, 1/bar	4.35×10^{-5}
Density of water, kg/m^3	1000
Viscosity of water, cp	1
Well radius, m	0.091
Production rate of the production wells, kg/s	110

4.2.1 One production well in the southeast and constant pressure boundary in the west

In this case, a system shown in Figure 4.6 with the parameters shown in Table 4.2, with a well located in the southeast part of the reservoir is considered. Also, there is a constant pressure boundary on the west part of the reservoir which is shown in Figure 4.7.

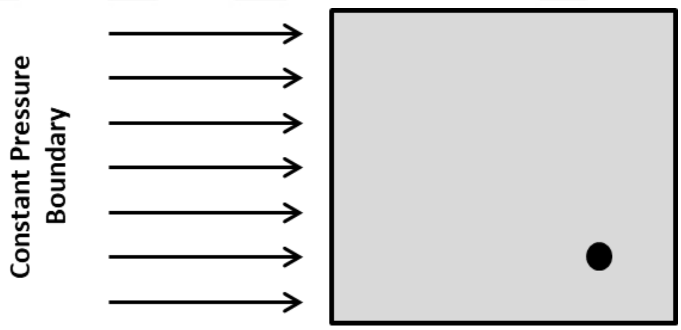

Figure 4.7 : Schematic for the case having one well in southeast and a constant pressure boundary on west.

After 10 years of production, the absolute percentile difference of the pressures for each grid with the average reservoir pressure is shown in Figure 4.8.

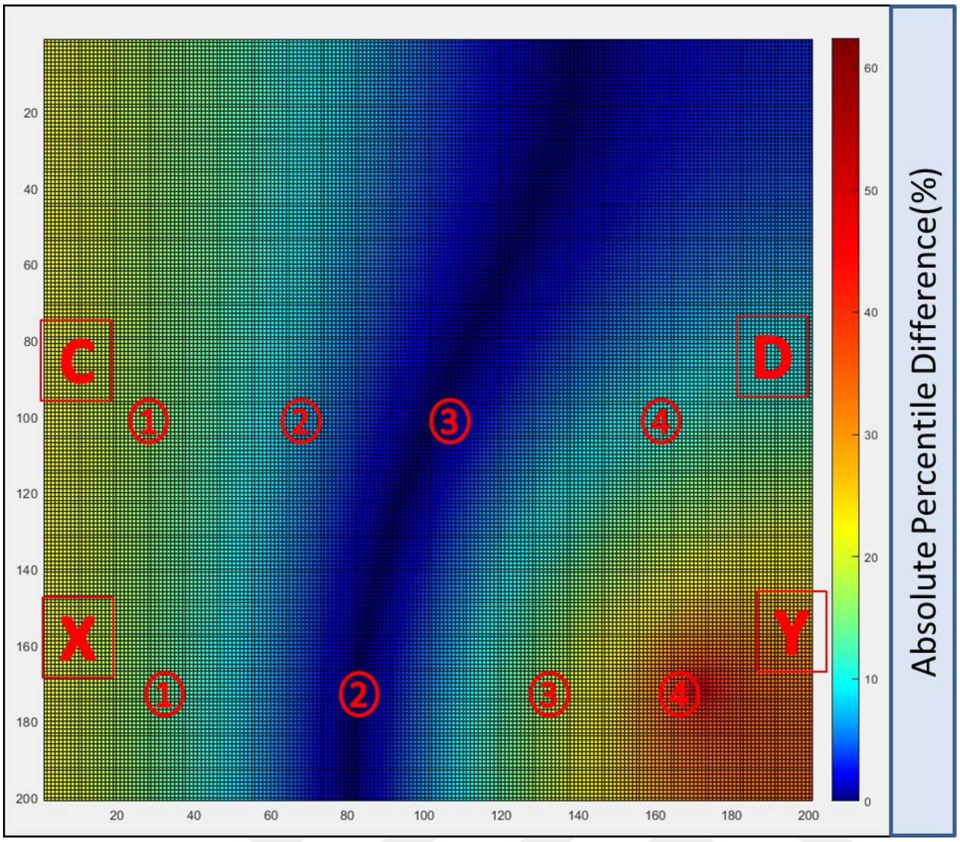

Figure 4.8 : Absolute percentile difference output and the points chosen among the two lines for the case having one well in southeast and a constant pressure boundary on west.

From Figure 4.8, it can be seen that a dark blue region is generated where the average reservoir pressure can be observed after 10 years of production. The red locations also indicate the locations where grid pressure is deviating most. A blue-red scale is used to shown the absolute percentile difference output. From this figure two separate lines are taken and four observation well locations are chosen. A systematic analysis is done to understand the behavior of observation well location on prediction of storage capacity and recharge index in order to be used in lumped parameter models. The results will be shown for each line separately.

Line C-D

Along the C-D Line, 4 points are chosen. The inverse model which was generated is used and the lumped parameter model parameters are matched based on pressure data observed from these points. The matched tank model parameters are shown in Table 4.3.

Table 4.3 : Comparison of arbitrary points along line C-D for the case having one well in southeast and a constant pressure boundary on west.

Observation Points	Grid	Storage Capacity (kg/bar)	Recharge Index (kg/bar-s)
Match to true average pressure		1.9×10^8	2.021
1	5126	9.51×10^8	7.100
2	13166	3.60×10^8	2.864
3	19196	2.36×10^8	2.030
4	35276	1.25×10^8	1.312

After matching the recharge index and storage capacity for the lumped parameter model, a prediction run is done in order to understand the performance of these four observation well locations. The pressure prediction performances of the above chosen 4 points together with the average reservoir pressure observation are shown in Figure 4.9.

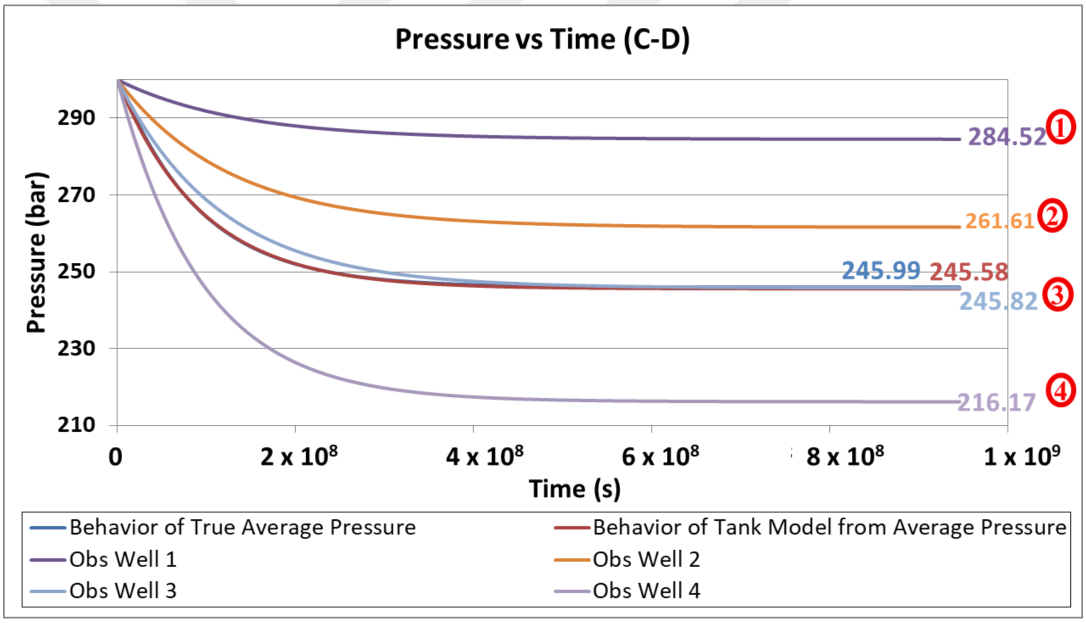

Figure 4.9 : Pressure matches for 4 points chosen from line C-D for the case having one well in southeast and a constant pressure boundary on west.

The best performing observation point is the 3rd one which also has the closest match in the recharge index. The rest of the points have worse performance in the pressure prediction. It is also important to note that 3rd point is the only observation well location placed on the dark blue region.

Line X-Y

Similar to C-D line, 4 arbitrary observation well locations are chosen along line X-Y. The matched tank model parameters for single tank open lumped parameter model are shown in Table 4.4.

Table 4.4 : Comparison of arbitrary points along line X-Y for the case having one well in southeast and a constant pressure boundary on west.

Observation Points	Grid	Storage Capacity (kg/bar)	Recharge Index (kg/bar-s)
Match to true average pressure		1.9×10^9	2.021
1	6201	5.67×10^8	5.400
2	16251	1.85×10^8	2.052
3	30321	5.35×10^7	0.988
4	40371	4.31×10^7	0.862

The pressure prediction performances of the above chosen 4 points together with the average reservoir pressure observation are shown in Figure 4.10.

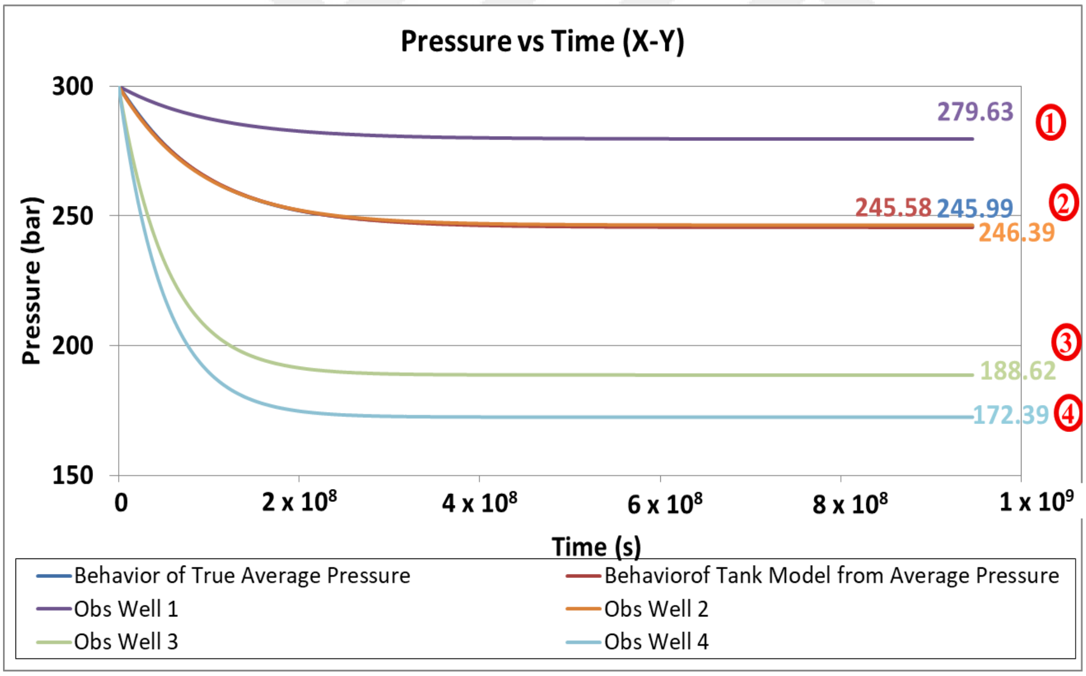

Figure 4.10 : Pressure matches for 4 points chosen from line X-Y for the case having one well in southeast and a constant pressure boundary on west.

As it can be seen matching to the history of the 2nd observation well location gives the best prediction, which has the best match for recharge index and storage capacity. It is also important to note that this point is again located on the dark blue region. The other points are not giving accurate pressure predictions.

4.2.2 One production well in middle and constant pressure boundary in the west

In this case, there is a production well located in the center of the reservoir. The production rate of this well is constant, 110 kg/s for the entire production campaign (10 years). There is a constant pressure boundary connected to the left side of the reservoir as shown in Figure 4.11.

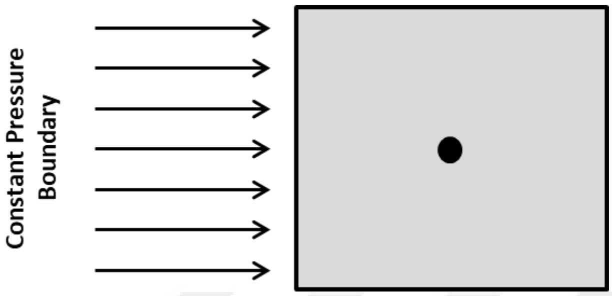

Figure 4.11 : Schematic for the case having one well in center and a constant pressure boundary on west.

The input parameters of the example are the same as the previous one and are shown in Table 4.2. After 10 years of production, Figure 4.12 shows the absolute percentile difference results for the example.

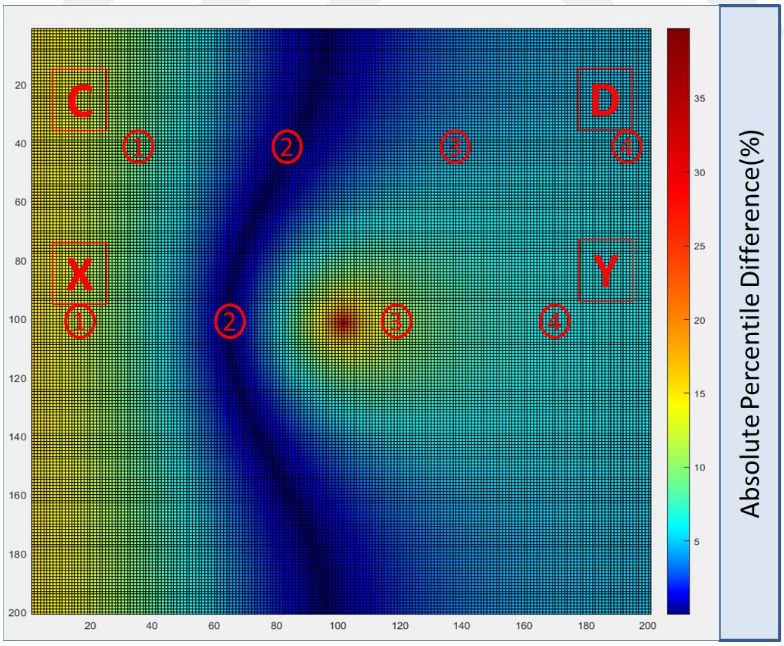

Figure 4.12 : Absolute percentile difference output and the points chosen among the two lines for the case having one well in center and a constant pressure boundary on west.

The dark blue region indicates the location where the average reservoir pressure is observed. A systematic analysis is conducted to understand the behavior of observation well location on prediction of storage capacity and recharge index in order to use in lumped parameter models. Along these two lines 4 different points are chosen and the results are shown for each line separately.

Line C-D

For the 4 points selected along the C-D line, the observed pressures are used to predict the recharge index and storage capacity with the help of the nonlinear optimization model. The matched tank model parameters for single tank open lumped parameter model are shown in Table 4.5.

Table 4.5 : Comparison of arbitrary points along line C-D for the case having one well in center and a constant pressure boundary on west.

Observation Points	Grid	Storage Capacity (kg/bar)	Recharge Index (kg/bar-s)
Match to true average pressure		2.30×10^8	2.667
1	5056	7.00×10^8	8.255
2	18121	2.30×10^8	2.615
3	30181	2.16×10^8	2.005
4	40231	2.27×10^8	1.906

By using the above matched parameters for the 4 grids prediction runs were made for 20 years more and the results are shown in Figure 4.13.

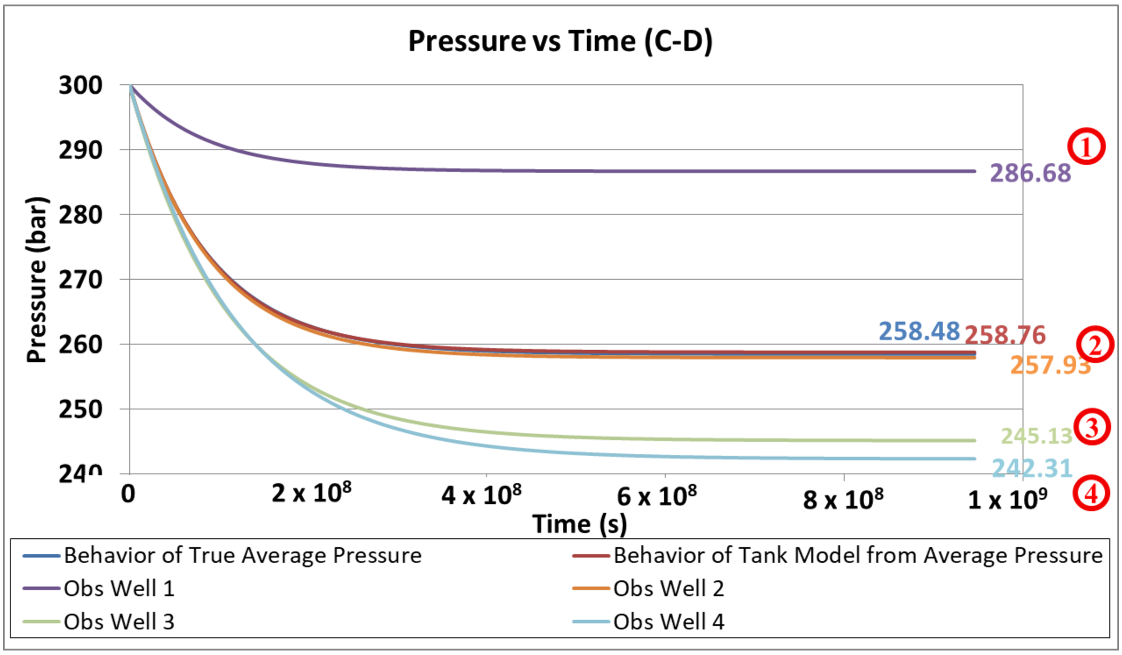

Figure 4.13 : Pressure matches for 4 points chosen from line C-D for the case having one well in center and a constant pressure boundary on west.

The above pressure predictions show that the best prediction run is done with matching to the history of observation well at point 2 which is located in the dark blue region. It was an expected result since the recharge index and storage capacity index matches are the best among the other grids on line C-D. However, the other pressure predictions show great differences from the average reservoir pressure matched tank model parameter predictions.

Line X-Y

Similar to C-D line, 4 arbitrary points are chosen and their performances are obtained. The matched tank model parameters for single tank open lumped parameter model are shown in Table 4.6.

Table 4.6 : Comparison of arbitrary points along line X-Y for the case having one well in center and a constant pressure boundary on west.

Observation Points	Grid	Storage Capacity (kg/bar)	Recharge Index (kg/bar-s)
Match to true average pressure		2.30×10^8	2.667
1	101	4.33×10^9	219.520
2	13166	2.18×10^8	2.686
3	25226	1.08×10^8	1.743
4	35276	1.93×10^8	1.868

20 year long prediction runs for the above given matched parameters are done and results are given in Figure 4.14.

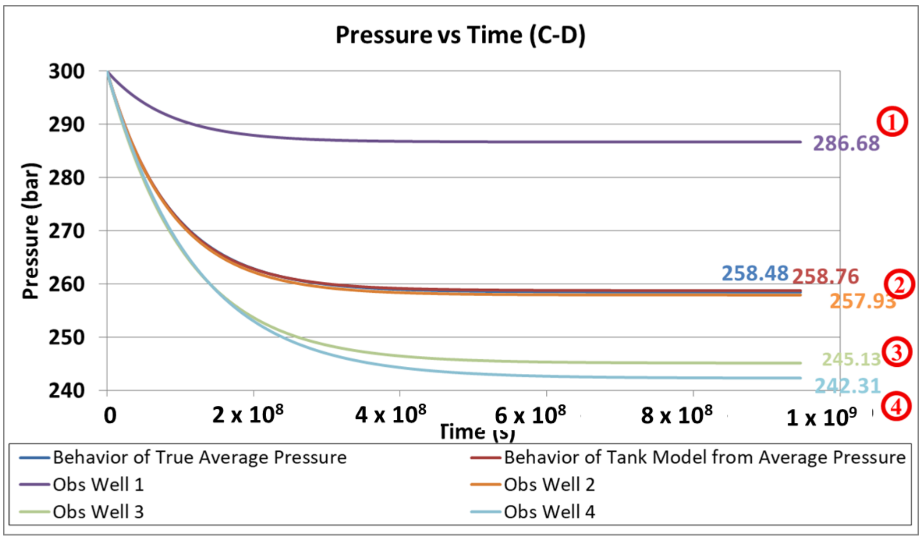

Figure 4.14 : Pressure matches for 4 points chosen from line X-Y for the case having one well in center and a constant pressure boundary on west.

The best prediction made by matching to the history of the 2nd observation well location also has the best match for the tank model parameters. It is also important to underline that observation well location is located on the dark blue region in Figure 4.12. The remaining points do not give a good prediction.

These two examples show that the best location for the observation well is the place where the dark blue region is located. When a grid from the dark blue region is chosen both recharge index and storage capacity values give reasonable estimates, which can be used in prediction runs. It is also important to underline that the grids located next to constant pressure boundary and production wells will not give good storage capacity and recharge index matches. It can easily be seen from Figure 4.12 and Figure 4.8, the grids in the vicinity of the production well and the constant pressure boundaries give great differences with average reservoir pressure value. Even the grids not located on the dark blue region and far away from interference effects give a pressure difference value between 5% and 15%. The observation wells chosen from this region cannot give reliable pressure predictions, which means that only the grids located in the dark blue region should be considered for the observation well location selection. In the upcoming parts of the study, for the sake of simplicity, the color output of absolute percentile difference graphs (i.e. Figure 4.12) are replaced with the black and white graphs (i.e. Figure 4.5e), in which the dark blue region is shown as the black region with 1% absolute percentile difference. Knowing that in the white region, the absolute percentile difference values are different and the pressure values are not same, the observation wells located on the black region give an acceptable pressure prediction. Thus, in the remaining part of the study, the black region is aimed to be located.

4.3 Effects of Different Boundary Conditions and Location of Production/ Reinjection Wells on Average Reservoir Pressure Location

The following examples aim to determine the best location for observation wells with varying boundary conditions and production/reinjection scenarios. It was previously shown that as the production starts the transient period takes over and dominates the pressure response for the reservoir. However after a certain amount of time passes and if there is a constant pressure boundary connected to the reservoir, the reservoir reaches the steady-state period and pressure response of the reservoir becomes static. In this study, the reservoirs that are in the steady-state period are taken into account which means the dark region shown for the absolute percentile difference outputs will remain the same. The main reason for this simplicity is that transient flow period is dependent on many different parameters. Furthermore it should be noted that transient periods may end rather quickly.

In this example, ten different cases are studied which are:

- Reservoir having one production well and a constant pressure boundary from west side.
- Reservoir with one production well and constant pressure boundaries from two sides.
- Reservoir with one production well and constant pressure boundaries from three sides.
- Reservoir with one production well and constant pressure boundaries from all four directions.
- Reservoir with one production well, one reinjection well and constant pressure boundaries from west.
- Reservoir with one production well, two reinjection wells and no-flow boundaries from all four directions.
- Reservoir with two production wells, one reinjection well and no-flow boundaries from all four directions.
- Reservoir with one production well, two reinjection wells and constant pressure boundary from west.
- Reservoir with one production well, two reinjection wells and constant pressure boundaries from all four directions.
- Reservoir with a fault.

In most cases only one production well is present in the system. It should be noted that this well can be considered to represent a region of multiple production wells. Again in the same logic, one injection well shown in the case can be considered as a region where injection wells are gathered. This means that the results obtained in this section are not representing the cases that have only one well but also representing the cases where production or injection wells are concentrated.

In most of the real life cases, the recharge source is connected to either one side or two sides of the reservoir. In other words, cases such as constant pressure boundary are connected on one side (west side) or connected on two sides (south and west side) are the ones that are most likely to be observed in geothermal fields. However, that does not mean that cases with a connection on three or four sides are not useful. The other cases are provided to illustrate what could happen if such cases had been present. At this point, it is important to mention that in the studied cases, the recharge sources are considered to be connected from the sides of the reservoir. For the sake of simplicity, the cases where the recharge sources are connected from below are not studied. There is nearly infinite number of well placement cases possible in a reservoir; however the studied cases are the ones that are most likely to occur.

The reservoirs presented in all cases are formed of 201×201 identical grids. The initial pressure for each grid is 300 bars. The wells assumed to have no wellbore storage and zero skin factor in order to keep the simplicity. The wells produce with 110 kg/s and the reinjection rate is 70% which means that 77 kg/s is reinjected. However, there are some cases where varying reinjection rate is used. The remaining input parameters are shown in Table 3.1. It is also important to note that in all the figures presented in this example, the solid line represents the no-flow boundary whereas the dashed line means that there is a constant pressure boundary connected to the reservoir from that side. As shown in the previous chapter example, the absolute percentile difference used for all cases is 1%. The dark region represents the location where the average reservoir pressure can be observed. Thus it should be considered as the best location for placement of an observation well.

4.3.1 Reservoir with one production well and constant pressure boundary from the west side

In this case, a constant pressure boundary is connected to the reservoir from the west side and the remaining boundaries are no-flow boundaries. For various production well locations, the steady-state absolute percentile difference outputs can be seen in Figure 4.15.

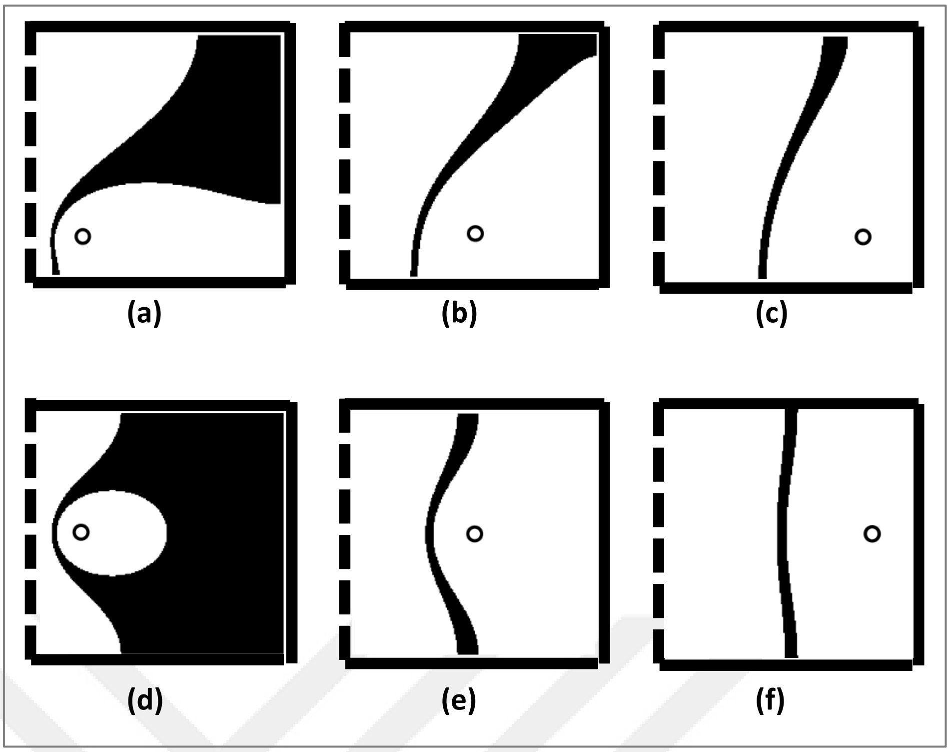

Figure 4.15 : Absolute percentile difference output for the cases having constant pressure boundary on west side and a production well.

From Figure 4.15, it can be seen that the dark region is formed between the production well and the constant pressure boundary for all cases. In the neighborhood of production well, the pressures tend to be lower. The pressures of the grids near to the constant pressure boundary are higher, thus the placement of dark region between these two points is the best option. When the production region comes closer to the boundary, the dark region can be seen in two different places. For the cases shown in Figure 4.15a and Figure 4.15d, the second location where the dark region is observed is between the production region and the closed boundary. If the production well is placed further away from the constant pressure boundary and closer to the no-flow boundary, the dark region has a limited region between the production region and the constant pressure boundary (compare Figure 4.15d and Figure 4.15f). The dark region area tends to decrease, as the production well is located further away from the constant pressure boundary. This case shows that the best possible location for an observation well should be between the constant pressure boundary and production region.

4.3.2 Reservoir with one production well and constant pressure boundaries from two sides

In this case, the constant pressure boundary is connected to the reservoir from the south and west sides. For various production well locations, the steady-state absolute percentile difference outputs are given in Figure 4.16.

This case gives similar results to the previous case. The black region is formed between the production region and the constant pressure boundaries and only the shape of the region changes between these two cases. Figure 4.16e shows an arc shaped dark region around the production well which is located in the center of the reservoir. This arc is located between the production region and constant pressure boundaries. For the cases where the production region is located closer to the constant pressure boundaries (Figure 4.16d, Figure 4.16g, Figure 4.16h), a second location for the average reservoir pressure which is located in the opposite part of the constant pressure boundary can be seen.

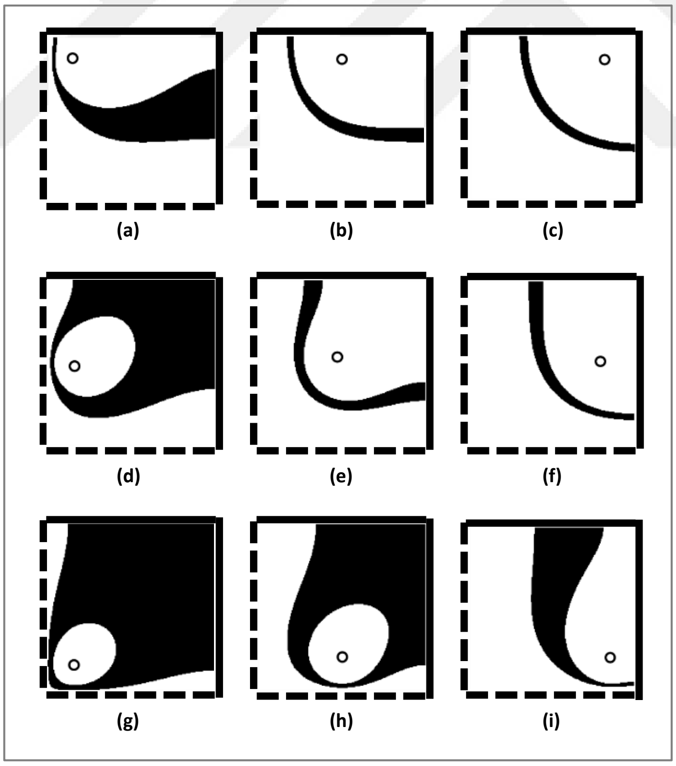

Figure 4.16 : Absolute percentile difference output for the cases having constant pressure boundary on west and south sides and a production well.

Cases which has constant pressure boundary in the east and west part of the reservoir are also studied and results are shown in Figure 4.17.

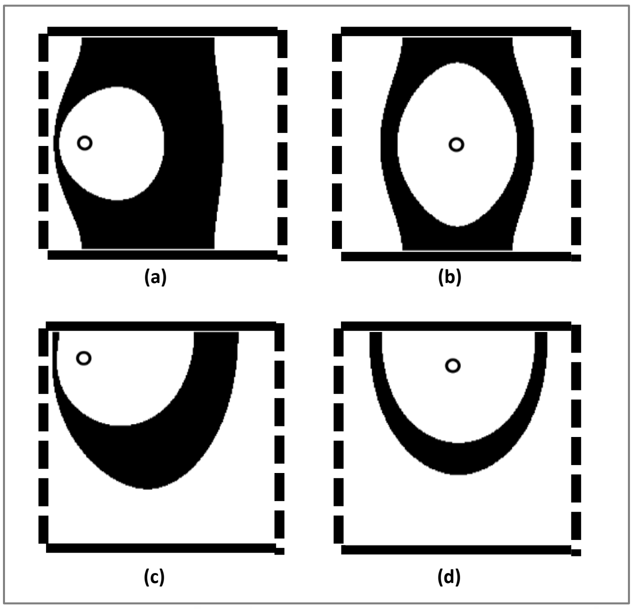

Figure 4.17 : Absolute percentile difference output for the cases having constant pressure boundary on west and east sides and a production well.

It can easily be observed that the dark region is located between constant pressure boundaries and the production region. Furthermore, it can be said that when the production region is located in the center of the reservoir (Figure 4.17a and Figure 4.17b) the dark region can be seen on all sides of the production well. As the production well moves closer to the no-flow boundaries (Figure 4.17c and Figure 4.17d), an arc shaped dark region can be observed around the production region. Lastly, if the production location moves closer to one of the constant pressure boundaries, a thicker dark region is formed between the production region and the farther constant pressure boundary.

4.3.3 Reservoir with one production well and constant pressure boundaries from three sides

In this case, the constant pressure boundary is connected from the south, east and west sides to the reservoir. For various production well locations, the steady-state absolute percentile difference outputs can be seen in Figure 4.18.

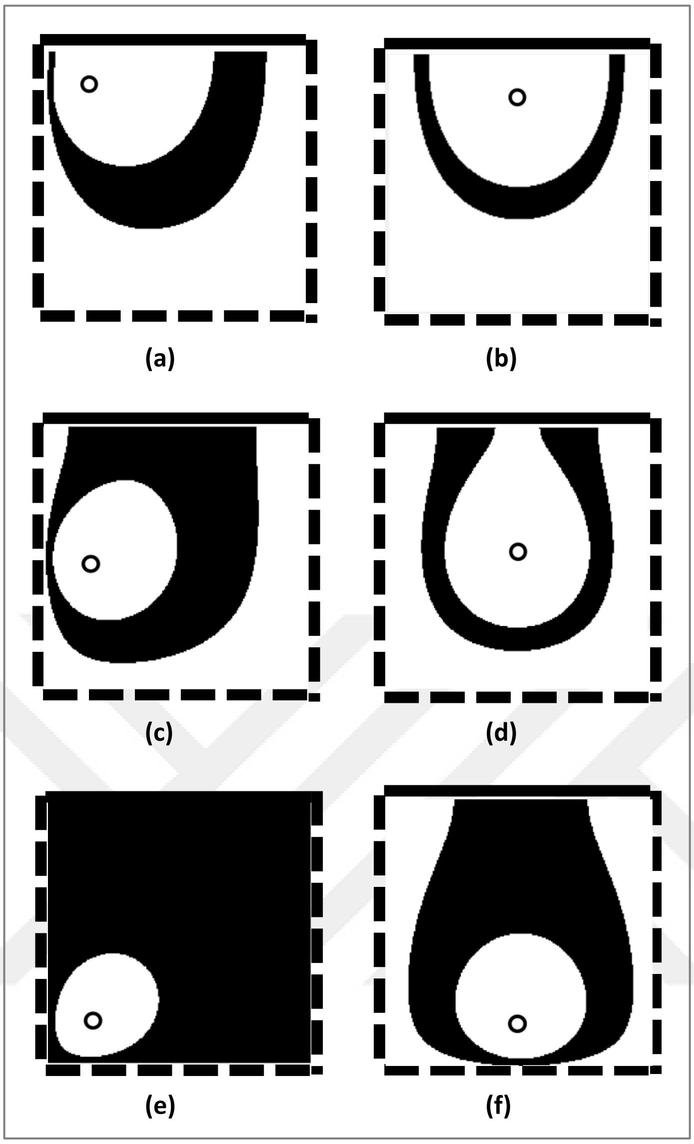

Figure 4.18 : Absolute percentile difference output for the cases having constant pressure boundary on west, east and south sides and a production well.

Similar to previous cases, if an observation well is going to be placed in the reservoir, it should be located in between the production well and one of the constant pressure boundaries. For the cases where the production well is located near one or two of the constant pressure boundaries, a dark region is formed at the opposite side of the constant pressure boundary that the production well is close to.

4.3.4 Reservoir with one production well and constant pressure boundaries on all sides

In Figure 4.19 various cases are shown for the case with constant pressure boundaries on all sides. Again it is important to note that the production well in the system is producing with 110 kg/s.

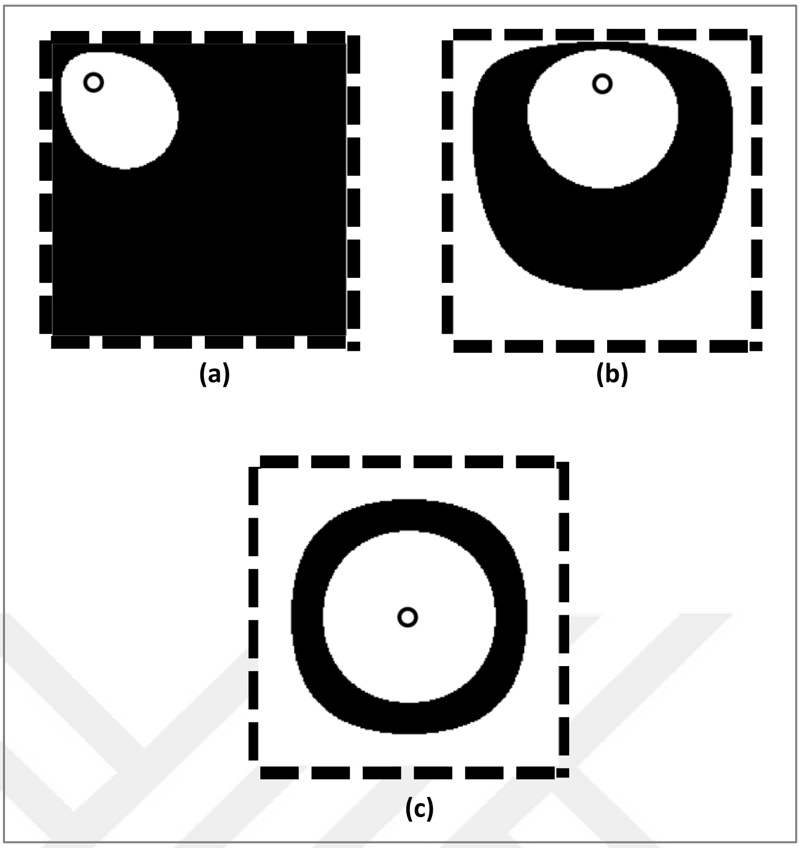

Figure 4.19 : Absolute percentile difference output for the cases having constant pressure boundary on all sides and a production well.

For this case (Figure 4.19c) where the well is located in the center of the reservoir, the dark region is nearly circular shaped. Actually, this case is formerly shown in Figure 2.1a, where the average reservoir pressure region is observed at $0.61r_e$. For this case the equivalent circular radius is calculated as 5641.2 m and the average reservoir region is observed at 3442 m which is equal to $0.61r_e$. Again for this case, if the well moves closer to one or two of the constant pressure boundaries, a dark region is formed opposite the constant pressure boundary that the production region is close to.

4.3.5 Reservoir with one production well, one reinjection well and constant pressure boundary on west side

In the following cases, a reinjection well is inserted near the production well. This reinjection well can also be treated as a gathering point for a set of reinjection wells. A constant pressure boundary is connected to the reservoir. For various reinjection rates, the location of the average reservoir pressure region is investigated. Figure 4.20 shows the outputs of these cases.

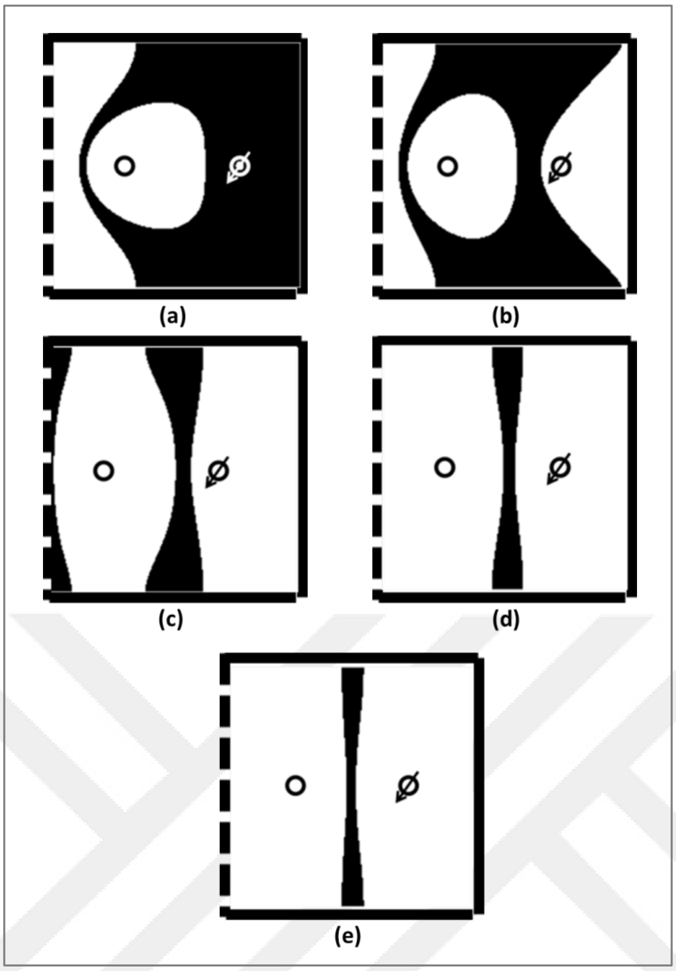

Figure 4.20 : Absolute percentile difference output for the case having constant pressure boundary on west side with (a) 10% reinjection rate, (b) 25% reinjection rate, (c) 50% reinjection rate, (d) 75% reinjection rate and (e) 100% reinjection rate.

It can clearly be seen from Figure 4.20 that a dark region is formed between the reinjection and production regions. Also for the cases with more than 50% reinjection rate, the average reservoir pressure region disappears between the production region and constant pressure boundary. An important outcome for the cases with high reinjection rates is that the observation well should be placed in between the production and reinjection regions.

4.3.6 Reservoir with one production well, two reinjection wells and no-flow boundaries on all sides

The previous case shows that the effect of constant pressure boundary disappears when choosing the observation well location, as the reinjection rate is quite high in a typical reservoir. In this case, all the boundaries are no-flow boundaries which means that the reservoir is a closed one. In the center of the reservoir, a production well is placed and two injection wells are located on each side of the reservoirs. The total reinjection rate is kept 100%, with varying weights for each reinjection well. The results for this case are shown in Figure 4.21.

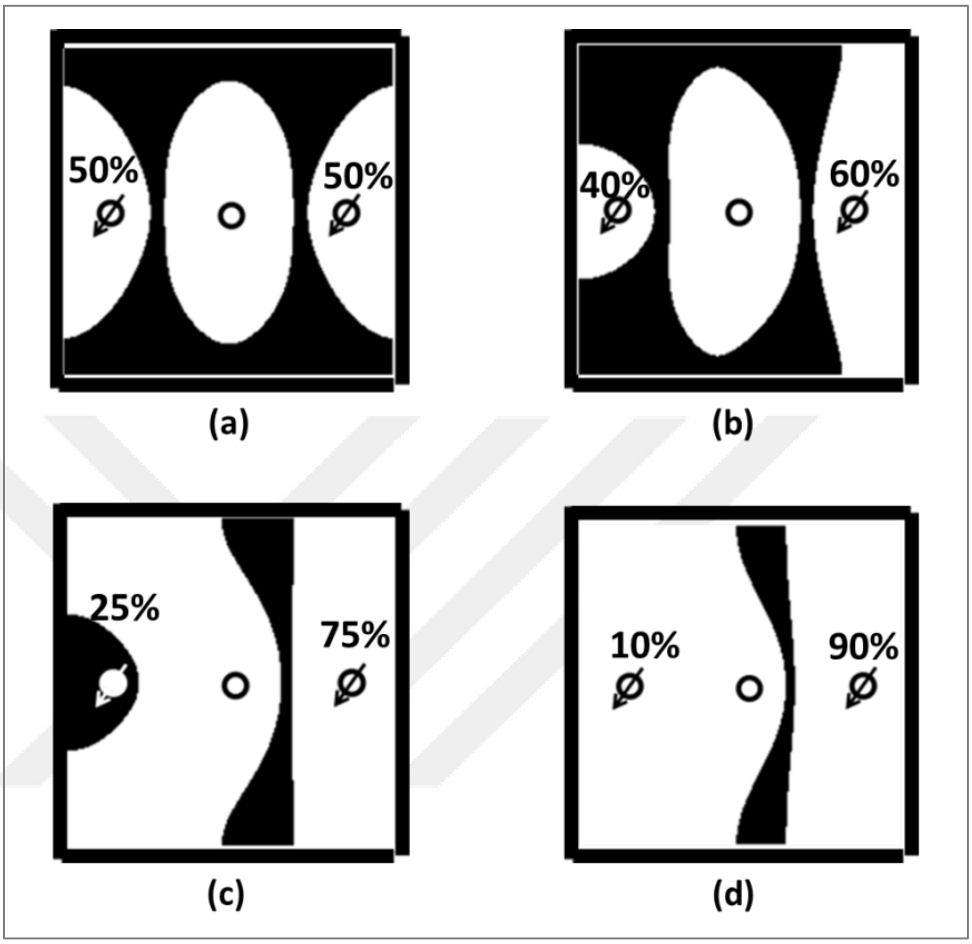

Figure 4.21 : Effect of reinjection weight between two injection wells on volumetric average reservoir pressure location.(a) 50% west, 50% east reinjection rates, (b) 40% west, 60% east reinjection rates, (c) 25% west, 75% east reinjection rates and (d) 10% west, 90% east reinjection rates.

It can easily be seen that, for cases with same or close reinjection rates (Figure 4.21a and Figure 4.21b), the black region can easily be placed between reinjection wells and production well. However, for the remaining cases where 25%-75% split and 10%-90% split, the black region is formed between only the reinjection well with the highest rate and the production well. This is an important outcome, which indicates that the observation well should be placed between the dominant reinjection region and the production region when there is a great difference between the reinjection rates of the reinjection regions.

4.3.7 Reservoir with two production wells, one reinjection well and no-flow boundaries on all sides

In this case, the number of production wells is increased. For this case the reinjection rate is kept constant at 100%, however, this time weight of the production regions is changed. The results for this case are shown in Figure 4.22.

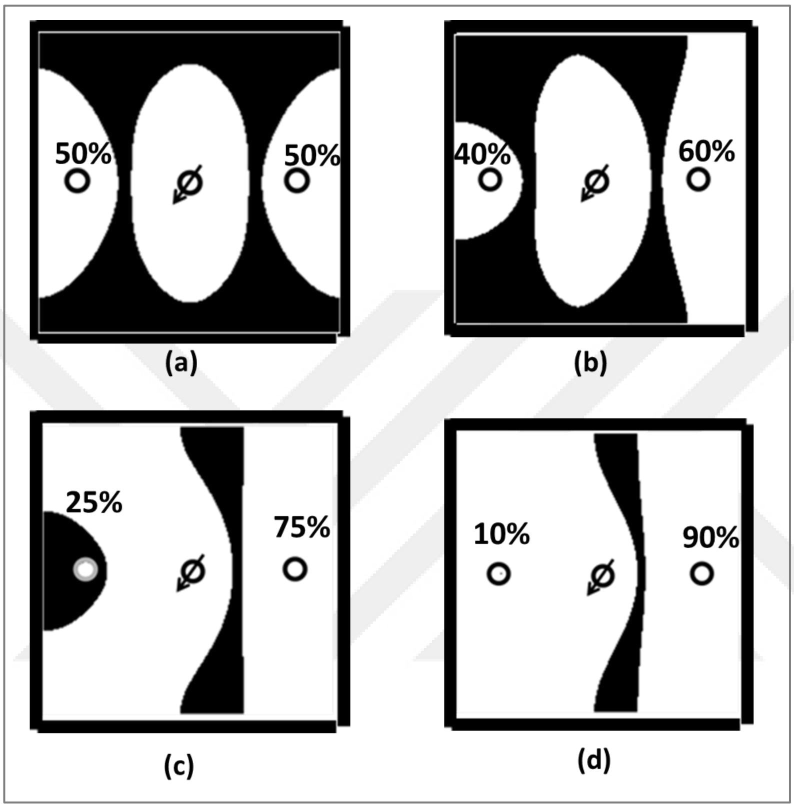

Figure 4.22 : Effect of production weight between two production wells on volumetric average reservoir pressure location.(a) 50% west, 50% east production weight, (b) 40% west, 60% east production weight, (c) 25% west, 75% east production weight and (d) 10% west, 90% east production weight.

Figure 4.22 shows that similar outcomes are obtained with that given in the previous section. The observation well should be chosen taking into account the most dominant production well in the system and the reinjection well when there is two separate production region in the field.

4.3.8 Reservoir with one production well, two reinjection wells and constant pressure boundary on the west side

The previous two cases are both closed cases and the outcome was clear that for the observation well selection, dominant reinjection/production well should be taken into account. In this case, a constant pressure boundary is connected to the reservoir and again the reinjection rates varied for each case. The results of this case are shown in Figure 4.23.

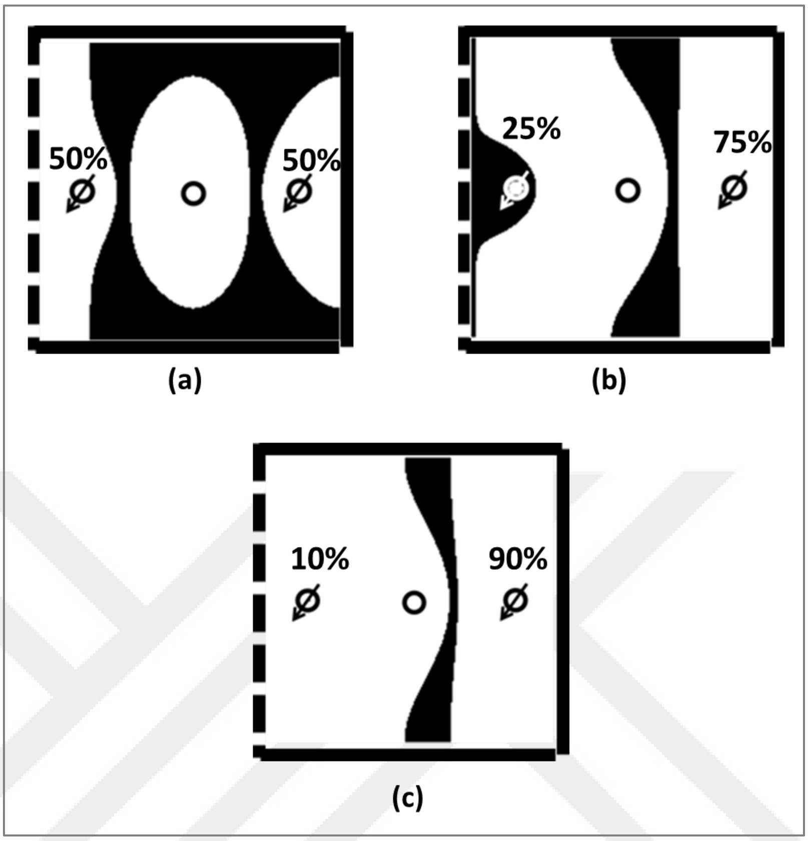

Figure 4.23 : Effect of reinjection weight between two injection wells on volumetric average reservoir pressure location when there is constant pressure boundary from west.(a) 50% west, 50% east reinjection rates, (b) 25% west, 75% east reinjection rates and (c) 10% west, 90% east reinjection rates.

Figure 4.23 shows that the effect of constant pressure boundary decreases (on black region generation) if there is a dominant reinjection region. One should choose the location of the observation well based on the dominant reinjection well and the production well even there is a constant pressure boundary is connected to the reservoir.

4.3.9 Reservoir with one production well, two reinjection wells and constant pressure boundary on all sides

In this case, two injection wells are present in the system, and a constant pressure boundary is connected to all sides of the reservoir. Again the total reinjection rate is kept as 100% but with varying reinjection weights for each reinjection well. The results obtained by this case are shown in Figure 4.24.

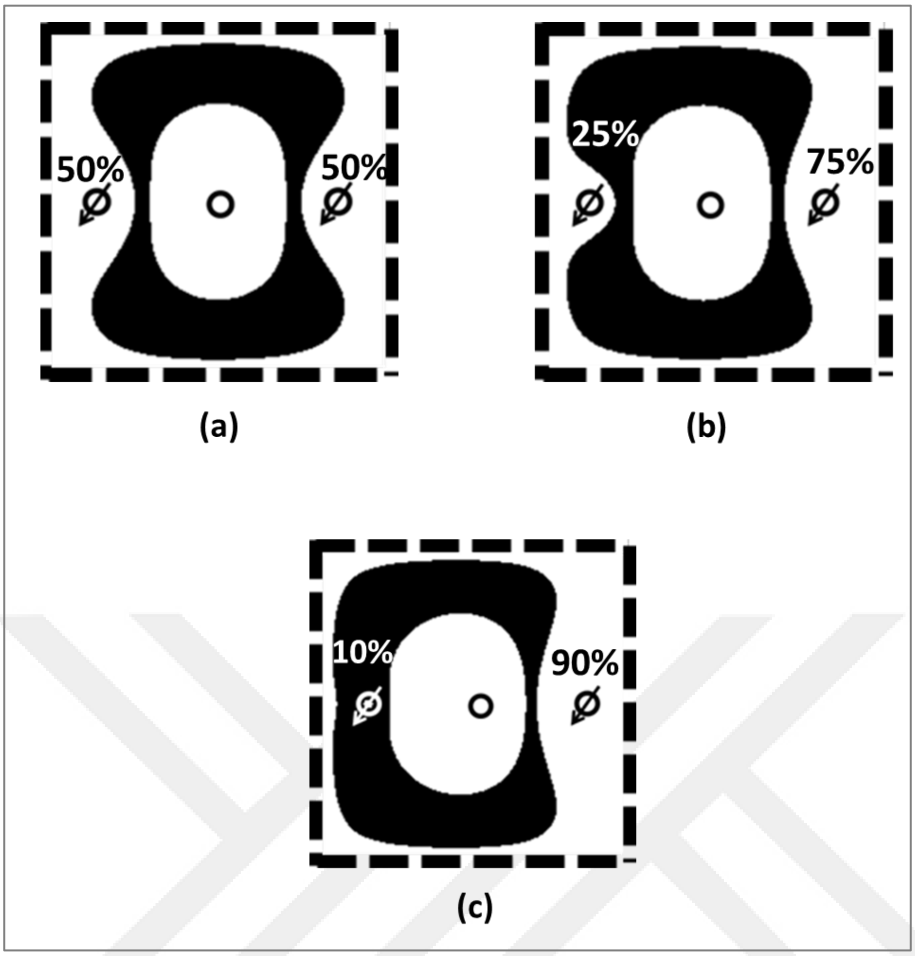

Figure 4.24 : Effect of reinjection weight between two injection wells on volumetric average reservoir pressure location when there is constant pressure boundary from all sides.(a) 50% west, 50% east reinjection rates, (b) 25% west, 75% east reinjection rates and (c) 10% west, 90% east reinjection rates.

Like in the previous cases, even though there is a constant pressure boundary connected to the reservoir from all sides, the black region exists between the dominant reinjection well and the production well. The injection well with less weight does not give a clear location for the observation well location. One should choose the observation well located between the production well and the dominant reinjection well.

4.3.10 Effect of heterogeneity on the region of average pressure

In real life, some geothermal reservoirs might have fault features that may affect the flow and pressure distribution throughout the reservoir. In this subsection, some measure of heterogeneity is introduced to the reservoir system by inserting faults. The recharge indices between the grids in the faults are taken as 1000 kg/bar-s for simplicity. The recharge indices between the reservoir grids are kept the same which is 1 kg/bar-s. For the reservoir and fault connection grids, harmonic average values for the recharge indices are used. A fault is three grid wide and throughout the figures, it is shown with a grey solid line. Four different cases are studied with faulted structures.

In the first case, a fault is inserted into the system which has a constant pressure boundary in the west part and the well located in the center of the reservoir. The fault is located in the center laterally by connecting the constant pressure boundary and the well. The output of the case is shown in Figure 4.25.

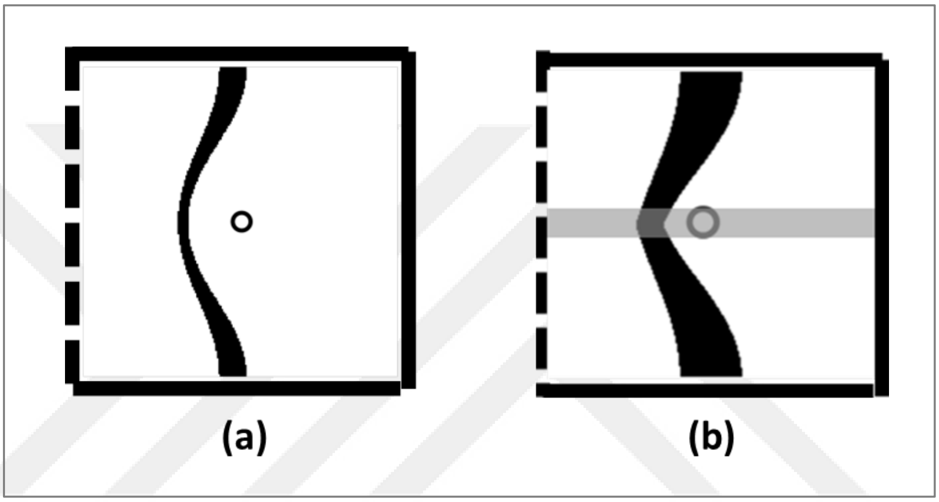

Figure 4.25 : Case with constant pressure boundary from the west with production well in the center. (a) Case without fault (Figure 4.16e), (b) Case with fault in communication with the constant pressure boundary.

Figure 4.25 shows the comparison of the faulted and non-faulted cases. It can be easily seen that not much is changed in the results of the two cases when the black regions are compared. The faulted case shows a little bit thicker result but with a similar shape. The observation well should be located in between the constant pressure boundary and the production well.

In the next case, the fault is located vertically, again passing through the production well but with no connection with the constant pressure boundary. The result obtained from this case is shown in Figure 4.26.

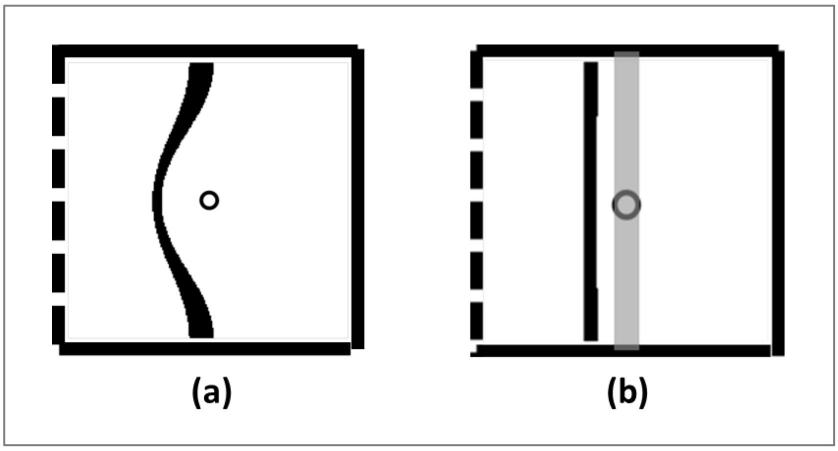

Figure 4.26 : Case with constant pressure boundary from the west with production well in the center. (a) Case without fault (Figure 4.16e), (b) Case with fault that is no-in communication with the constant pressure boundary.

It can clearly be seen that there is a difference between the two cases. The dark region formed with the faulted case is linear. The main reason for this is that the fault is acting as the production well. Since fault has high permeability, when production started, the water located in or around the neighborhood of the fault is produced. First water moves from neighboring grids to the fault and then from fault to the production well. This makes the fault act as if it were a linear producer, therefore creating a linear region of average reservoir pressure.

In the previous cases, the fault is inserted to the place where the production well is located. However, in the following case, fault will be inserted with a connection with the constant pressure boundary. The comparison of the results obtained in this case is shown in Figure 4.27.

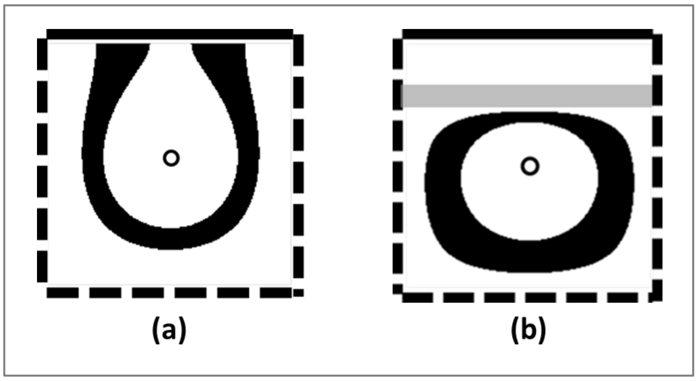

Figure 4.27 : Case with constant pressure boundary from the east, west and south with production from the center. (a) Case without fault (Figure 4.19d), (b) Case with fault that is in communication with the constant pressure boundary.

The result obtained from the faulted case show some difference with the non-faulted case. In the non-faulted case, the black region is formed between the constant pressure boundaries and the production well; however, in the faulted cases the black region appeared between the production well and the no-flow boundary, being located on the same side with the fault. The main reason for this outcome is that since the fault is in communication with the constant pressure boundary, it acts as a constant pressure boundary. When the well is producing, water starts to move from fault to reservoir as if the fault is a constant pressure boundary.

In the last case, a production and an injection well are present in the system. Both of the wells are located in two different faults. The output of this case is shown in Figure 4.28.

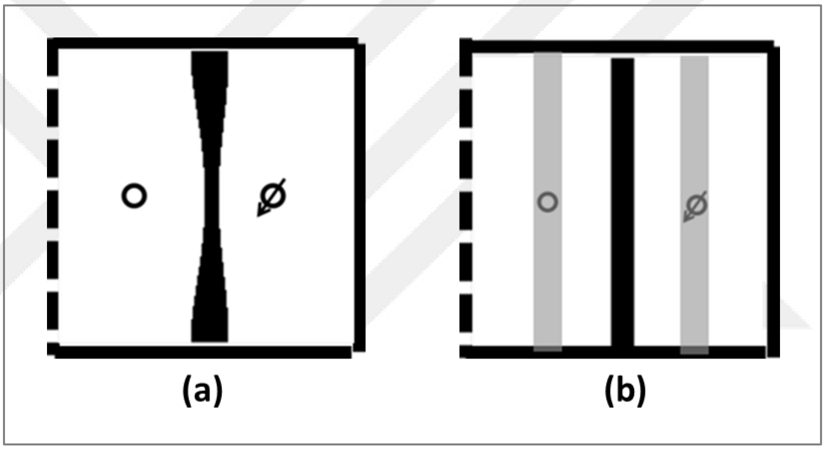

Figure 4.28 : Case with constant pressure boundary from the east with a producer and an injector. (a) Case without fault (Figure 19d), (b) Case with two faults that contain the production and reinjection wells that are not in communication with the constant pressure boundary.

It can be seen from the no faulted case the black region is a concave-like shape, on the other hand, the faulted case gives us a straight like black region. Like in the previous cases, when a well is located in a fault, the fault acts like the well and the pressure outputs are affected by this feature. For this case, a linear average reservoir pressure region is formed.

In cases with heterogeneity, two major outcomes can be observed. The first one is if a well is producing from a fault, the fault acts as a production well and the pressure outputs are affected respectively. The second outcome is that if the fault is connected to the recharge source, then it also acts as if it were a constant pressure boundary simply because fluid is transmitted from the recharge source into the fault easily because of the high permeability of the fault compared to the reservoir permeability. Hence, an average pressure region tends to form between the wells and the fault.

In this section, various cases are run with different outer boundary conditions and well compositions in order to find the best possible location for the observation well. The outcomes of these can be summarized as follows:

- If there is only a production well in the field, then the region of volumetric average reservoir pressure forms between the production well and any constant pressure boundary. Hence if there are only production wells in a reservoir (that are gathered in a certain region of the reservoir), then it is best to place an observation well between the production region and the constant pressure boundary or boundaries.

- Observation wells should not be placed close to the production well or the reinjection wells. The interference effect from these wells will cause the observation well pressures to be either lower than what it is supposed to be or higher than what it is supposed to be based on the well, being closer to a production well or a reinjection well respectively. Similarly, it can be stated that the observation wells should not be placed closer to the production region or the reinjection region in a reservoir.

- In the case where there exists only one production well and no reinjection wells, if the production well is placed close to the constant pressure boundary, then the region of volumetric average reservoir pressure could be in two places. First in the region between the production well and the constant pressure boundary (as mentioned above) and second in the region opposite the constant pressure boundary that the well is closer to.

- When a reinjection well is present in the reservoir, the volumetric average pressure region forms between the production well and the reinjection well. Hence the observation well in such a case should be placed in between the two wells. For an actual field where there exists a reinjection zone with many reinjection wells and a production zone with many production wells, then the observation well should be placed between the production region and the reinjection region.

- With high reinjection rates, the effects of the outer boundaries become negligible while selecting ideal location of the observation well.
- In the case of more than one production region or more than one reinjection region, the location of the observation well should be between the production/reinjection pairs where there are higher ratios of either production or reinjection. In other words, the observation well should be placed where higher rates of production/reinjection are involved.
- It is important to note that with the addition of new wells or production reinjection regions, the location of average reservoir pressure regions could change. Hence the locations of observation wells may need to be changed accordingly. The location of an observation well should be considered to change with time.
- Having high permeability, fluid flows from the recharge source through the connected fault easily which causes the fault to act as if it were a constant pressure boundary. As a result average reservoir pressure can be observed between the wells and the fault. It is also important to note that, in the cases having a well located in the fault, the fault acts as if it is either a producer or an injector. As a result, instead of the well, the shape of the fault defines the average reservoir pressure region

4.4 Determining the Location of the Average Reservoir Pressure Region between Production and Reinjection Well

In the previous section for the cases having reinjection well, it was understood that it is better to place observation well between the production well and reinjection well even though there is a constant pressure boundary in the system. In this section, four different sets of cases are studied and the results of these cases for different reinjection rates are investigated. It is aimed to understand the exact location of the region that average reservoir pressure can be seen by varying reinjection rates.

The whole reservoir system is formed of 201x201 grids which are identical. The system is isothermal and single-phase water. The width and the length of a grid is 49.75m. The height of the reservoir is 500m. Storage capacity of a grid is 5384.93 kg/bar and the recharge indexes between the grids are same which is 1 kg/bar-s.

The initial pressure is 300 bars and for the wells created in the system, they are assumed to have no wellbore storage and Peaceman WI values are equal to 1.3 kg/bar-s in order to keep the simplicity of the case.

In the first three of the studied cases, the production well is producing with a constant flow rate of 110 kg/s. And for the last set of cases the production well is producing with 55 kg/s. The reinjection rate is varying between 10% and 100% with 10% increments.

As shown in the previous chapter example, the absolute percentile difference used for all cases is 1%. The dark region represents the location where the average reservoir pressure can be observed.

4.4.1 Reservoir with one production well on west, one reinjection well on east and constant pressure boundary from west side

This example composes of a production well, which is located on the west side of the reservoir, and a reinjection well that is located on the east side of the reservoir. A constant pressure boundary is present in the system with a connection from the west side of the reservoir as shown in Figure 4.29.

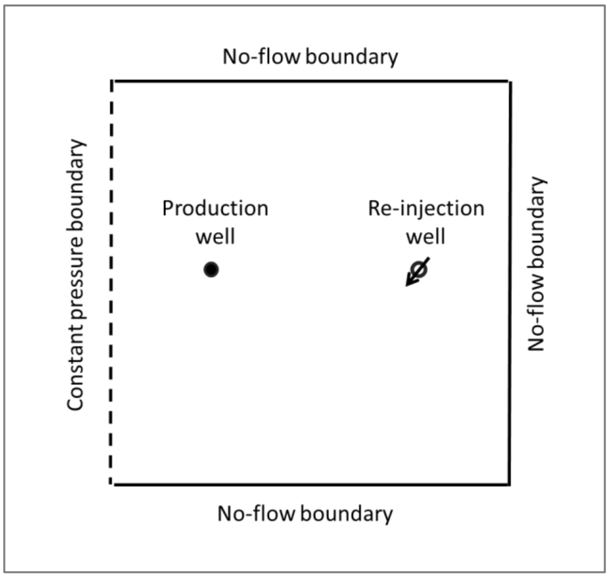

Figure 4.29 : Schematic of the reservoir with one production well on west, one reinjection well on east and constant pressure boundary from west side.

For the reservoir as shown in Figure 4.29, the average reservoir pressure region for different reinjection rates is calculated. Between the 10% and 100% reinjection rates each 10% is studied and the results are shown in Figure 4.30.

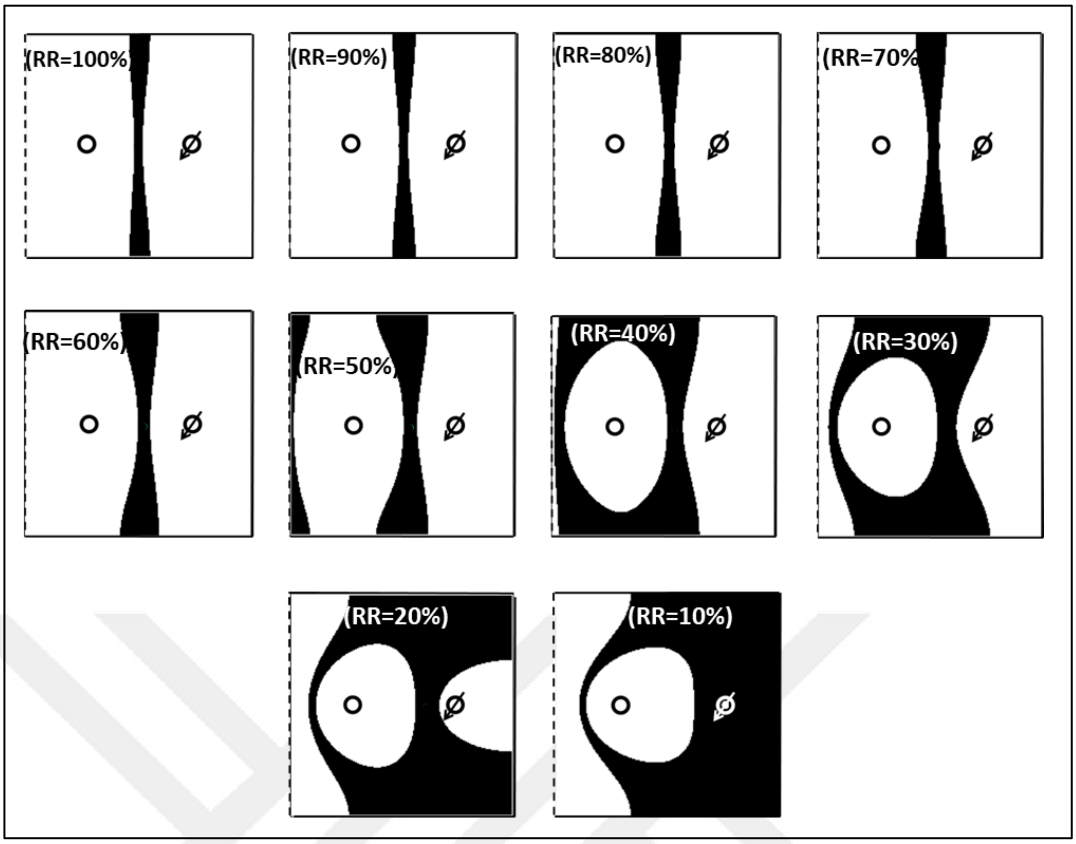

Figure 4.30 : Case with reinjection well on east and constant pressure boundary from west with varying reinjection rates.

It can be seen in Figure 4.30 that black region is always located between reinjection and production well. It is important to note that, as the reinjection rate decreases the black region moves towards the reinjection well. For the cases having low reinjection rates, a second black region occur between the production well and the constant pressure boundary. With the decreasing reinjection rates this black region moves towards the production well.

4.4.2 Reservoir with one production well on east, one reinjection well on west and constant pressure boundary from west side

This example has similar composition except with a small difference where the places of reinjection and production well are switched. By this way, the reinjection well is placed on the side of the constant pressure boundary. Again the results of the cases are observed for varying reinjection rates. Figure 4.31 shows the system.

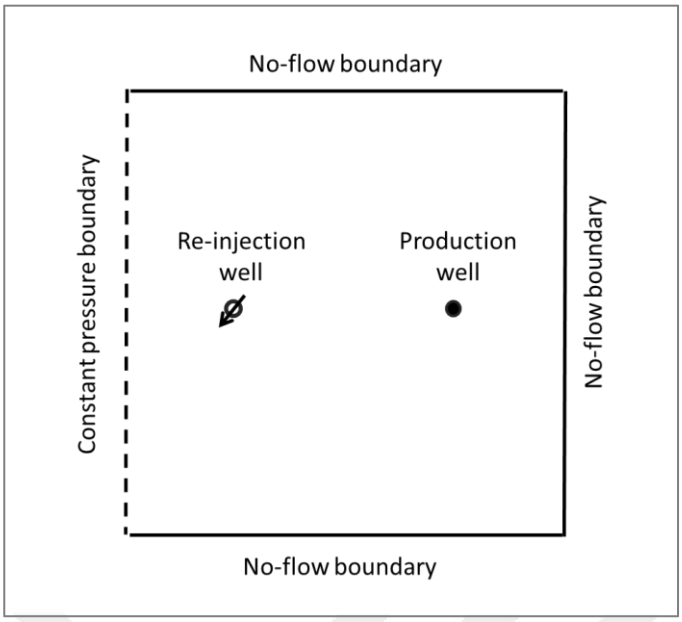

Figure 4.31 : Schematic of the reservoir with one production well on east, one reinjection well on west and constant pressure boundary from west side.

For the composition of the reservoir as shown in Figure 4.31, the average reservoir pressure region for different reinjection rates is calculated. **Error! Reference source not found.** shows the results obtained.

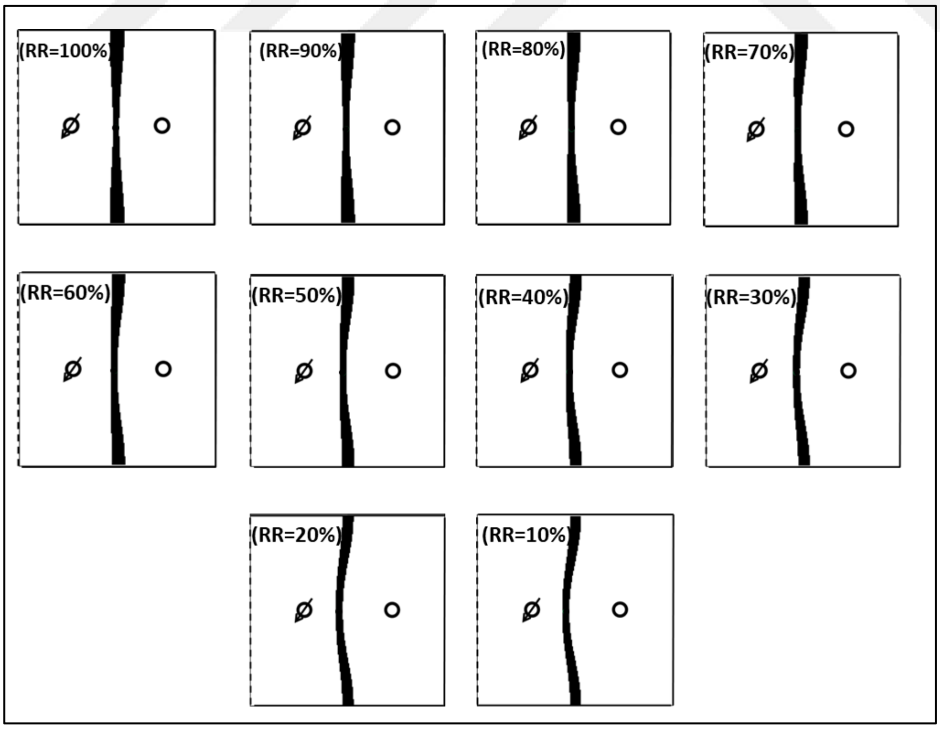

Figure 4.32 : Case with reinjection well on west and constant pressure boundary from west with varying reinjection rates.

Again in this case it can be seen from Figure 4.32 that the black region moves towards the reinjection well with the decreasing reinjection rates. For all cases there is only one black region occurs which is between production and reinjection wells..

4.4.3 Reservoir with one production well on west, one reinjection well on east and constant pressure boundary from all sides

In the previous two examples, the constant pressure is connected from one side of the reservoir. However, in this example, the constant pressure boundary is connected from all sides of the reservoir. The production well is located in the west and the reinjection well is located on the east side of the reservoir. In Figure 4.33 the composition of the reservoir is shown.

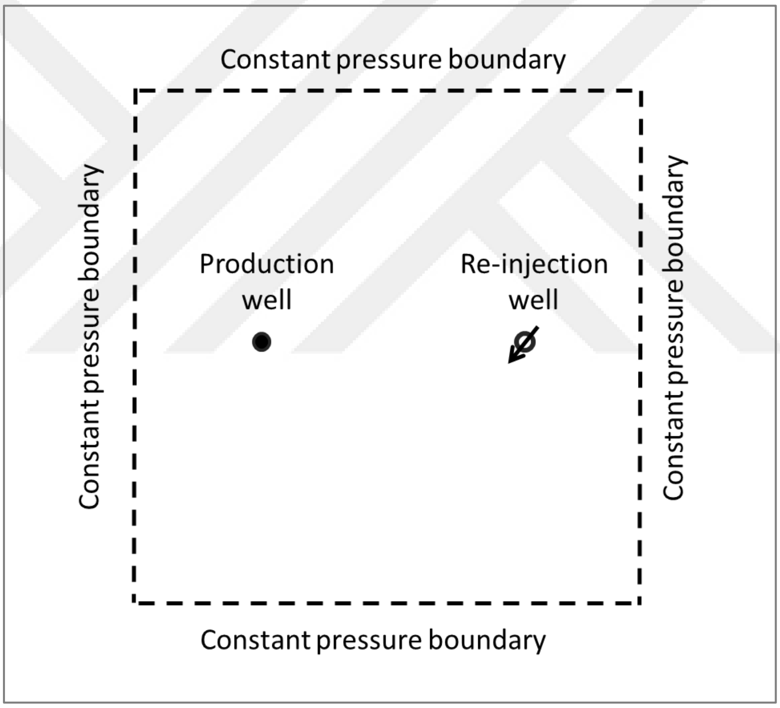

Figure 4.33 : Schematic of the reservoir with one production well on west, one reinjection well on east and constant pressure boundary from all sides.

For the reservoir given in Figure 4.33, cases for varying reinjection rates are studied and the pressure outputs of the cases are shown in Figure 4.34.

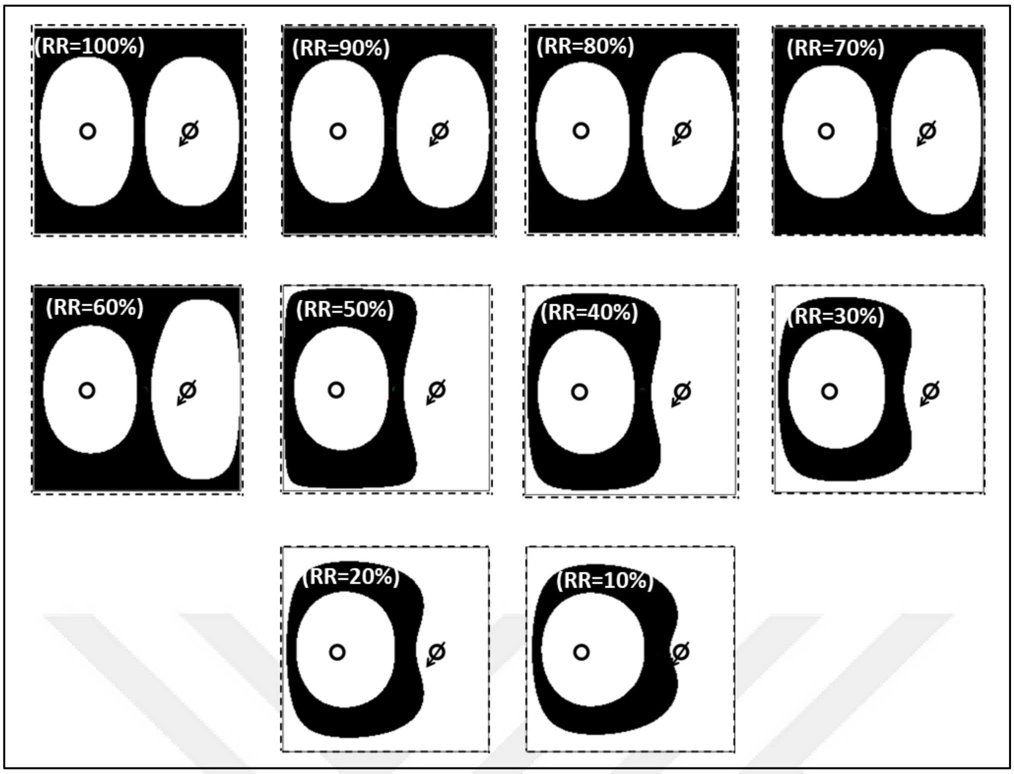

Figure 4.34 : Case with reinjection well on east and constant pressure boundary from all sides with varying reinjection rates.

Figure 4.34 shows that as the reinjection rate decreases the density of the dark region decreases as well. Also it is clearly seen that from the above table, the dark region moves towards the reinjection well as the reinjection rates decreases.

4.4.4 Reservoir with one production well on west, one reinjection well on east and no-flow boundary from all sides

All the previous three examples were giving results for open systems. However, in this example, a closed reservoir is considered with a production well in the west and an injection well in the east side of the reservoir. The production rate of the well is 55 kg/s and the results are observed for different reinjection rates. Since it is a closed system, the dark region is shown for the pseudo-steady-state period outputs. Figure 4.35 shows the system used in this example.

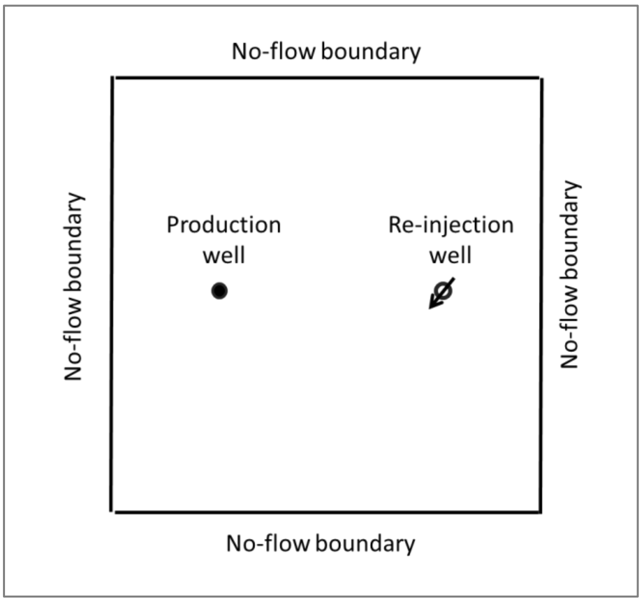

Figure 4.35 : Schematic of the reservoir with one production well on west, one reinjection well on east and no-flow boundary from all sides.

For the varying reinjection rates, the pressure output of the cases is shown in Figure 4.36.

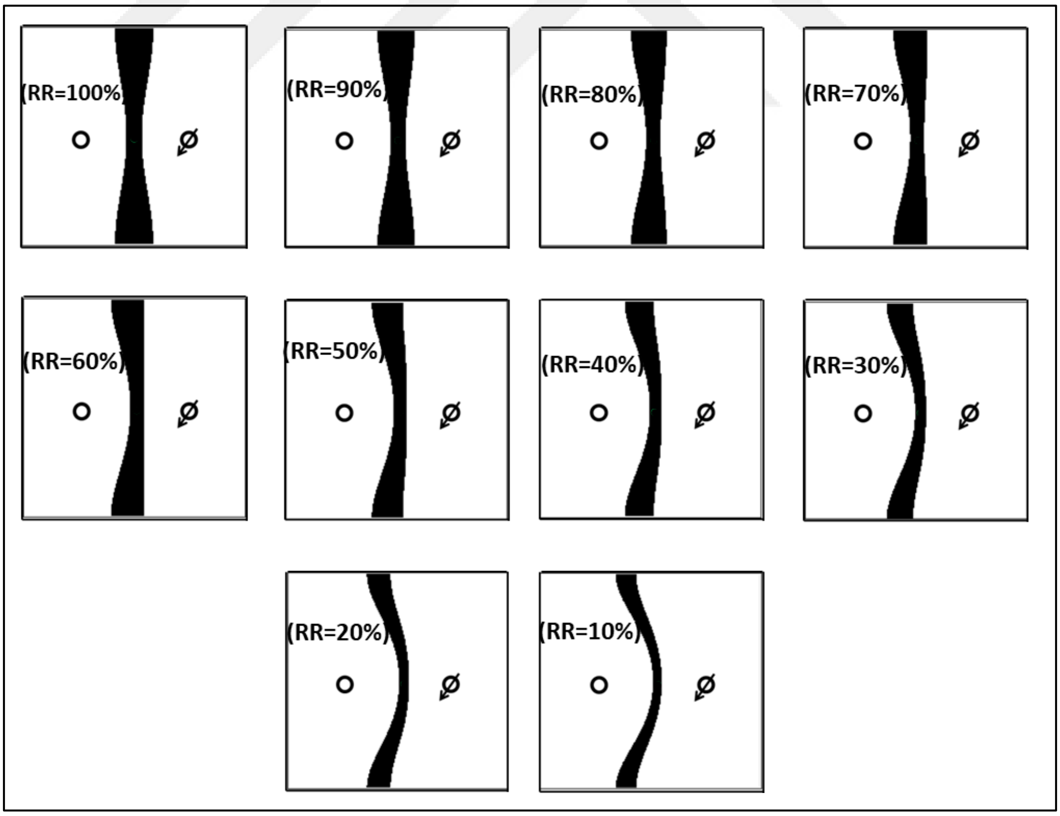

Figure 4.36 : Case with reinjection well on east and no-flow boundary from all sides with varying reinjection rates.

All of the cases in Figure 4.36 show similar results except the concavity of the dark region. As the reinjection rate decreases the concave-like shape moves towards the production well.

As the examples in this suggest suggests, as the reinjection rate decreases, the location of the dark region moves towards the reinjection well. For the cases having constant pressure boundary and no-flow boundary from all sides, this movement is less when it is compared with the other cases.

5. CONCLUSIONS AND RECOMMENDATIONS

In this chapter, the conclusions obtained from the thesis study and recommendations for future works are given. Also, a section for the applications that can be adapted to the Oil and Gas Sector is discussed.

5.1 Conclusions

In this thesis, optimum location of an observation well is studied. Firstly a two-dimensional numerical model is generated. The validation of this numerical model is achieved by way of different analytical models in literature.

In the second part of the thesis, several lumped parameter models are presented. The crucial effect of observation well location on lumped parameter models is given. The prediction deviations and misjudgments about reservoir characteristics caused by poor observation well placement are illustrated with several examples. Appropriate locations for the observation wells are illustrated in several examples. It was understood that the dark region’s location in steady-state flow period gives the best matches for lumped parameter models and pressure predictions with these matched lumped parameter models.

In the last part of the thesis study, a superposition-based method, Larsen method, is presented for steady-state solutions and validation of this model is done with the already validated numerical model. A multi well approach with superposition is carried out for this superposition-based Larsen method. By this way the solutions of steady-state cases can be obtained based on using the superposition principle twice. Different examples are run with varying boundary conditions and well compositions both with the superposition model and the numerical model. In these cases usually, single production or injection well is used which also represents the location for a gathering place of production or injection wells. The effect of reinjection rate and the heterogeneity of the reservoir is investigated by the insertion of faults into the system. The major outcomes from these cases can be summarized as follows:

- For the cases having only production wells (and gathered in a region), the region of volumetric average pressure forms between the production region and constant pressure boundary. An observation well should be placed into this region.
- Having great interference on the pressure observation, one should not place observation wells close to the production and reinjection wells. The injection operation causes an increase in the readings and similarly, production operations cause a decrease in the readings.
- For the cases having production well close to a constant pressure boundary, a second location for observation well can be chosen which is in the region opposite the constant pressure boundary where the well is close to.
- If there are reinjection wells present in the system, the observation well should be placed between the reinjection well and the production well where volumetric average pressure formed.
- The effect of boundaries is neglected on the location of observation well selection when the reinjection rate is high in the reservoir.
- If there is more than one production region or one reinjection region, an observation well should be placed between the most dominant production region and the most dominant reinjection region.
- When there are faults in the system, and the fault is connected with the constant pressure boundary, these faults act as a constant pressure boundary and the volumetric average reservoir pressure region can be observed between the fault and production well. When a well is located in the fault, with the effect of high permeability among the fault, the fault acts as a producer or an injector. Thus, the volumetric average pressure forms based on the shape of the fault.
- Insertion of new wells into the system might change the location of average reservoir pressure. One should consider whether the change of observation well is needed based on this insertion of new wells.
- In Figure 5.1 a simple guide to find proper locations of observation wells is given.

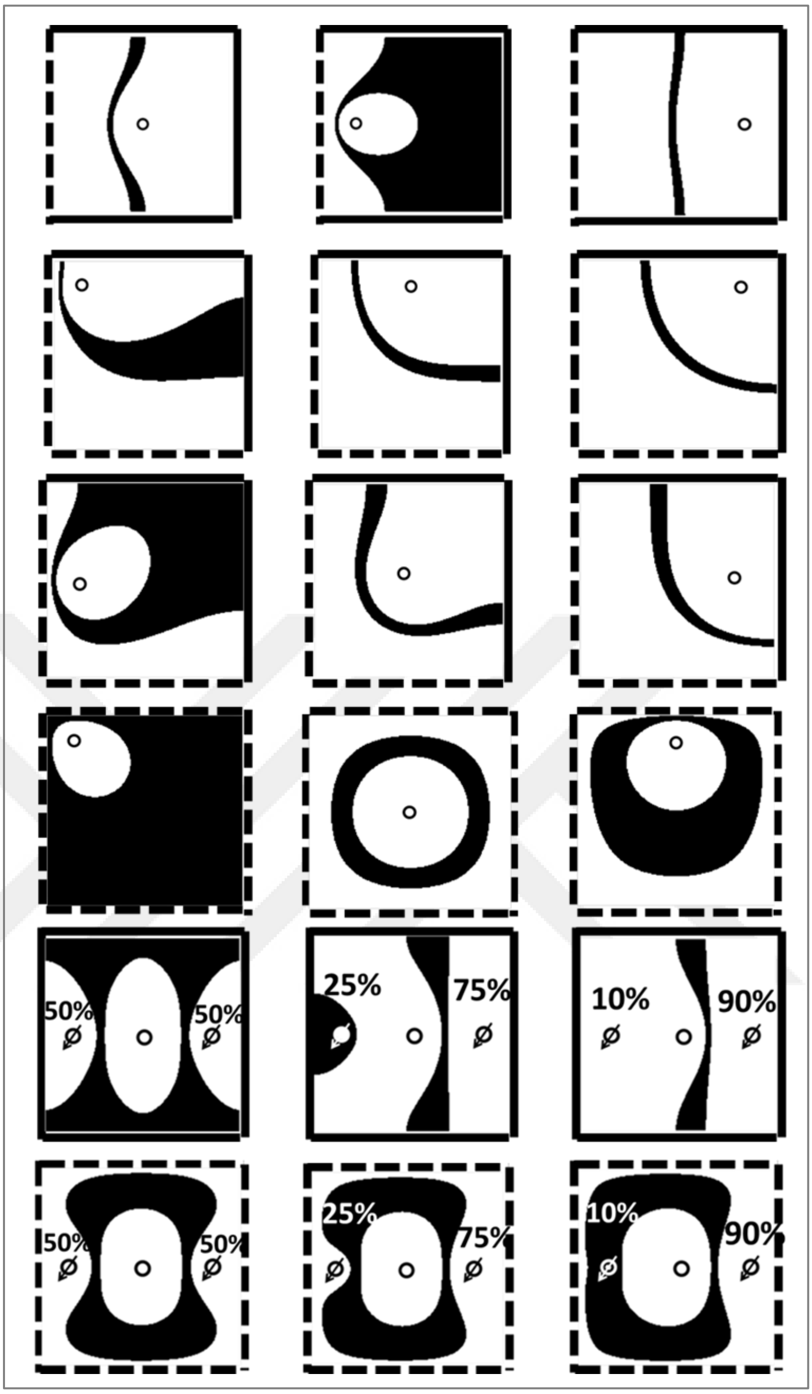

Figure 5.1 : Summary of the cases provided for various boundary conditions.

5.2 Recommendations for Future Studies

Based on this thesis study, the following recommendations and suggestions are given for future studies. Further improvements can be made with the help of these suggestions.

In this study, a 2D numerical model is used and results of the observation well location are shown based on this assumption. With the insertion of gravitation effects and the 3rd dimension, a guide for the perforations of observation well can be investigated. Some parts of the observation well might not represent the average reservoir pressure and the effect of the datum in pressure readings should be included.

In our study, the boundaries are connected to the reservoir from the sides. In a 2D environment, the insertion of a constant pressure boundary from the bottom of the reservoir will give an unrealistic case since every grid in the system will be connected to the boundary which indirectly means that producing from that boundary. With the 3D model and insertion of constant pressure boundaries from the bottom of the reservoir might contribute to the understanding of the observation well placement.

The effect heterogeneity is tried to be measured by the insertion of faults to the system. Insertion of heterogeneity by the means of grid property distributions like using kriging and Gaussian distribution may contribute to the study and might give some indications about the relation between the heterogeneity level and average reservoir pressure region in the reservoir.

The geothermal reservoirs are studied in this study. Being a porous medium and having similar production concepts and relations, the results obtained from this study might be implemented to the oil fields. One should consider the multiphase system in the oil reservoirs. In an under-saturated oil reservoir, the results obtained from our study might be similar, however, since the injection is conducted with a second type of fluid, mainly water, a second phase automatically enters the system. The sweep efficiencies may also affect the results.

The regions where the grid pressure is high can be marked with the numerical model, and possible candidates for the new oil wells can be chosen with the help of this output.

REFERENCES

Ahmed,T. (2001). *Reservoir Engineering Handbook*. Gulf Professional Publishing, Houston, Texas.

Ahmed, T., Mckinney, P.D. (2005). *Advanced Reservoir Engineering*. Gulf Professional Publishing, Houston, Texas.

Aksoy, N., Serpen, U., Filiz, S. (2008). Management of the Balcova-Narlidere Geothermal Reservoir Turkey. *Geothermics, 37*, 444-466.

Akyapı, E. (2010). *A New Non-Isothermal Tank Model for Liquid Dominated Geothermal Reservoirs* (Master's thesis). ITU, Istanbul, Turkey.

Alkan, H., and Satman, A. (1990). A New Lumped Parameter Model for Geothermal Reservoirs in Presence of Carbon Dioxide. *Geothermics, 19*, 469-479.

Arihara, N., Yoshida, H., Hanano, M., Ikeuchi, K. (1995). A Simulation Study on Hydrothermal System of the Kakkonda Geothermal Field. *Proceedings of World Geothermal Congress '95*, Florence, 18-31 May 1995, 1715-1720.

Axelsson, G. (1989). Simulation of Pressure Response Data from Geothermal Reservoirs by Lumpd Parameter Models. *14th Workshop on Geothermal Reservoir Engineering*, Stanford University, 257-263.

Bodvarsson, G.S., Benson, S.M., and, Witherspoon, P.A. (1982). Theory of the Development of Geothermal Systems Charged by Vertical Faults. *Journal of Geophysical Research*, September, *87*, 9317-9328.

Bodvarsson, G.S., Pruess, and K., Lippmann, M.J. (1986). Modeling of Geothermal Systems. *Journal of Petroleum Technology*, September, *38*, 1007-1021.

Bromley, C., Brockbank, K., Glynn-Morris, T., Rosenberg, M., Pender, M., O'Sullivan, M., Currie, S. (2013). Geothermal Subsidence Study at Wairake-Tauhara, New Zeland. *Proceedings of the Institution of Civil Engineers- Geotechnical Engineering*, *166*, 211-223.

Butler, S.J., Sanyal, S.K., Henneberger, R.C., Klein, C.W., Gutierrez, H., de Leon, J.S. (2000). Numerical Modeling of the Cerro Prierto Geothermal Field, Mexico. *Proceedings of World Geothermal Congress 2000*; Kyushu, Japan, 2545-2550.

Castanier, L.M., Sanyal, K.S., and Brigham, W.E. (1980). A Practical Analytical Model for Geothermal Reservoir Simulation. *50th Annual California Regional Meeting of SPE*, Los Angeles, California, April 9-11, SPE 8887.

Coats, K.H. (1977). Geothermal Reservoir Modeling. *52nd Annual Fall Technical Conference and Exhibition*, October 9-12, SPE 6892.

Dastan, A., Kamal, M., Collins, J.R., Neubauer, E.B. (2012). Calculation of Average Reservoir Pressure during Primary and Secondary Recovery and Under Variable Boundary Conditions. *SPE Annual Technical Conference and Exhibition*, San Antonio, Texas, USA, October 8-10, SPE 159568.

Dykstra, H. (1979). Average Pressure from Buildup Data for A Rectangle with Constant Pressure Boundary. *SPE California Regional Meeting*, April 18-20, SPE 7980.

Feng, G., Tianfu, G.,, Jiang, Z.J., Bellani, S. (2017). Geothermal Assessment of the Pisa Plain, Italy: Coupled Thermal and Hydraulic Modeling. *Renewable Energy*, *111*, 416-427.

Golan, M., Whitson, C. H. (1991).*Well Performance* (2nd ed.). Prentice Hall, Englewood Cliffs, New Jersey.

Goyal, K.P., and Kassoy, D.R. (1980). A Plausible Two-Dimensional Vertical Model of the East Mesa Geothermal Field, California, USA. *Journal of Geophysical Research*, *86*, November, 10719-10733.

Horne, R.N., and O'Sullivan, M.J. (1977). Numerical Modeling of the Wairakei Geothermal Reservoir. *47th Annual California Regional Meeting of the SPE*, April 13-15, SPE 6536.

Horne. R. (1990). *Modern Well Test Analysis*. Petroway Inc. USA.

Hoşgör, F. B., Tureyen, O. I., and Satman, A., (2016). Keeping Inventory of Carbon Dioxide in Liquid Dominated Geothermal Reservoirs. *Geothermics*, *64*, 55-60.

International Energy Agency (IEA). (2020). *Renewables 2020: Analysis and forecast to 2025*. Retrieved from https://www.iea.org

Kappa Engineering. (2005). *Ecrin User Guide*.

Kazemi, H. (1974). Determining Average Reservoir Pressure from Pressure Buildup Tests. *SPE Journal*, *14*, February, 55-62, SPE 4052.

Konuksal, H. (2007). *Boyutsuz Rezervuar Modellerinin Numerik Olarak Çözümlenmesi* (Master's thesis). ITU, Istanbul, Turkey.

Korkmaz, E. D., Serpen, U., Satman, A. (2014). Geothermal boom in Turkey: Growth in identified capacities and potentials. *Renewable Energy*, *68*, August 2014, 314-325.

Kuchuk, F., Ayestaran, L. (1985). Analysis of Simultaneously Measured Pressure and Sandface Flow Rate in Transient Well Testing. *Journal of Petroleum Technology*, February, 323-334.

Larsen, L. (1985). A Simple Approach to Pressure Distributions in Geometric Shapes. *SPE Journal*. February, 113-120.

Lee. J. (1982). *Well Testing*. Society of Petroleum Engineering Textbook Series Vol.1. USA.

Li, Y., Juliusson, E., Palsson, H., Stefansson, H., Valfells, A. (2017). Machine Learning for Creation of Generalized Lumped Parameter Tank Models of Low Temperature Geothermal Reservoir Systems. *Geothermics, 70*, 62-84.

Llanos, E.M., Zarrouk, S.J., Hogarth, R.A. (2015). Numerical Model of the Habanero Geothermal Reservoir, Australia, *Geothermics, 53,* 308-319.

Marcou, J.A., and Gudmundsson, J.S. (1986). Development Model for Geothermal Reservoirs. *56th California Regional Meeting of the SPE*, Oakland, California, April, 265-269.

Matthews, C.S., Brons, F., Hazebroek. (1954). A Method for Determination of Average Pressure in a Bounded Reservoir. *Trans, 201*, December, 182-191, SPE 296.

More, J.J. (1978). The Levenber-Marquardt Algorithm: Implementation and Theory. *Numerical Analysis*. 105-116.

Nurlaela, F., Sutopo. (2015). Non-Isothermal Lumped Parameter Model for Two Phase High Temperature Geothermal Reservoirs. *Proceedings World Geothermal Congress 2015*, Melbourne, Australia, April 19-25.

Onur, M., Sarak, H., Türeyen, Ö.İ., Çınar M., and Satman, A. (2008). A New Non-isothermal Lumped-parameter Model for Low Temperature Liquid Dominated Geothermal Reservoirs and Its Applications. *33rd Workshop on Geothermal Reservoir Engineering*, Stanford University, Stanford, January, 28-30.

Olsen, G. (1984). *Depletion Modeling of Liquid Dominated Geothermal Reservoirs. Technical Report*, SGP-TR-80, Stanford Geothermal Program, Stanford University.

O'Sullivan, M.J., and Bullivant, D.P., Follows, S.E., Mannington, W.I. (1998). Modelling of the Wairakei – Tauhara Geothermal System. *Proceedings of the New Zealand Geothermal Workshop*, 59-66.

Peaceman, D.W. (1977). Interpretation of Well-Block Pressures in Numerical Reservoir Simulation. *52nd Annual Fall Technical Conference and Exhibition*, Oct. 9-12, SPE-6893.

Pruess, K., and Schroeder, R.C. (1979). Geothermal Reservoir Simulation with SHAFT79. *Proceedings of the 5th Workshop on Geothermal Reservoir Engineering*, 183-188.

Pruess, K. (1987). *TOUGH User's Guide*. Lawrence Berkeley Laboratory Report, No LBL-20700.

Pruess, K. (1991). *TOUGH2 A General Purpose Numerical Simulator for Multiphase Fluid and Heat Flow. Lawrence Berkeley Laboratory Report*, No LBL-29400.

Qin, Z., Valfells, A., Gudjonsdottir, M.S. (2017). The Lumped-Parameter Model on Two-Phase and Superheated Geothermal Reservoir. *Energy Procedia, 142*, 481-487.

Quinao, J.J.D., Zarrouk, S.J. (2018). Geothermal Resource Assessment Using Experimental Design and Response Surface Methods: The Ngatamariki Geothermal Field, New Zeland. *Renewable Energy*, *116*, 325-334.

Raghavan. R.(1993). Well Test Analysis, Prentice Hall Petroleum Engineering. USA.

Ramey, J. and Cobb, W.M. (1971). A General Pressure Buildup Theory for a Well in a Closed Drainage Area. *Journal of Petroleum Technology, 23*: 1493-1505. SPE-3012.

Sarak, H. (2004). *Düşük Sıcaklıklı Jeothermal Rezervuarlar için Boyutsuz Rezervuar Modelleri* (Doctoral dissertation). ITU, Istanbul, Turkey.

Sarak, H., Onur, M., and Satman, A. (2005a). Lumped-parameter Models for Low Temperature Geothermal Reservoirs and Their Applications. *Geothermics*, *34*, 728-755.

Sarak, H., Onur, M., and Satman, A. (2005b). New Lumped-parameter Models for Simulation of Low Temperature Geothermal Reservoirs. *28th Workshop on Geothermal Reservoir Engineering*, Stanford University, Stanford, California, 27-29.

Satman, A. (2012). *Geothermal Engineering* [Class notes], Istanbul, Turkey: Petroleum and Natural Gas Engineering Department, ITU.

Schilthuis. R.J. (1936). Active Oil and Reservoir Energy. *Trans*. AIME, *118*, 33-52.

Schroeder, R.C., Goranson, C.B., Benson, S.M., Lippmann, M.J. (1980). Well Interference Tests at the Cerro Prieto Geothermal Field. *Geothermics*, *9*, 179-187.

Türeyen, Ö.İ., and Akyapı, E. (2011). A Generalized Nonisothermal Tank Model for Liquid Dominated Geothermal Reservoirs. *Geothermics*, *40*, March, 50-57.

Türeyen, Ö.İ., Onur, M., and Sarak, H. (2009). A Generalized Nonisothermal Lumped-Parameter Model for Liquid Dominated Geothermal Reservoirs. *34th Workshop on Geothermal Reservoir Engineering*, Stanford University, Stanford, February, 9-11.

URL-1 <http://lsa.colorado.edu/essence/texts/geothermal.html>, date retrieved 01.05.2021.

URL-2 < https://www.worldenergy.org/assets/images/imported >, date retrieved 03.10.2021.

URL-3 < https://www.energy.gov/eere/geothermal/history-geothermal-energy-america>, date retrieved 22.05.2021.

URL-4 < https://www.iea.org/articles/renewables-2020-data-explorer?mode =market&region=World&product=Geothermal >, date retrieved 01.05.2021.

URL-5 <https://www.thinkgeoenergy.com/thinkgeoenergys-top-10-geothermal-countri -2020-installed-power-generation-capacity-mwe/>, date retrieved 03.10.2021.

URL-6 < http://www.oil-gasportal.com/reservoir-management/integrated-reservoir-modeling/>, date retrieved 02.05.2021.

Whiting, R.L., and Ramey, H.J.Jr. (1969). Application of Material and Energy Balance to Geothermal Steam Production. *Journal of Petroleum Technology*, *21*, July, 893-900.

Zhakupov, M., Ilk, D., Blasingame, T.A. (2007). Application of Convolution and Average Pressure Approximation for Solving Nonlinear Flow Problems – Constant Wellbore Pressure Case. *SPE Annual Technical Conference and Exhibition*, Anaheim, California, USA, November 11-14, SPE 110820.

Zyvoloski, G.A., and O'Sullivan, M.J. (1980). Simulation of a gas-dominated, two-phase geothermal reservoir. *Journal of Petroleum Technology*, *20*, February, 52-57.

APPENDICES

APPENDIX A: Superposition Related Formulas

APPENDIX B: Analytical Formulas Used in Validation

APPENDIX A: Superposition Related Formulas

Superposition method with line source solution

Consider a system composed of 2 wells located on points B and C as shown in Figure A.1.

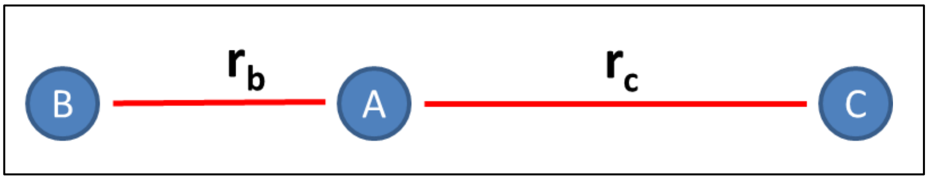

Figure A.1 : Schematic of two well system.

Assuming that wells B and C are both line source wells without wellbore storage, the pressure drop can be formulated as in Equation (A.1) (Ahmed &McKinney, 2005):

$$\Delta p_A = -\frac{70.6 q_B B\mu}{kh}\left[\left(Ei\left(\frac{-948\Phi\mu c_t {r_B}^2}{kt}\right)\right)\right] + -\frac{70.6 q_C B\mu}{kh}\left[\left(Ei\left(\frac{-948\Phi\mu c_t {r_C}^2}{kt}\right)\right)\right] \tag{A.1}$$

where;

q_B is the flow rate of well B, bbl/d,

q_C is the flow rate of well C, bbl/d,

B is the water formation volume factor, bbl/rbbl,

μ viscosity of the water, cp,

k permeability of the reservoir, md,

t elapsed time, hr,

c_t is the total compressibility, 1/psi,

h is the height of the production zone, ft,

Φ porosity, %.

Consider a case shown in Figure A.2.

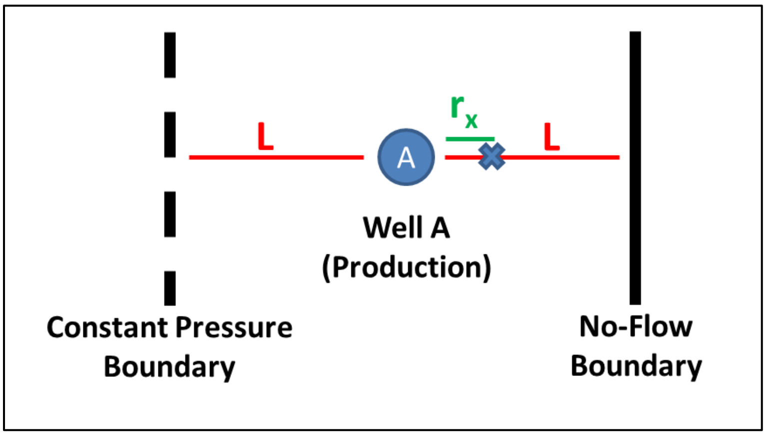

Figure A.2 : Well and boundaries location in example.

By applying superposition and inserting image wells Figure A.3 is obtained.

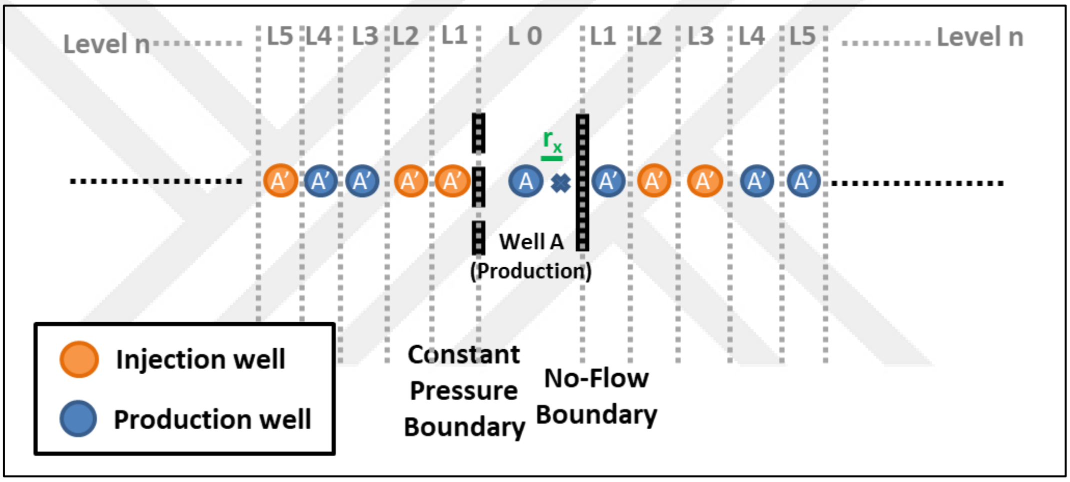

Figure A.3 : The image well insertion.

By using the Equation (A.1) the pressure drop at point x caused by the production and injection wells according to the level of insertion can be written as:

Level 0 pressure drop can be written as in Equation (A.2):

$$\Delta \mathrm{p}_{xL0} = -\frac{70.6\mathrm{q}B\mu}{kh}\left[\left(Ei\left(\frac{-948\Phi\mu c_t r_x{}^2}{kt}\right)\right)\right] \tag{A.2}$$

Let $\frac{70.6\mathrm{q}B\mu}{kh}$ be θ, $\frac{948\Phi\mu c_t}{k}$ be α for the simplicity. Equation (A.2) can be written as in Equation (A.3):

$$\Delta \mathrm{p}_{xL0} = -\theta\left[\left(Ei\left(\frac{-\alpha r_x{}^2}{t}\right)\right)\right] \tag{A.3}$$

Level 1 pressure drop can be written as in Equation (A.4):

$$\Delta p_{xL1} = -\theta\left[Ei\left(\left(-\frac{\alpha(2L-r_x)^2}{t}\right)\right)\right] + \theta\left[Ei\left(\left(-\frac{\alpha(2L+r_x)^2}{t}\right)\right)\right] \quad (A.4)$$

By adding (A.3) and (A.4) we obtain Equation (A.5):

$$\Delta p_{xL0-1} = -\theta\left[\left(\left(Ei\left(\frac{-\alpha {r_x}^2}{t}\right)\right) + Ei\left(\left(-\frac{\alpha(2L-r_x)^2}{t}\right)\right)\right.\right. \\ \left.\left. - Ei\left(\left(-\frac{\alpha(2L+r_x)^2}{t}\right)\right)\right)\right] \quad (A.5)$$

Like with same logic level 2 pressure drop can be written as in Equation (A.6):

$$\Delta p_{xL2} = \theta\left[Ei\left(\left(-\frac{\alpha(4L-r_x)^2}{t}\right)\right)\right] + \theta\left[Ei\left(\left(-\frac{\alpha(4L+r_x)^2}{t}\right)\right)\right] \quad (A.6)$$

Level 3 pressure drop is shown in Equation (A.7):

$$\Delta p_{xL3} = \theta\left[Ei\left(\left(-\frac{\alpha(6L-r_x)^2}{t}\right)\right)\right] - \theta\left[Ei\left(\left(-\frac{\alpha(6L+r_x)^2}{t}\right)\right)\right] \quad (A.7)$$

Level 4 pressure drop is shown in Equation (A.8):

$$\Delta p_{xL4} = -\theta\left[Ei\left(\left(-\frac{\alpha(8L-r_x)^2}{t}\right)\right)\right] - \theta\left[Ei\left(\left(-\frac{\alpha(8L+r_x)^2}{t}\right)\right)\right] \quad (A.8)$$

Level 5 pressure drop is shown in Equation (A.9):

$$\Delta p_{xL5} = -\theta\left[Ei\left(\left(-\frac{\alpha(10L-r_x)^2}{t}\right)\right)\right] \\ + \theta\left[Ei\left(\left(-\frac{\alpha(10L+r_x)^2}{t}\right)\right)\right] \quad (A.9)$$

From the above equations, a general expression for the pressure drop for n levels can be written as in Equation (A.10):

$$\Delta \mathrm{p}_{xL0-n} = -\sum_{i=1}^{n} \theta c_k \left[\left(Ei \left(-\frac{\alpha(2iL - r_x)^2}{t} \right) \right) \right] - \sum_{i=1}^{n} \theta d_k \left[\left(Ei \left(-\frac{\alpha(2iL + r_x)^2}{t} \right) \right) \right] \tag{A.10}$$

where;

c_k is a function giving two times positive and two times negative one value recurrently,

d_k is a function giving two times positive and two times negative one value recurrently.

The above problem can also be solved by using dimensionless terms. In the following formulas, the dimensionless equations are given (Ramey&Cobb, 1971).

$$\mathrm{P}_D = -\frac{1}{2} E_i \left(-\frac{{r_D}^2}{4t_D} \right) \tag{A.11}$$

$$\mathrm{t}_D = \frac{0.000264kt}{\Phi \mu c_t {r_w}^2} \tag{A.12}$$

$$\mathrm{r}_D = \frac{r}{r_w} \tag{A.13}$$

$$\mathrm{p}_D = \frac{2\pi kh}{qB\mu} \left(p_i - p_{wf} \right) \tag{A.14}$$

where;

P_D is the dimensionless pressure,

r_D is the dimensionless radius,

t_D is the dimensionless time,

B water formation volume factor, bbl/rbbl,

μ viscosity of the water, cp,

k permeability of the reservoir, md,

t elapsed time, hr,

Φ porosity, %,

c_t is compressibility, 1/psi,

r_w is the well radius, ft,

r is the radial distance from the well, ft,

P_i is the initial pressure, psi,

P_{wf} is the well flowing pressure, psi.

By using the Equations (A.11), (A.12), (A.13) and (A.14) together, the following expression can be obtained:

$$\Delta\mathrm{p} = \frac{-\frac{1}{2}E_i\left(-\frac{r^2}{{r_w}^2 4\mathrm{t}_D}\right)qB\mu}{2\pi kh} \tag{A.15}$$

By inserting Equation (A.15) into (A.10) the general expression with the dimensionless terms is obtained in equation (A.16):

$$\Delta\mathrm{p}_{xL0-n} = \sum_{i=1}^{n} -\frac{\theta}{2}c_k E_i\left(\frac{-(2iL - r_x)^2}{{r_w}^2 4\mathrm{t}_D}\right) + \sum_{i=1}^{n} -\frac{\theta}{2}d_k E_i\left(\frac{-(2iL + r_x)^2}{{r_w}^2 4\mathrm{t}_D}\right) \tag{A.16}$$

At this point, one may ask what should be the latest level that should be taken as n in the Equation (3.24). In order to answer this question, model is developed which checks the pressure drop values caused by each level of image wells. It was suspected that after some level, as the distance between the newly added image well and the point x increases, the pressure disturbance effect will decrease.

An example is solved to check the above formulation and the validity of the optimum level of image wells. Let the configuration of the boundaries be the same as in Figure 5. Distance between two boundaries is 10000 ft and the well is located in the center of the reservoir with 40000 bbl/d flowrate. The height of the reservoir is 100 ft and the pressure drop from 1000 ft away from the production well is investigated. The permeability is 100 mD, porosity is 10%, the viscosity of water is taken as 1 cp, and formation volume factor of the water is taken as 1 bbl/sb. The compressibility is taken as 1 $\times 10^{-5}$ 1/psi. After 100000 hrs of production, the pressure drop at point x is calculated with the help of the program. The obtained results can be seen in Table A.1.

Table A.1 : Pressure difference as the image well level increase.

Image Well Level	Pressure Difference (psi)	Image Well Level	Pressure Difference (psi)	Image Well Level	Pressure Difference (psi)
Level 0	2.77	Level 9	1.82	Level 18	1.72
Level 1	2.89	Level 10	1.67	Level 19	1.72
Level 2	1.15	Level 11	1.67	Level 20	1.72
Level 3	1.11	Level 12	1.74	Level 21	1.72
Level 4	2.04	Level 13	1.75	Level 22	1.72
Level 5	2.06	Level 14	1.71	Level 23	1.72
Level 6	1.54	Level 15	1.71	Level 24	1.72
Level 7	1.53	Level 16	1.72	Level 25	1.72
Level 8	1.82	Level 17	1.72	Level 26	1.72

It can be seen that in the initial levels, the pressure difference value deviates highly. However, as the number of levels increases, the changes between the levels decrease. After level sixteen the pressure difference keeps the same as the new level of image wells inserted. We can conclude that there is an optimum number of levels for the insertion of image wells.

APPENDIX B: Analytical Formulas Used in Validation

Single tank open model

In Sarak (2004) the analytical formula for the pressure difference of a single tank open model is given by Equation (B.1):

$$\Delta p(t) = \frac{w_{well}}{\alpha_r}\left[1 - \exp(\frac{-\alpha_r t}{\kappa_r})\right] \tag{B.1}$$

where;

α_r is the recharge index, kg/bar-s,

$\Delta p(t)$ is the pressure change, bar,

$p(t)$ is the average pressure in the tank at a given time, bar,

κ_r is the storage capacity of the reservoir, kg/bar,

w_{well} is the production from the well, kg/s,

t is the time, s.

Two tank closed model

In Sarak (2004) the analytical formula for the pressure difference of a two tank closed model is given in Equation (B.2):

$$\begin{aligned} p_r(t) = \; & p_i - \frac{w_{p,net}}{(\kappa_r + \kappa_a)}\, t \\ & - \frac{w_{p,net}}{\alpha_r}\left(\frac{\kappa_a}{(\kappa_r + \kappa_a)}\right)^2 \left[1 - \exp\left(-\frac{\alpha_r(\kappa_r + \kappa_a)t}{\kappa_r\kappa_a}\right)\right] \end{aligned} \tag{B.2}$$

where;

w_r is the recharge of water from the aquifer to the reservoir, kg/s,

$w_{p,net}$ is the production from reservoir, kg/s,

κ_a is the storage capacity of the aquifer, kg/bar,

κ_r is the storage capacity of the reservoir, kg/bar,

p_a is the pressure of the aquifer tank, bar,

p_r is the pressure of the reservoir tank, bar,

p_i is the initial pressure, bar,

α_r is the recharge index between the aquifer and the reservoir, kg/bar-s,

t is the time, s.

Three tank open model

The analytical formula that is used for three tank open model was given in Sarak (2004) can be shown as in Equation (B. 3):

$$\Delta p_r(t) = \frac{w_{p,net}}{\kappa_r}\left[A + B\exp(-\mu_1 t) + C\exp(-\mu_2 t) + D\exp(-\mu_3 t)\right] \quad (B.3)$$

where the values A, B, C, and D is calculated as shown in Equations (B.4)- (B.7):

$$A = \frac{a_2}{\mu_1\mu_2\mu_3} \quad (B.4)$$

$$B = -\frac{{\mu_1}^2 - a_1\mu_1 + a_2}{\mu_1(\mu_2 - \mu_1)(\mu_3 - \mu_1)} \quad (B.5)$$

$$C = -\frac{{\mu_2}^2 - a_1\mu_2 + a_2}{\mu_2(\mu_1 - \mu_2)(\mu_3 - \mu_2)} \quad (B.6)$$

$$D = -\frac{{\mu_3}^2 - a_1\mu_3 + a_2}{\mu_3(\mu_1 - \mu_3)(\mu_2 - \mu_3)} \quad (B.7)$$

where μ_1, μ_2, and μ_3 are calculated as shown in Equations (B.8) - (B. 10):

$$\mu_1 = 2\sqrt{Q}cos\left(\frac{\theta}{3}\right) + \frac{a_3}{3} \quad (B.8)$$

$$\mu_2 = 2\sqrt{Q}cos\left(\frac{\theta + 2\pi}{3}\right) + \frac{a_3}{3} \quad (B.9)$$

$$\mu_3 = 2\sqrt{Q}cos\left(\frac{\theta + 4\pi}{3}\right) + \frac{a_3}{3} \quad (B.10)$$

where Q, R and θ is given with the Equations (B.11) – (B.13):

$$Q = \frac{{a_3}^2 - 3a_4}{9} \quad (B.11)$$

$$R = \frac{2{a_3}^3 - 9a_3a_4 + 27a_5}{54} \quad (B.12)$$

$$\theta = arccos\left(\frac{R}{\sqrt{Q^3}}\right) \quad (B.13)$$

And a_1, a_2, a_3, a_4, and $a_5$are calculated by Equations (B.14) – (B.18):

$$a_1 = \frac{\kappa_{ia}(\alpha_{ia} + \alpha_{oa}) + \kappa_{oa}(\alpha_{ia} + \alpha_r)}{\kappa_{ia}\kappa_{oa}} \tag{B.14}$$

$$a_2 = \frac{\alpha_{ia}\alpha_r + \alpha_{oa}\alpha_r + \alpha_{ia}\alpha_{oa}}{\kappa_{ia}\kappa_{oa}} \tag{B.15}$$

$$a_3 = \frac{\kappa_{oa}\kappa_r(\alpha_{ia} + \alpha_r) + \kappa_{ia}\kappa_r(\alpha_{ia} + \alpha_{oa}) + \kappa_{ia}\kappa_{oa}\alpha_r}{\kappa_{ia}\kappa_{oa}\kappa_r} \tag{B.16}$$

$$a_4 = \frac{\kappa_r(\alpha_{ia}\alpha_{oa} + \alpha_{ia}\alpha_r + \alpha_r\alpha_{oa}) + \kappa_{ia}(\alpha_{ia}\alpha_r + \alpha_r\alpha_{oa}) + \kappa_{oa}(\alpha_{ia}\alpha_r)}{\kappa_{ia}\kappa_{oa}\kappa_r} \tag{B.17}$$

$$a_5 = \frac{\alpha_{ia}\alpha_r\alpha_{oa}}{\kappa_{ia}\kappa_{oa}\kappa_r} \tag{B.18}$$

where ; κ_{ia} is the storage capacity of the inner aquifer, kg/bar,

κ_{oa} is the storage capacity of the inner aquifer, kg/bar,

κ_r is the storage capacity of the reservoir, kg/bar,

α_r is the recharge index between the inner aquifer and the reservoir, kg/bar-s,

α_{ir} is the recharge index between the inner aquifer and the outer aquifer, kg/bar-s,

α_{or} is the recharge index between the outer aquifer and recharge source, kg/bar-s.

Two reservoir tanks with aquifer model

Sarak (2004) described the pressure behavior of the shallow reservoir with the analytical Equation (B.19):

$$\begin{aligned}\Delta p_{r1}(t) = \frac{w_{well1}}{\kappa_{r1}}\Bigg[&\frac{a_1a_9 - a_3a_7}{\mu_1\mu_2\mu_3} \\ &- \frac{{\mu_1}^2 - (a_1 + a_9)\mu_1 + a_1a_9 - a_3a_7}{\mu_1(\mu_2-\mu_1)(\mu_3-\mu_1)}\exp(-\mu_1 t)\Bigg] \\ + \frac{w_{well1}}{\kappa_{r1}}&\left[-\frac{{\mu_2}^2 - (a_1 + a_9)\mu_2 + a_1a_9 - a_3a_7}{\mu_2(\mu_1-\mu_2)(\mu_3-\mu_2)}\exp(-\mu_2 t)\right] \\ + \frac{w_{well1}}{\kappa_{r1}}&\left[-\frac{{\mu_3}^2 - (a_1 + a_9)\mu_3 + a_1a_9 - a_3a_7}{\mu_3(\mu_1-\mu_3)(\mu_2-\mu_3)}\exp(-\mu_3 t)\right] \\ + \frac{w_{well2}}{\kappa_{r2}}&\left[\frac{a_1a_6 - a_3a_4}{\mu_1\mu_2\mu_3} - \frac{-a_6\mu_1 + a_1a_6 + a_3a_4}{\mu_1(\mu_2-\mu_1)(\mu_3-\mu_1)}\exp(-\mu_1 t)\right]\end{aligned} \tag{B.19}$$

$$+\frac{w_{well2}}{\kappa_{r2}}\left[-\frac{-a_6\mu_2+a_1a_6+a_3a_4}{\mu_2(\mu_1-\mu_2)(\mu_3-\mu_2)}\exp(-\mu_2 t)\right]$$

$$+\frac{w_{well2}}{\kappa_{r2}}\left[-\frac{-a_6\mu_3+a_1a_6+a_3a_4}{\mu_3(\mu_1-\mu_3)(\mu_2-\mu_3)}\exp(-\mu_3 t)\right]$$

For the deep reservoir analytical expression is shown in Equation (B.20):

$$\Delta p_{r2}(t)=\frac{w_{well1}}{\kappa_{r1}}\left[\frac{a_1a_8+a_2a_7}{\mu_1\mu_2\mu_3}-\frac{-a_8\mu_1+a_1a_8+a_2a_7}{\mu_1(\mu_2-\mu_1)(\mu_3-\mu_1)}\exp(-\mu_1 t)\right]$$

$$+\frac{w_{well1}}{\kappa_{r1}}\left[-\frac{-a_8\mu_2+a_1a_8+a_2a_7}{\mu_2(\mu_1-\mu_2)(\mu_3-\mu_2)}\exp(-\mu_2 t)\right]$$

$$+\frac{w_{well1}}{\kappa_{r1}}\left[-\frac{-a_8\mu_3+a_1a_8+a_2a_7}{\mu_3(\mu_1-\mu_3)(\mu_2-\mu_3)}\exp(-\mu_3 t)\right]$$

$$+\frac{w_{well2}}{\kappa_{r2}}\left[\frac{a_1a_5-a_2a_4}{\mu_1\mu_2\mu_3}-\frac{{\mu_1}^2-(a_1+a_5)\mu_1+a_1a_5-a_2a_4}{\mu_1(\mu_2-\mu_1)(\mu_3-\mu_1)}\exp(-\mu_1 t)\right] \quad \text{(B.20)}$$

$$+\frac{w_{well2}}{\kappa_{r2}}\left[-\frac{{\mu_2}^2-(a_1+a_5)\mu_2+a_1a_5-a_2a_4}{\mu_2(\mu_1-\mu_2)(\mu_3-\mu_2)}\exp(-\mu_2 t)\right]$$

$$+\frac{w_{well2}}{\kappa_{r2}}\left[-\frac{{\mu_3}^2-(a_1+a_5)\mu_3+a_1a_5-a_2a_4}{\mu_3(\mu_1-\mu_3)(\mu_2-\mu_3)}\exp(-\mu_3 t)\right]$$

The parameters μ_1, μ_2 and μ_3 can be calculated with the Equations (B.21) - (B.23):

$$\mu_1 = 2\sqrt{Q}cos\left(\frac{\theta}{3}\right)+\frac{(a_1+a_5+a_9)}{3} \quad \text{(B.21)}$$

$$\mu_2 = 2\sqrt{Q}cos\left(\frac{\theta+2\pi}{3}\right)+\frac{(a_1+a_5+a_9)}{3} \quad \text{(B.22)}$$

$$\mu_3 = 2\sqrt{Q}cos\left(\frac{\theta+4\pi}{3}\right)+\frac{(a_1+a_5+a_9)}{3} \quad \text{(B.23)}$$

where Q, R and θ is given with the Equations (B.24) – (B.26):

$$Q = \frac{(a_1+a_5+a_9)^2-3(a_5a_9-a_6a_8+a_1a_5+a_1a_9-a_2a_4-a_3a_7)}{9} \quad \text{(B.24)}$$

$$R = \left[\frac{2(a_1+a_5+a_9)^3-9(a_1+a_5+a_9)(a_5a_9-a_6a_8+a_1a_5+a_1a_9-a_2a_4-a_3a_7)}{54}\right] \quad \text{(B.25)}$$

$$+\left[\frac{27(a_1a_5a_9 - a_1a_6a_8 - a_2a_4a_9 - a_2a_6a_7 - a_3a_4a_8 - a_3a_5a_7)}{54}\right]$$

$$\theta = arccos\left(\frac{R}{\sqrt{Q^3}}\right) \quad (B.26)$$

And a_1, a_2, a_3, a_4, a_5, a_6, a_7, a_8, a_9,are calculated by Equations (B.27) – (B.35):

$$a_1 = \frac{\alpha_a + \alpha_{r1} + \alpha_{r2}}{\kappa_a} \quad (B.27)$$

$$a_2 = \frac{\alpha_{r1}}{\kappa_a} \quad (B.28)$$

$$a_3 = \frac{\alpha_{r2}}{\kappa_a} \quad (B.29)$$

$$a_4 = \frac{\alpha_{r1}}{\kappa_{r1}} \quad (B.30)$$

$$a_5 = \frac{\alpha_{r1}+\alpha_{r12}}{\kappa_{r1}} \quad (B.31)$$

$$a_6 = \frac{\alpha_{r12}}{\kappa_{r1}} \quad (B.32)$$

$$a_7 = \frac{\alpha_{r2}}{\kappa_{r2}} \quad (B.33)$$

$$a_8 = \frac{\alpha_{r12}}{\kappa_{r2}} \quad (B.34)$$

$$a_9 = \frac{\alpha_{r2}+\alpha_{r12}}{\kappa_{r2}} \quad (B.35)$$

where;

κ_{r1} is the storage capacity of the shallow reservoir (kg/bar),

κ_{r2} is the storage capacity of the deep reservoir (kg/bar),

κ_{ar} is the storage capacity of the aquifer (kg/bar),

α_{r1} is the recharge index between the aquifer and the shallow reservoir, kg/bar-s,

α_{r2} is the recharge index between the aquifer and the deep reservoir, kg/bar-s,

α_{r12} is the recharge index between the deep and the shallow reservoir, kg/bar-s,

α_a is the recharge index between the aquifer and recharge source, kg/bar-s,

w_{well1} is the production from well1 in the shallow reservoir, kg/s,

w_{well2} is the production from well2 in the deep reservoir, kg/s.

CURRICULUM VITAE

Name Surname **:** Ufuk ÖZTÜRK

EDUCATION **:**

- **B.Sc.** **:** 2005, Middle East Technical University, Faculty of Engineering, Petroleum and Natural Gas Engineering Department
- **M.Sc.** **:** 2009, Middle East Technical University, Faculty of Engineering, Industrial Engineering Department

PUBLICATIONS, PRESENTATIONS AND PATENTS ON THE THESIS:

- **Öztürk U.,** Türeyen Ö.İ., Satman, A**.** 2016. Effects of Observation Well Location in Lumped Parameter Models., *41st Workshop on Geothermal Reservoir Engineering*, February 22-24, 2016 California, USA.
- **Öztürk U.,** Türeyen Ö.İ., Satman, A. 2021: A Study on the Proper Location of Observation Wells for Various Boundary Conditions for Geothermal Reservoirs, *Journal of Petroleum Science and Engineering*, *203.*